

## **Distribution Agreement**

In presenting this thesis or dissertation as a partial fulfillment of the requirements for an advanced degree from Emory University, I hereby grant to Emory University and its agents the non-exclusive license to archive, make accessible, and display my thesis or dissertation in whole or in part in all forms of media, now or hereafter known, including display on the world wide web. I understand that I may select some access restrictions as part of the online submission of this thesis or dissertation. I retain all ownership rights to the copyright of the thesis or dissertation. I also retain the right to use in future works (such as articles or books) all or part of this thesis or dissertation.

Signature:

---

Caroline S Jansen

---

Date

An intratumoral immune niche sustains the anti-tumor immune response and supports the response to immunotherapy

By  
Caroline S. Jansen  
Doctor of Philosophy

Graduate Division of Biological and Biomedical Science  
Cancer Biology

---

Haydn T. Kissick  
Advisor

---

Mandy L. Ford  
Committee Member

---

Gregory B. Lesinski  
Committee Member

---

Bernardo Mainou  
Committee Member

---

Viraj A. Master  
Committee Member

Accepted:

---

Kimberly Jacob Arriola, Ph.D, MPH  
Dean of the James T. Laney School of Graduate Studies

---

Date

An intratumoral immune niche sustains the anti-tumor immune response and supports the response to immunotherapy

By

Caroline S. Jansen  
B. S., the University of Virginia, 2015

Advisor: Haydn T. Kissick, PhD

An abstract of  
A dissertation submitted to the Faculty of the  
James T. Laney School of Graduate Studies of Emory University  
in partial fulfillment of the requirements for the degree of  
Doctor of Philosophy  
in the Graduate Division of Biological and Biomedical  
Science, Cancer Biology  
2022

## Abstract

An intratumoral immune niche sustains the anti-tumor immune response and supports the response to immunotherapy

By Caroline S. Jansen

Tumor infiltrating lymphocytes have been associated with a survival benefit in many tumor types, as well as with the response to immunotherapy. However, it is not clear why some tumors are infiltrated by many T cells, but others have relatively few. Herein, we investigate the mechanisms required for maintaining a strong anti-tumor T cell response in human cancers. We demonstrate that the T cell response is both functionally compartmentalized and physically organized, where a stem-like T cell both self-renews, as well as differentiates into more terminally differentiated, effector-like daughter cells. We show that the presence of these two cell types, and the critical differentiation of the stem-like cells, is integral to a robust anti-tumor immune response. Furthermore, we show that these stem-like T cells reside in antigen presenting cell-dense immune niches within the tumor, and that tumors with an absence or loss of these niches fail to maintain a strong anti-tumor T cell response. Importantly, we illustrate that this biology is translatable across multiple tumor types, reporting these findings in renal cell carcinoma, prostate cancer, and brain metastases from patients with diverse tumor types. Importantly, in renal cell carcinomas and brain metastases, we find the substantial presence of these immune niches leads to significantly improved clinical outcomes. As such, the data presented here provides a strong foundation for understanding the mechanisms of the T cell response to human cancer and provides a springboard for future investigation and continued clinical translation for the benefit of patients of many different tumor types.

An intratumoral immune niche sustains the anti-tumor immune response and supports the response to immunotherapy

By

Caroline S. Jansen  
B. S., the University of Virginia, 2015

Advisor: Haydn T. Kissick, PhD

A dissertation submitted to the Faculty of the  
James T. Laney School of Graduate Studies of Emory University  
in partial fulfillment of the requirements for the degree of  
Doctor of Philosophy  
in the Graduate Division of Biological and Biomedical Science  
in Cancer Biology  
2022

## Acknowledgements

While a noteworthy experience, this dissertation is all but a reflection of my own accomplishments, and rather a crystalline reflection of the immensely vast and valuable support in which I find myself surrounded. They say it takes a village to raise a child, while my own experience has found that to undoubtedly true, I might argue that it also takes the strength of a community to complete a PhD. I owe an immense debt of gratitude, thanks, and appreciation to countless individuals who I hope to name many of here, but I must especially thank my advisor, Dr. Haydn Kissick. You have not only shepherded me along the path to a PhD, but you have also truly taught me to be a scientist, a colleague, a collaborator, a writer, a mentor, and an authentic champion for the shared success of others along the way. Our path to this point has held much interesting science, many failed experiments, an ongoing pandemic, and plenty of laughter and fun, and I truly cannot think of another mentor who could have walked this road with me quite so well. Thank you, from the depths of who I am, for all you have given me and how you have helped set my course in this career.

I would also like to thank many of my other mentors who have been invaluable sources of wisdom, encouragement, and inspiration along the way. To Dr. Bill Petri, who first taught me what it means to be a physician scientist as an undergraduate at UVa and has continued to be a treasured mentor and advocate, thank you for setting me on my course in this career and continually empowering me to stay that course. To Dr. Larry Boise and Dr. Anita Corbett, who have always given me a space to be my most unapologetic, unfiltered, and passionate self, thank you for always keeping your doors open to me, for keeping me grounded, and for always encouraging me, both in my scientific endeavors and my extracurricular ones. To those who span the boundaries between friend, mentor, and inspiration in the best of ways, Dr. Jenny Carlisle, Dr. Zach Buchwald, and Dr. Scott Wilkinson, thank you for the countless hours of scientific counsel, career advice, and true friendship, and for the inspiring example each of you sets ahead of me for my career. To Dr. Scott Wilkinson, thank you particularly for being a mentor, a sponsor, an advisor, an advocate, a collaborator, a teacher, and, most importantly, a truest friend for all seasons. To my committee, Dr. Mandy Ford, Dr. Bernado Mainou, Dr. Viraj Master, and Dr. Greg Lesinski, thank you for your willingness, your patience, your enthusiasm, and your guidance as I learned to ask good scientific questions, to test hypotheses, and to pursue this doctoral degree.

I would also like to thank those in our scientific community, both at Emory and beyond. To our friends and collaborators, particularly those in the Ahmed, Sowalsky, Buchwald, Lesinski, Balk, and Larsen labs who especially greeted me with open arms and have walked with me throughout my PhD, thank you for your friendship and your partnership over these years. I look forward to continuing to work together and enjoy good science together for many years to come. To our Emory Cancer Biology community past and present, especially Dr. Scott Wilkinson, Dr. Jackie Zoine, Dr. Brandon Ware, Emily Greene, Amanda Ruggieri, Gianna Branella, and Alyssa Duffy, to our Emory MSTP community, especially our 2022 re-entry cohort, and to our Behind the Microscope team, Dr. Bejan Saeedi, Dr. Joe Behnke, and Dr. Michael Sayegh, thank you for your friendship, your support, and the comradery from our very first days together to all those yet to come.

To the Kissick lab, especially my fellow graduate students, Nataliya Prokhevskaya, who has been by my side in the lab since day one, Maria Cardenas, and Ewelina Sobierajska, and our labmates past

and present, including Luke del Balzo, Adriana Moon Reyes, Petra Gregorova, Dr. Baohan Vo, and Rachel Greenwald, thank you for always being there for me and for each other, for never hesitating to lend a helping hand, and for always being a source of valuable feedback, of lively scientific discussion, and of an assuredly good time. To the Integrated Cellular Imaging Core, the Cancer Tissue and Pathology Core, the Yerkes Genomics Core, especially Kathryn Pellegrini, and the Flow Cytometry Core, especially Bob Karaffa and Kametha Fife, thank you for your patience, flexibility, and willingness to teach and work with me.

There is not a way to express enough thanks for the role that my family and friends have played in my journey up to this point. To my family, thank you to my Papa, Dr. Greg Stewart, for being my first and earliest inspiration in learning to love the discipline of science and the art of medicine, for always cheering me on, and for never failing to take an interest in my dreams. Thank you to my Mom, Robin Stewart, for being my most faithful friend and constant encourager, for being my inspiration in motherhood, for always listening to my problems and my victories, big and small, for loving my family like your own, and for always answering the call to love, nurture, and play with Mary Caroline at a moment's notice. Thank you to my sister, Dr. Kate Timberlake, for being the best big sister, my first and best friend, and my inspiration as a mother and a woman in medicine.

To my dear friends, of whom I will surely fail to name all, thank you so very much for everything that you mean to me, and most especially for being my village. To the Quaranteam, Mary Featherstone and Mary, Joe, and Joseph Devlin, thank you for being my people, for showing up for me at a moment's notice, for always cheering me on, for celebrating me, for picking me up when I'm down, and for just being who you are. To the friends who have been by my side since before this degree was only a pipedream, mused over on a sunny day on the UVa Lawn, especially Renee Redman Nixon, Lauren Baetsen Corless, Kaila Grenier Ott, Naomi Bishop Lopes, Natalie Khalil, Jalen Ross, TJ Potter, and Sky Miller, and to the friends who have welcomed me and my family to Atlanta and made it feel like home, especially Hanson, Catherine, Preston, and James Schultz, Fr. Robbie Cotta, Fr. Mike Metz, and Nick Molinet, thank you for your enduring friendship and unwavering belief in my dreams. To my childhood best friend, Vanessa Utley, thank you for walking through so many seasons of life with me, for being a constant amidst an ever-changing world, and for just being who you are.

To my sweet, smart, beautiful, kind, and sparkly daughter, Mary Caroline, thank you for shining the brightest of lights in my life, for running joyfully into my arms every day, for giggling my troubles away, for always reminding me of the greater and utmost purposes in life, and for being my greatest inspiration, especially in advocating for the advancement of equality and dignity of women and girls, not just in science and medicine, but across the globe and in all things.

Finally, and most especially, to my incredible, dedicated, thoughtful, and kind husband, Patrick, the words are wholly inadequate, but thank you. I can't imagine that I would have made it to this point without your support and your encouragement. For always encouraging me to chase this dream and cheering me on throughout it, for always understanding when the days start early and run late, for believing in me when I can't believe in myself, for simply being who you are, and most of all, for loving me, thank you. I'll never be able to say it enough, but I love you, and thank you, yesterday, today, and every day to come.

## **Table of Contents**

Abstract.....	ii
Acknowledgements.....	iv
Table of Contents.....	vi
List of Figures.....	viii
List of Tables.....	xi
List of Abbreviations.....	xii
<b>Chapter 1: Introduction.....</b>	<b>1</b>
1.1 Introduction.....	1
1.2 The importance of the immune system in the control and prevention of cancer.....	1
1.3 T cell dynamics in the environment of chronic antigen exposure.....	5
1.4 Summary, scope, and goals for this project.....	8
<b>Chapter 2: An intra-tumoral niche maintains and differentiates stem-like CD8 T-cells.....</b>	<b>10</b>
2.1 Author's Contribution and Acknowledgement of Reproduction.....	10
2.2 Abstract.....	11
2.3 Introduction.....	12
2.4 Results.....	13
2.5 Discussion.....	42
2.6 Materials & Methods.....	47
2.7 Acknowledgements.....	56
2.8 Tables.....	58
<b>Chapter 3: Stem-like CD8 T cells are present in intra-tumoral immune niches in diverse tumor types.....</b>	<b>60</b>

3.1 Author’s Contribution and Acknowledgement of Reproduction.....	60
3.2 Introduction.....	61
3.3 Results.....	63
3.4 Discussion.....	90
3.5 Materials & Methods.....	94
3.6 Acknowledgements.....	98
3.7 Tables.....	99
<b>Chapter 4: Clinical outcomes following immunotherapy in renal cell carcinoma patients is associated with a pre-existing immune response in tumor tissue.....</b>	<b>101</b>
4.1 Introduction.....	101
4.2 Results.....	103
4.3 Discussion.....	114
4.4 Materials & Methods.....	118
4.5 Acknowledgements.....	120
4.6 Tables.....	121
<b>Chapter 5: General Discussion and Closing Remarks.....</b>	<b>124</b>
5.1 Introduction.....	124
5.2 TCF1+ stem-like T cells in human tumors.....	124
5.3 Stem-like T cells reside in an intratumoral immune niche.....	126
5.4 Immune niches and the response to immunotherapy.....	130
5.5 Future studies and concluding remarks.....	131
<b>Chapter 6: References.....</b>	<b>141</b>

## List of Figures

Figure 1.1 Models of T cell differentiation in the setting of acute or chronic antigen exposure....	7
Figure 2.1 Clinical characteristics, statistical methods, and clinical outcomes in renal cell carcinoma.....	14
Figure 2.2 The anti-tumor T cell response is supported by a stem-like CD8 T cell, which gives rise to terminally differentiated CD8 T cells in the tumor.....	17
Figure 2.3 CD8 T cell infiltration is associated with improved survival and is independent of standard risk assessment tools, tumor features, and patient demographics.....	19
Figure 2.4 Flow cytometry profiling and functional analysis of CD8 T cells in human RCC tumor samples.....	20
Figure 2.5 Sorting schema, practical, and statistical approach to T cell receptor analysis in RCC..	22
Figure 2.6 Stem cell differentiation to the terminally differentiated state is associated with transcriptional and epigenetic changes.....	25
Figure 2.7 Transcriptional and Epigenetic analysis of T cell subsets in tumors.....	27
Figure 2.8 Antigen presenting cells (APCs) form a supportive, intratumoral niche for TCF1+ stem-like CD8 T cells.....	32
Figure 2.9 Comparing flow cytometry and histo-cytometry methods for analysis of immune infiltrate in RCC.....	33
Figure 2.10 Comparison of tertiary lymphoid structures and intratumoral antigen presenting niches in RCC tumor samples.....	35
Figure 2.11 Highly infiltrated kidney tumors are well vascularized and contain lymphatic vessels.....	38

Figure 2.12 Clinical features and clinical association of clinical outcomes with imaging-based assessment of tumor immune infiltrate.....	40
Figure 2.13 Loss of APC niche is associated with impaired CD8 T cell response and disease progression.....	43
Figure 2.14 PDL1 status is not associated with CD8 T cell infiltration in human RCC tumor samples.....	45
Figure 3.1 Evaluation of antigen-presenting cell (APC) niches within PCa cases.....	65
Figure 3.2 Multiplex, quantitative immunofluorescence imaging analysis of human brain metastasis samples. ....	68
Figure 3.3 TCF1+ stem-like CD8 T cells are present in brain metastases in both irradiated and unirradiated samples.....	71
Figure 3.4 Flow cytometry identification of TCF1+ stem-like CD8 T cells and Tim3+ terminally differentiated CD8 T cells in brain metastases.....	74
Figure 3.5 Flow cytometry comparison of T cell infiltration in irradiated and unirradiated brain metastasis samples.....	75
Figure 3.6 Flow cytometry comparison of the phenotype of stem-like and terminally differentiated CD8 T cells in irradiated and unirradiated brain metastasis samples.....	76
Figure 3.7 TCF1+ stem-like CD8 T cells reside in dense antigen presenting immune niches in brain metastases.....	78
Figure 3.8 Comparison between highly and poorly infiltrated brain metastases samples.....	80
Figure 3.9 Higher levels of TCF1+ stem-like CD8 T cells and higher proportions of intratumoral immune niches in brain metastases are associated with improved local control.....	83

Figure 3.10 Exposure to radiation therapy attenuates the CD8 T cell response, but TCF1+ stem-like cells, MHC-II+ cells, and immune niches persist.....	85
Figure 3.11 The effect of timing between exposure to radiation therapy and surgical resection on the immune response in brain metastases.....	87
Figure 4.1 Identification of TCF1+ stem-like CD8 T cells in renal cell carcinoma tumors by flow cytometry and quantitative immunofluorescence imaging.....	105
Figure 4.2 Presence TCF1+ stem-like CD8 T cells in intratumoral immune niches is associated with clinical benefit following immune checkpoint blockade.....	110
Figure 4.3 Increased intratumoral infiltration of CD8 T cells is associated with improved progression free and overall survival in renal cell carcinoma patients following immune checkpoint blockade.....	113
Figure 5.1 The intratumoral immune niche.....	129
Figure 5.2 Features of tertiary lymphoid structures.....	136

## List of Tables

Table 2.1 Flow Cytometry Antibodies.....	58
Table 2.2 Immunofluorescence Antibodies.....	58
Table 2.3 CellProfiler Primary Object Parameters.....	59
Table 3.1 Immunofluorescence Antibodies.....	99
Table 3.2 Immunofluorescence Antibodies.....	100
Table 3.3 Flow Cytometry Antibodies.....	100
Table 4.1 Immunofluorescence Imaging Cohort Patient Characteristics.....	121
Table 4.2 Flow Cytometry Cohort Patient Characteristics.....	122
Table 4.3 Flow Cytometry Antibodies.....	123
Table 4.4 Immunofluorescence Antibodies.....	123

## List of Abbreviations

<b>ACK</b>	Ammonium-Chloride-Potassium
<b>AF</b>	alexa-fluor
<b>AID</b>	activation induced cytidine deaminase
<b>AJCC</b>	American Joint Committee on Cancer
<b>ANOVA</b>	analysis of variance
<b>APC</b>	allophycoyanin
<b>APC</b>	antigen presenting cell
<b>BD</b>	Becton-Dickinson
<b>BIDMC</b>	Beth Israel Deaconess Medical Center
<b>BV</b>	brilliant violet
<b>CAST</b>	cluster affinity search technique
<b>CB</b>	clinical benefit
<b>CCL19</b>	C-C Motif Chemokine Ligand 19
<b>CCL21</b>	C-C Motif Chemokine Ligand 21
<b>CCR7</b>	C-C chemokine receptor type 7
<b>CD11b</b>	Cluster of Differentiation 11b
<b>CD11c</b>	Cluster of Differentiation 11c
<b>CD127</b>	Cluster of Differentiation 127
<b>CD19</b>	Cluster of Differentiation 19
<b>CD2</b>	Cluster of Differentiation 2
<b>CD226</b>	Cluster of Differentiation 226

<b>CD244</b>	Cluster of Differentiation 244
<b>CD25</b>	Cluster of Differentiation 25
<b>CD28</b>	Cluster of Differentiation 28
<b>CD3</b>	Cluster of Differentiation 3
<b>CD31</b>	Cluster of Differentiation 31
<b>CD38</b>	Cluster of Differentiation 38
<b>CD39</b>	Cluster of Differentiation 39
<b>CD4</b>	Cluster of Differentiation 4
<b>CD45RA</b>	Cluster of Differentiation 45RA
<b>CD45RO</b>	Cluster of Differentiation 45RO
<b>CD68</b>	Cluster of Differentiation 68
<b>CD69</b>	Cluster of Differentiation 69
<b>CD8</b>	Cluster of Differentiation 8
<b>CG</b>	germinal center
<b>Chr</b>	chromosome
<b>CR</b>	complete response
<b>CT</b>	computerized tomography
<b>CT</b>	tumor core
<b>CTLA4</b>	cytotoxic T-lymphocyte-associated protein 4
<b>CXCL13</b>	C-X-C Motif Chemokine Ligand 13
<b>CXCR5</b>	C-X-C chemokine receptor type 5
<b>DAPI</b>	4',6-diamidino-2-phenylindole
<b>DEG</b>	differentially expressed genes

<b>DFS</b>	disease free survival
<b>DMR</b>	differentially methylated regions
<b>DNA</b>	deoxyribonucleic acid
<b>ECOG</b>	Eastern Cooperative Oncology Group (performance status score)
<b>EDTA</b>	ethylenediaminetetraacetic acid
<b>EFCC</b>	Emory Flow Cytometry Core
<b>EM</b>	expectation maximization
<b>FACS</b>	fluorescence activated cell sorting
<b>FBS</b>	fetal bovine serum
<b>FDA</b>	Food and Drug Administration
<b>FDC</b>	follicular dendritic cell
<b>FFPE</b>	formalin fixed paraffin embedded
<b>FITC</b>	fluorescein
<b>FOXP3</b>	forkhead box P3
<b>FRC</b>	fibroblastic reticular cell
<b>FSC</b>	forward scatter
<b>GSEA</b>	gene set enrichment analysis
<b>GZMB</b>	granzyme B
<b>H&amp;E</b>	hematoxylin & eosin
<b>HBSS</b>	Hank's Balanced Salt Solution
<b>HEV</b>	high endothelial venule
<b>HIPAA</b>	Health Insurance Portability and Accountability Act
<b>HPC</b>	high performance computing

<b>HPF</b>	high powered field
<b>HR</b>	hazard ratio
<b>HRP</b>	horseradish peroxidase
<b>ICI</b>	immune checkpoint inhibition
<b>IF</b>	immunofluorescence
<b>IFNg</b>	interferon gamma
<b>IHC</b>	immunohistochemistry
<b>IL2</b>	interleukin 2
<b>IL2RA</b>	interleukin 2 receptor alpha
<b>IL7R</b>	interleukin 7 receptor
<b>IM</b>	invasive margin
<b>IO</b>	immunotherapy
<b>IR</b>	infrared
<b>IRB</b>	institutional review board
<b>IU</b>	international units
<b>KM</b>	Kaplan-Meier
<b>LCMV</b>	lymphocytic choriomeningitis virus
<b>MACS</b>	magnetic-activated cell sorting (buffer)
<b>mCRPC</b>	metastatic castration resistant prostate cancer
<b>MD</b>	medical doctor
<b>MFI</b>	mean fluorescence intensity
<b>MHC</b>	major histocompatibility complex
<b>MRI</b>	magnetic resonance imaging

<b>MSI-H</b>	microsatellite instability - high
<b>NA</b>	numerical aperture
<b>NCB</b>	no clinical benefit
<b>NCCN</b>	National Comprehensive Cancer Network
<b>NCI</b>	National Cancer Institute
<b>NHP</b>	non-human primate
<b>NIH</b>	National Institutes of Health
<b>NP</b>	no progression/non-progressor
<b>OS</b>	overall survival
<b>P</b>	progression/progressor
<b>PBMC</b>	peripheral blood mononuclear cell
<b>PBS</b>	phosphate buffered saline
<b>PCa</b>	prostate cancer
<b>PCA</b>	principle component analysis
<b>PD</b>	progressive disease
<b>PD1</b>	programmed death 1
<b>PDCD1</b>	Programmed cell death protein 1
<b>PDL1</b>	Programmed death-ligand 1
<b>PDPN</b>	podoplanin
<b>PE</b>	phycoerythrin
<b>PFS</b>	progression free survival
<b>PR</b>	partial response
<b>R<sup>2</sup></b>	coefficient of determination

<b>RBC</b>	red blood cell
<b>RCC</b>	renal cell carcinoma
<b>RECIST</b>	response evaluation criteria in solid tumors
<b>RNA</b>	ribonucleic acid
<b>RNAseq</b>	RNA sequencing
<b>RP</b>	radical prostatectomy
<b>RPMI</b>	Roswell Park Memorial Institute (medium)
<b>SAS</b>	statistical analysis system
<b>SD</b>	stable disease
<b>SOC</b>	standard of care
<b>SRS</b>	stereotactic radiosurgery
<b>SSC</b>	side scatter
<b>SSIGN</b>	size, stage, grade, necrosis
<b>Tbet</b>	T-box expressed in T cells
<b>TBX21</b>	T-box transcription factor 21
<b>TCF</b>	T cell receptor
<b>TCF1</b>	T cell factor 1
<b>TD</b>	terminally differentiated
<b>TIGIT</b>	T cell immunoreceptor with Ig and ITIM domains
<b>TIL</b>	tumor infiltrating lymphocytes
<b>Tim3</b>	T-cell immunoglobulin and mucin-domain containing-3
<b>TLS</b>	tertiary lymphoid structure
<b>TNF<math>\alpha</math></b>	Tumor necrosis factor alpha

<b>TNM</b>	tumor node metastasis
<b>TOX</b>	Thymocyte selection-associated high mobility group box protein TOX
<b>TURBT</b>	transurethral resection of bladder tumor
<b>UISS</b>	UCLA Integrated Staging System
<b>WD</b>	working distance
<b>YF</b>	yellow fever

## **Chapter 1: Introduction**

### **1.1 Introduction**

It is estimated that some 1.9 million new cancer diagnoses will be made by the end of 2022 and that an unfortunate more than 600,000 cancer deaths will occur in the same year in the United States alone, reinforcing the idea that cancer-related illness and cancer-related death remains a forefront issue facing the health of not only the United States, but also the entire world<sup>1</sup>. In kidney cancers specifically, disease incidence continues to increase, and 2022 is expected to hold nearly 80,000 new kidney cancer diagnoses and nearly 14,000 kidney cancer deaths<sup>1</sup>. With major risk factors for kidney cancer including excess body weight, smoking and tobacco use, chronic hypertension, and chronic renal failure, the increasing prevalence of these conditions raises additional concern for continued increases in kidney cancer incidence<sup>2-4</sup>. Thus, there is great urgency for improvement in biomarkers for diagnosing or risk-stratifying kidney cancer, as well as for uncovering opportunities for new or enhanced therapeutic options for kidney cancer patients.

### **1.2 The importance of the immune system in the control and prevention of cancer**

To begin considering what research questions might be most impactful in diagnosing and treating cancer, it is useful to consider what the unifying features of cancer development and progression are, especially across multiple tumor types. One such framework for doing so is the “hallmarks of cancer,” which were first outlined by Weinberg and Hanahan in the early 2000s, when they proposed six common features and functionalities that cells acquire as they transform to become malignant<sup>5</sup>. The original set of six hallmarks included: self-sufficiency in growth signals, insensitivity to anti-growth signals, tissue invasion & metastasis, limitless replicative potential,

sustained angiogenesis, and evading apoptosis<sup>5</sup>. In the early 2010s, they updated this list to propose the six hallmarks to be sustaining proliferative signaling, evading growth suppressors, resisting cell death, enabling replicative immortality, inducing/accessing vasculature, and activating invasion and metastasis, with reprogramming cellular metabolism and evading immune destruction denoted as “emerging hallmarks<sup>6</sup>”. Most recently, especially given the leaps in understanding these two emerging hallmarks that have been made in the decade since this update, it has been agreed that these emerging hallmarks should now be considered core hallmarks, alongside the original six<sup>7</sup>.

Most particularly, the importance of the immune system in restraining cancer growth and development—and strategically harnessing that for use as therapeutics—has been a strong focus of cancer research in recent history, most famously culminating with awarding Tasuku Honjo and Jim Allison with the Nobel Prize. This prize was awarded for their “their discovery of cancer therapy by inhibition of negative immune regulation<sup>8</sup>”, which is a discovery that hinges upon the central role of the T lymphocyte in combatting cancer growth. Importantly, T cells have long been placed as key players in keeping tumors at bay. For example, it was observed that mice with profound lymphocyte deficiencies develop spontaneous tumors<sup>9-13</sup>, and that interfering with important effector molecules produced by T cells (e.g. IFN $\gamma$  and perforin) made mice more susceptible to tumors<sup>14-20</sup>.

Additionally, similar observations have long been made in human patients, where immunosuppressed organ transplant patients have increased cancer risk<sup>14, 21-23</sup> and where transfer of bone marrow cells can result in a “graft versus leukemia” effect that can contribute to controlling

leukemia cell expansion<sup>24-26</sup>, again underscoring the importance of the immune system in curtailing the development of cancer.

Many studies have demonstrated that the presence of T cells, particularly CD8 T cells, is a predictor of favorable patient prognosis in several tumor types, and this finding continues to be replicated in many tumor types<sup>27-43</sup>. For example, much of the landmark work establishing tumor infiltrating lymphocytes (TILs) as a predictor of patient outcomes was accomplished by the Galon group, who first showed that the type, density, and location of TILs in primary colorectal cancer are significant predictors of both disease free and overall survival<sup>27-31</sup>. This seminal work led them to establish a scoring system for measuring TILs—the “Immunoscore”—which considers the density of infiltrating CD8+ and CD45RO+ T-cells at the tumor core (CT) and invasive margin (IM), with higher scores reflecting greater lymphocyte invasion<sup>31</sup>. Validation of this scoring system showed that patients with higher scores (i.e. higher T-cell densities within primary tumors) had increased DFS and OS compared to low scores, and that the Immunoscore scoring system was a better predictor of survival than TNM staging methods<sup>32</sup>. Further study has indicated that patients with dense CD8 T-cell infiltration of lung metastases colorectal cancer also have improved overall survival<sup>33</sup>. Importantly, after this leading work in colorectal cancer, similar findings have been reported in many additional tumor types, with T cell infiltration having been found to be a positive prognostic indicator in melanoma, breast cancer, head and neck cancer, ovarian cancer, non-small cell lung cancer, esophageal cancer, small cell lung cancer, hepatocellular carcinoma, and renal cell carcinoma<sup>34-38, 43</sup>.

In addition to being an intrinsic predictor of patient prognoses, tumor infiltrating lymphocytes have

also been associated with the response to immunotherapies, such as immune checkpoint blockade<sup>39-42</sup>. In melanoma patients, those who responded to anti-PD1 therapy have proliferation of intratumoral CD8 T cells that corresponds with subsequent radiographic reduction of tumor size<sup>39</sup>. Interestingly, in this study, analysis of pre-treatment samples from responding patients shows higher density of CD8, PD1, and PDL1 expressing cells in and near the tumor, which implies that patients with a strong pre-existing T cell response may be more poised to mount a productive response to immune checkpoint blockade<sup>39</sup>, and this finding was replicated in a study of desmoplastic melanoma patients, where patients with more CD8 T-cells near the tumor margin were gleaned the most clinical benefit following anti-PD1 therapy<sup>40</sup>. Interestingly, more recent studies have shown that a specific subset of tumor infiltrating T cells (TCF1+ CD8 T cells), which harbors both a capacity to persist and self-renew as well as differentiate, are those that are most mechanistically important for the effective response to immune checkpoint blockades, and indeed, this subset of cells is associated with therapeutic efficacy in patients with melanoma<sup>44-48</sup>.

Importantly, PDL1 expression status is used as a strategy for predicting which patients will benefit from immunotherapy, but typical immunohistochemistry-based evaluation of expression levels falls short in comprehensively identifying patient populations who will benefit from these therapies<sup>49-51</sup>. Thus, these and other studies indicate that the presence of infiltrating lymphocytes in the tumor microenvironment is an important factor in predicting the response to immunotherapy<sup>27, 31, 37, 39, 44, 45, 52-54</sup>, which could add to the utilization of PDL1 expression status or make up for it in those cancers which typically lack PDL1 expression or for which PDL1 expression status is poorly predictive of response<sup>51, 55-57</sup>. Thus, together with the aforementioned studies indicating that the intrinsic tumor infiltrating immune response can predict patient

outcomes<sup>27-45, 52-54</sup>, these studies also highlight a common feature of the immune response to cancer: while some patients may generate significant and efficacious anti-tumor T cell responses, others do not, and seeking to understand why this is is a critical question for the field, and much of the focus of the work presented herein.

In summary, all of these observations point to a central role for the immune system, and specifically for T lymphocytes, in combatting and controlling cancer development, growth, and advancement. However, given the widespread occurrence of cancer in otherwise healthy patients, it is clear that this T lymphocyte response is insufficient for completely preventing or controlling cancer. Accordingly, it is critically important to understand how this response works, how it fails, and how we might enhance the response to control and prevent cancer more effectively.

### **1.3 T cell dynamics in the environment of chronic antigen exposure**

In order to identify and understand the mechanisms of the CD8 T cell response to cancer, it is important to build upon the mechanisms of this response in other settings, such as in mouse models of both infection and cancer, as well as in other relevant human settings, such as chronic infections or solid organ transplant.

During the classic response to acute infection, it is well understood that naïve CD8 T cells undergo rapid effector differentiation, followed by contraction and the emergence of a population memory cells as antigen is cleared from the environment<sup>58-62</sup> (Figure 1.1). However, when antigen is not cleared, T cells are chronically exposed to cognate antigen, such as in the setting of tumors and chronic viral infections. This causes significant transcriptional and functional alterations in the T

cells, which can lead to a T cell state called “T cell exhaustion<sup>63-65</sup>.” This state of exhaustion was first and most extensively described in a mouse model of chronic viral infection (LCMV), in which virus-specific CD8 T cells progressively “exhaust”—gaining increasing expression of checkpoint and inhibitor receptors, while also experiencing a progressive decline in their ability to proliferate and kill target cells<sup>64, 65</sup>.

Importantly, more recent studies have added dimension to the understanding of the T cell exhaustion observed in the setting of chronic antigen exposure<sup>66</sup>. It is now appreciated that there are several distinct subsets of exhausted, antigen specific CD8 T cells in this setting<sup>46, 67-70</sup>. One such subset is a stem-like cell, which notably maintains the capacity for self-renewal, but also for differentiating into a more terminally differentiated cell subset (Figure 1.1). This terminally differentiated subset has diminished capacity for self-renewal, but importantly retains the ability to kill target cells<sup>46, 64, 67-69</sup>. These stem-like CD8 T cells are most readily defined by characteristic expression of the transcription factor TCF1, as well as high expression of costimulatory molecules, such as CD28. On the other hand, the more terminally differentiated CD8 T cells lack expression of TCF1 and instead have higher expression of checkpoint (e.g. Tim3, CTLA4, CD244) and effector molecule (e.g. granzymes, perforin) expression<sup>46, 64</sup>. Importantly, this establishes a new way of understanding the mechanisms of the T cell response in chronic antigen settings—these distinct cellular subsets compartmentalize the proliferative and cytotoxic functions of CD8 T cells. TCF1+ stem-like T cells orchestrate T cell maintenance, while killing is achieved by the more terminally differentiated cells, allowing for an organized, sustainable T cell response in the setting of chronic antigen exposure<sup>46, 66</sup>.

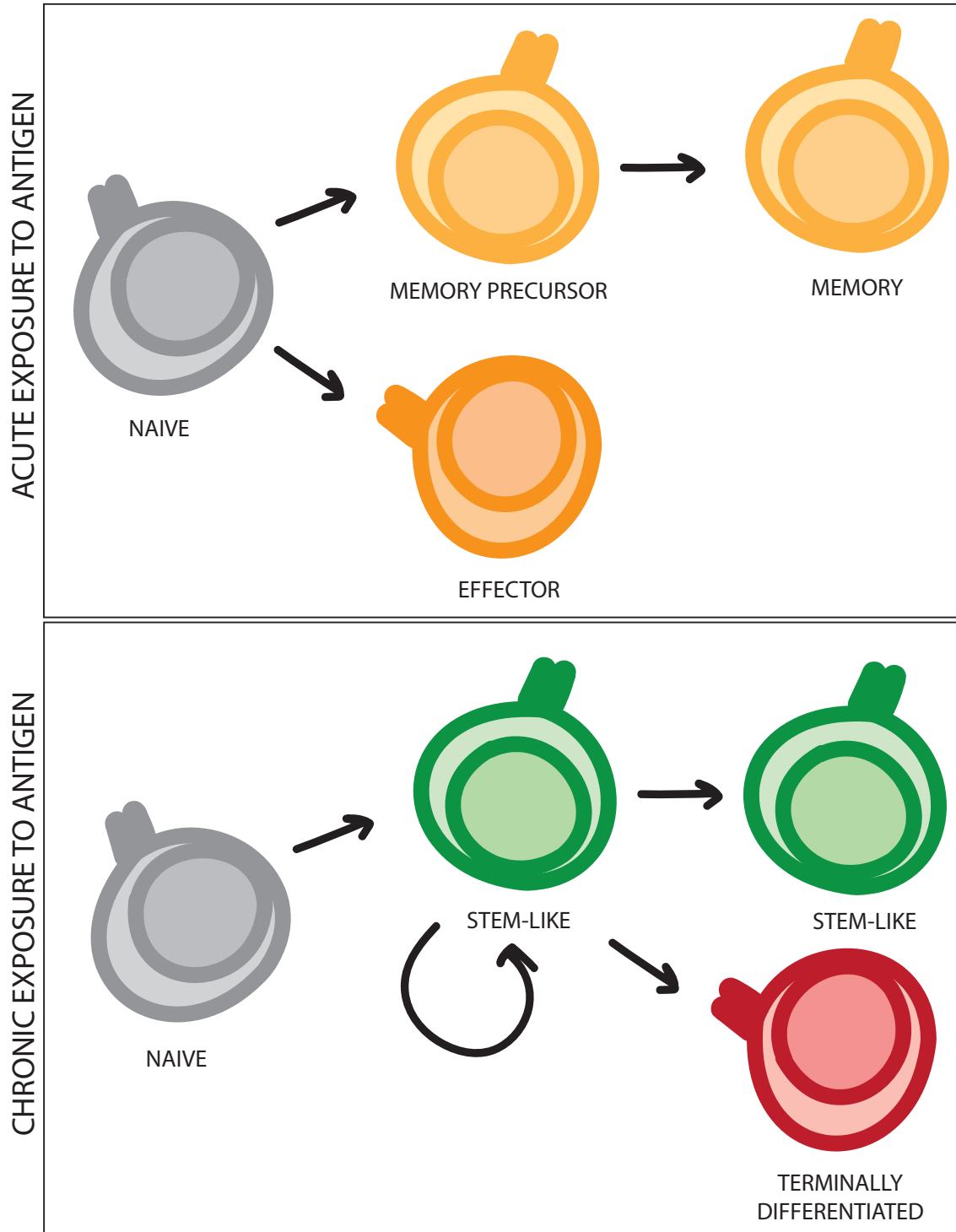


**Figure 1.1 Models of T cell differentiation in the setting of acute or chronic antigen exposure.**

This understanding is particularly important in the cancer-specific setting of chronic antigen exposure, and these stem-like and terminally differentiated cells have also been identified amongst tumor infiltrating T cells<sup>44, 45, 68, 71</sup>. In the work presented here, we identify these cell populations in human renal tumors and demonstrate the critical importance of these stem-like CD8 T cells in maintaining the anti-tumor immune response<sup>43</sup> (see also: Chapter 2). Having found that these stem-like T cells are critical to a durable anti-tumor T cell response, we propose that the ability to house these cells could be a factor in why some patient's harbor many T cells in the tumor, while others have very few.

#### **1.4 Summary, scope, and goals for this project**

In summary, while it has been well established in many tumor types that a productive anti-tumor T cell response is a positive predictor of patient prognosis<sup>27-33, 35-42</sup>, this remains to be clearly decided in other tumor types, such as in renal cell carcinoma, so one particular goal of this project was to define the association between clinical outcomes and T cell infiltration in renal tumors. Additionally, it remains unclear why some patients may mount such a productive immune response, while others may not. As others had previously described a stem-like model of maintaining a T cell response in chronic antigen settings<sup>46, 66-70</sup>, this work sought to probe whether an analogous or similar model was also responsible for supporting an enduring T cell response in renal tumors, as well to understand whether breakdowns in this biology could explain why some patients fail to mount a productive T cell response. A second part of this goal for the project included testing these same hypotheses in diverse tumor types, seeking to understand whether the stem-like model of the T cell response in tumors represents a biological feature that spans tumor types. Finally, this project sought to determine how this understanding of the mechanisms of the

intrinsic anti-tumor T cell response might affect the subsequent response to immunotherapy, in order to better understand why some patients glean great benefit from immune checkpoint blockade, while others do not. Thus, in this text, I describe my efforts and my findings in the pursuit of answering these scientific questions, in order to advance the understanding of the mechanisms of the anti-tumor T cell response in human tumors and in response to immune checkpoint blockade.

## Chapter 2: An intra-tumoral niche maintains and differentiates stem-like CD8 T-cells

### 2.1. Author's Contribution and Acknowledgement of Reproduction.

This chapter is reproduced with minor edits from Caroline S Jansen<sup>1</sup>, Nataliya Prokhnevskaya<sup>1</sup>, Viraj A Master<sup>1,2</sup>, Martin G Sanda<sup>1,2</sup>, Jennifer W Carlisle<sup>2,3</sup>, Mehmet Asim Bilen<sup>2,3</sup>, Maria Cardenas<sup>1</sup>, Scott Wilkinson<sup>4</sup>, Ross Lake<sup>4</sup>, Adam G Sowalsky<sup>4</sup>, Rajesh M Valanparambil<sup>5,6</sup>, William H Hudson<sup>5,6</sup>, Donald McGuire<sup>5,6</sup>, Kevin Melnick<sup>1</sup>, Amir I Khan<sup>1</sup>, Kyu Kim<sup>1</sup>, Yun Min Chang<sup>5</sup>, Alice Kim<sup>1</sup>, Christopher P Filson<sup>1,2</sup>, Mehrdad Alemozaffar<sup>1,2</sup>, Adeboye O Osunkoya<sup>1,2,7</sup>, Patrick Mullane<sup>7</sup>, Carla Ellis<sup>7</sup>, Rama Akondy<sup>5,6</sup>, Se Jin Im<sup>5,6</sup>, Alice O Kamphorst<sup>8</sup>, Adriana Reyes<sup>1</sup>, Yuan Liu<sup>2,9</sup>, Haydn Kissick<sup>10, 11, 12, 13</sup>, An intra-tumoral niche maintains and differentiates stem-like CD8 T-cells. *Nature*, 2019;576(7787):465-70. doi:10.1038/s41586-019-1836-5.

C.S.J. and H.K. conceived and designed the study and composed the manuscript. C.S.J., V.A.M., M.G.S., C.P.F., M.A. and H.K. designed experiments. C.S.J., N.P., J.W.C., M.C., R.M.V., W.H.H., D.M., K.M., A.I.K., K.K., Y.M.C., A.K., A.O.K., A.R. and H.K. collected flow cytometry data. C.S.J., N.P., M.C. and H.K. analyzed flow cytometry data. C.S.J., N.P., M.C., A.R. and H.K. performed fluorescence activated cell sorting. C.S.J., N.P. and M.C. performed RNA and DNA extractions. C.S.J., S.W., R.L. and A.G.S. optimized and performed immunofluorescence slide scanning. C.S.J. and H.K. developed quantitative immunofluorescence techniques and performed quantitative analysis of immunofluorescence data. W.H.H., D.M. and H.K. performed RNA sequencing analysis. N.P., M.C., K.K., Y.M.C., A.K. and H.K. performed in vitro T cell assays. N.P. and H.K. performed whole-genome methylation analysis. R.A., S.J.I. and A.O.K. provided

critical expertise and contributed specific analysis. V.A.M., M.G.S., C.P.F. and M.A. provided clinical samples. C.S.J., J.W.C. and A.R. collected and organized clinical data. K.M., A.O.O., P.M. and C.E. provided annotation and scoring of pathology specimen. Y.L. assisted with biostatistical analysis. All authors reviewed the manuscript.

#### Affiliations:

1. Department of Urology, Emory University School of Medicine, Atlanta, GA, USA. 2. Winship Cancer Institute of Emory University, Atlanta, GA, USA. 3. Department of Hematology and Oncology, Emory University School of Medicine, Atlanta, GA, USA. 4. Laboratory of Genitourinary Cancer Pathogenesis, National Cancer Institute, Bethesda, MD, USA. 5. Department of Microbiology and Immunology, Emory University School of Medicine, Atlanta, GA, USA. 6. Emory Vaccine Centre, Emory University School of Medicine, Atlanta, GA, USA. 7. Department of Pathology, Emory University School of Medicine, Atlanta, GA, USA. 8. Department of Oncological Sciences, Precision Immunology Institute, Icahn School of Medicine at Mount Sinai, New York City, NY, USA. 9. Rollins School of Public Health, Emory University, Atlanta, GA, USA. 10. Department of Urology, Emory University School of Medicine, Atlanta, GA, USA. 11. Winship Cancer Institute of Emory University, Atlanta, GA, USA. 12. Department of Microbiology and Immunology, Emory University School of Medicine, Atlanta, GA, USA. 13. Emory Vaccine Centre, Emory University School of Medicine, Atlanta, GA, USA.

## 2.2 Abstract.

Tumor-infiltrating lymphocytes are associated with a survival benefit in several tumor types and with the response to immunotherapy<sup>27, 31, 37, 39, 40, 52, 53, 72</sup>. However, the reason some tumors have

high CD8 T cell infiltration while others do not remains unclear. Here we investigate the requirements for maintaining a CD8 T cell response against human cancer. We find that CD8 T cells within tumors consist of distinct populations of terminally differentiated and stem-like cells. On proliferation, stem-like CD8 T cells give rise to more terminally differentiated, effector-molecule-expressing daughter cells. For many T cells to infiltrate the tumor, it is critical that this effector differentiation process occur. In addition, we show that these stem-like T cells reside in dense antigen-presenting-cell niches within the tumor, and that tumors that fail to form these structures are not extensively infiltrated by T cells. Patients with progressive disease lack these immune niches, suggesting that niche breakdown may be a key mechanism of immune escape.

### **2.3 Introduction.**

In many cancers, tumor infiltrating CD8 T cells predict patient survival and response to immunotherapy<sup>27, 31, 37, 39, 40, 53, 72, 73</sup>. These observations raise a fundamental question about the immune response to cancer: Why do some tumors have high CD8 T cell infiltration while others do not? A logical assumption has been made that T cell exhaustion drives a decline in the T cell response. T cell exhaustion has been extensively described in viral infections, where persistent antigen exposure reduces the ability of the CD8 T cells to proliferate and kill target cells<sup>65, 74</sup>. Acquisition of checkpoint molecules that inhibit T cell function are a hallmark of this exhausted state, and blockade of molecules like PD-1 can rescue exhausted cells in these models<sup>75, 76</sup>. Supporting the idea that T cell exhaustion is a factor limiting T cell function in cancer, many reports have found that T cells in tumors express high levels of these checkpoint molecules, and blockade of PD-1 and CTLA-4 are among the most successful treatments for many cancers<sup>77-81</sup>. However, the model of persistent antigen exposure driving T cell decline does not explain why

some patients have a strong T cell response to their tumor for decades, or why patients with controlled disease may have many CD8 T cells that are phenotypically exhausted. Here, we have investigated the CD8 T cell response to human tumors to better explain the mechanisms that control the magnitude of the T cell response to cancer.

## **2.4 Results.**

### *TCF1+ CD8 T cells reside in tumors*

Based on the observation that CD8 infiltration into tumors predicts survival and response to immunotherapy in other cancers<sup>27, 31, 37, 39, 53, 72, 73, 82, 83</sup>, we measured this parameter in a cohort of kidney cancer patients. To quantitate CD8 infiltration, tumor tissue was collected from patients undergoing surgery and analyzed by flow cytometry (Figure 2.1 A). CD8 T cell infiltration ranged from 0.002% to over 20% of the total tumor cells (Figure 2.2 A). For patients with any stage disease, having less than 2.2% CD8 T cell infiltration predicted a 4-fold more rapid progression after surgery (HR=3.84, p<0.01) (Figure 2.2 B, Figure 2.1 B-E, 2.3 A-B). CD8 T cell infiltration did not correlate with clinical parameters such as disease stage or patient age (Figure 2.3 C-K), suggesting that other biological mechanisms control the degree of T cell infiltration into tumors.

Reasoning that the composition of the tumor infiltrating CD8 T cells might offer insight into the mechanisms controlling T cell infiltration, we analyzed expression of checkpoint molecules, co-stimulatory molecules, and important transcription factors in tumor infiltrating CD8 T cells. We detected a distinct population of cells that resembled exhausted CD8 cells by their expression of high levels of checkpoint molecules, TIM3, PD1, CTLA4 and TIGIT (Figure 2.2 C-D, Figure 2.4 A-B). We also identified a population of cells with low checkpoint molecule expression, but high

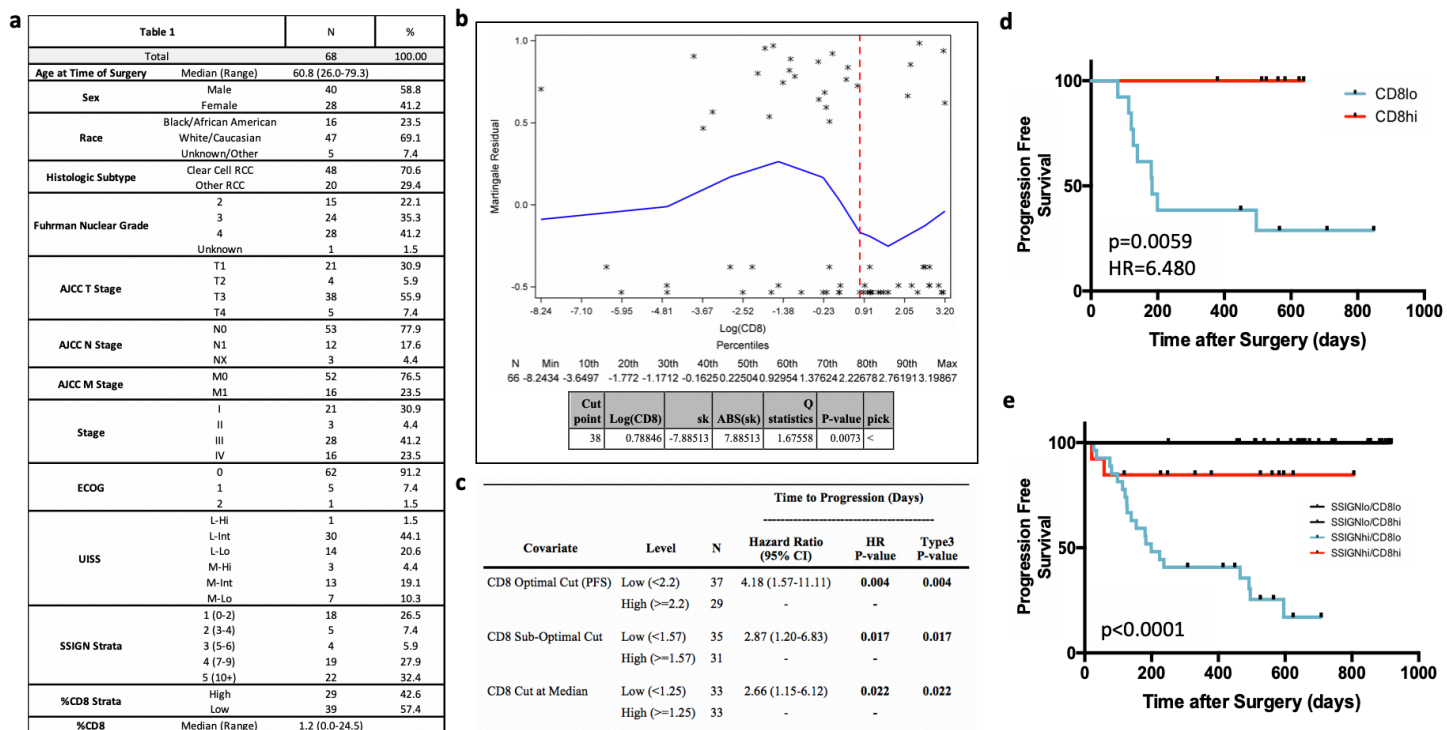


**Figure 2.1: Clinical characteristics, statistical methods, and clinical outcomes in renal cell carcinoma.** (a) Descriptive Statistics. Table details the demographic, disease stage, disease characteristic, and immune infiltrate breakdown of the cohort of kidney patients. (b) Martingale Residual Plot. Residual plot illustrating discovery of 2.2% CD8 “optimal cut”. (c) Comparison of Optimal Cut, Sub-Optimal Cut, and Median Cut. (d) CD8 T cell Infiltration predicts time to progression in stage III (T3N0M0) patients. Patients were stratified into high (>2.2%CD8) or low (<2.2%CD8) based on the optimal cut identified in a cohort of all-stage patients. CD8hi: n=13.; CD8lo: n=7.  $p=0.0059$ ,  $HR=0.1543$ , as determined using log-rank test. (e) CD8 T cell infiltration significantly improves prognostication in kidney cancer patients with high SSIGN (size, stage, grade, necrosis) scores.  $p=0.0292$ ,  $HR=0.1409$ , as determined using log-rank test. Patients were stratified into low (scores 1-6) and high (scores >6) SSIGN score groups and into low

(<2.2%CD8) and high (>2.2%CD8) T cell infiltration. SSIGNlo/CD8lo: n=11, SSIGNlo/CD8hi: n=16, SSIGNhi/CD8lo, n=28, SSIGNhi/CD8hi, n=13.

expression of co-stimulatory molecule CD28 and transcription factor TCF1 (encoded by *TCF7*) (Figure 2.2 C-D, Figure 2.4 A-B). TCF1 is a critical transcription factor that defines a stem-like T cell population in chronic murine lymphocytic choriomeningitis virus (LCMV) infection<sup>46, 67, 68</sup>. Importantly, others have described a TCF1+ CD8 T cell population in human and murine tumors that correlates with response to PD1 blockade<sup>44, 45, 47, 48, 68, 84</sup>. To functionally characterize the TCF1+ and checkpoint-high populations of CD8 T cells in tumors, checkpoint-high cells (PD1+, TIM3+) and stem-like cells (TCF1+TIM3-CD28+) were sorted from tumors, labeled with cell trace violet, and incubated with anti-CD3/CD28 stimulation beads. The TCF1+TIM3-CD28+ stem-like population consistently proliferated in response to bead stimulus, while the checkpoint-high population lacked proliferative potential (Figure 2.2 E-F). Importantly, after division, the stem-like T cells upregulated PD1, TIM3 and CD244 to a similar level seen *in vivo*, and downregulated TCF1, acquiring the phenotype of the checkpoint-high population (Figure 2.2 G-H, Figure 2.4 C-F). Together, these data suggest that TIM3- CD28+ T cells possess a stem-like capability; they can proliferate and give rise to more terminally differentiated, checkpoint-expressing T cells.

To further investigate the relationship between the intratumoral stem-like and terminally differentiated CD8 T cells, we examined the T cell receptor (TCR) repertoires of each population in 11 tumor samples. We found that TCRs significantly overlapped between the stem-like and terminally differentiated cell populations in all patients examined, suggesting a clonal relationship between these populations (Figure 2.2 I-J, Figure 2.5 H). In two patients for whom we recovered samples from distant sites within the same tumor, we found a high degree of TCR overlap between the stem-like and terminally differentiated populations at all locations (Figure 2.5 G). These data

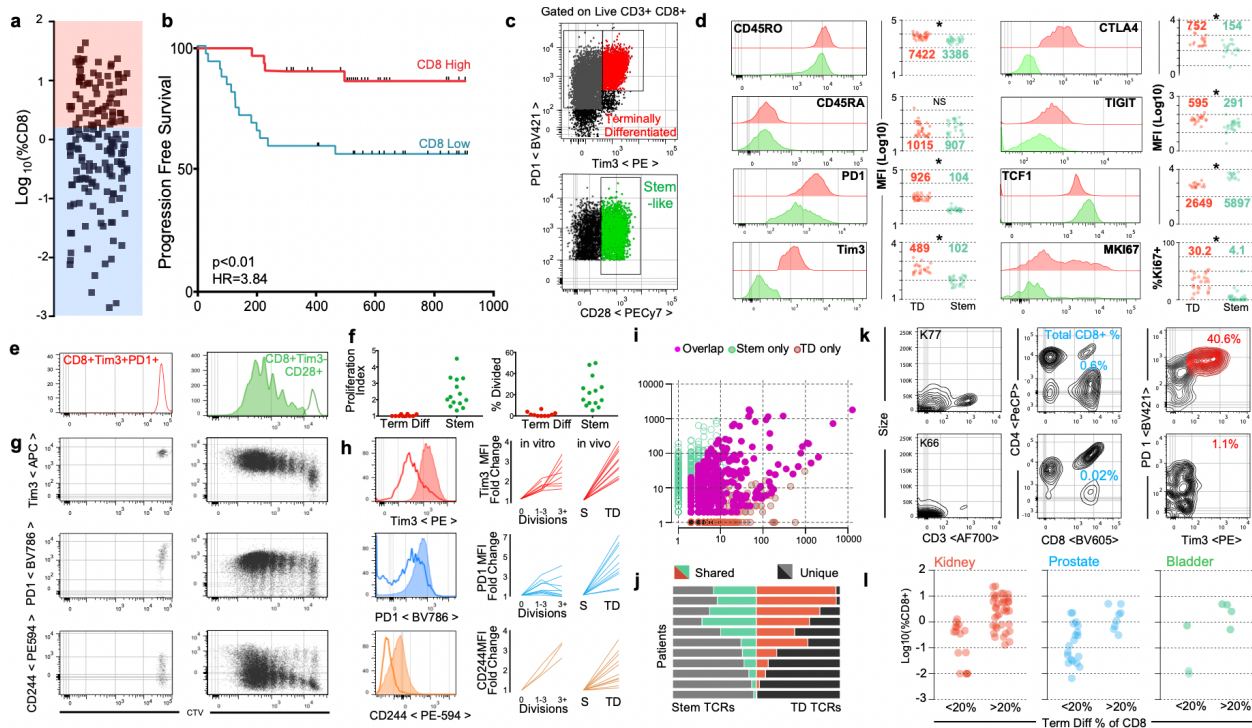


**Figure 2.2: The anti-tumor T cell response is supported by a stem-like CD8 T cell, which gives rise to terminally differentiated CD8 T cells in the tumor.** a) CD8 T cell proportion in kidney tumors shown as percent of total cells (n=68). b) Disease progression after surgery in kidney cancer patients stratified into high or low CD8 T cell infiltration (+/-2.2%) based on optimal cut methods. Time to progression is the number of days from surgery until death or progression by RECIST criteria. (n=66). c) Gating strategy to identify intratumoral CD8 T cell populations. Populations shown are gated on Live/CD3+/CD8+. d) Expression (MFI) of activation markers, checkpoint molecules, and transcription factors by Tim3+ and Tim3-CD28+ subsets, gated as in (c). e & f) Stem-like (Tim3-CD28+) and terminally differentiated (Tim3+) populations were sorted from kidney tumors, labeled with cell trace violet, and cultured with anti-CD3/anti-CD28 beads and 10U/mL of IL2 for 4-5 days. Proliferation index and percentage of cells divided is shown. g & h) Expression of Tim3, PD1, and CD244 after cells undergo proliferation. Summary plots from in vitro activation experiments compared to fold change in MFI observed between the populations in vivo. i) TCR repertoires of stem-like and terminally differentiated T cells sorted as shown in

Extended Data figure 4. TCR clones are represented by the number of reads detected in either T cell population. j) TCR repertoire overlap between stem-like and terminally differentiated T cells. The proportion of the detected TCR repertoire in each patient that is unique to each population or shared between the two is shown. k & l) Generation of checkpoint high cells correlates with total T cell infiltration. Patients were classified as having a low (<20%) or high (>20%) fraction of Tim3+ terminally differentiated cells. Data shows sample patients (k) and summary data in kidney (n=49), prostate (n=28), and bladder tumors (n=8) (l).

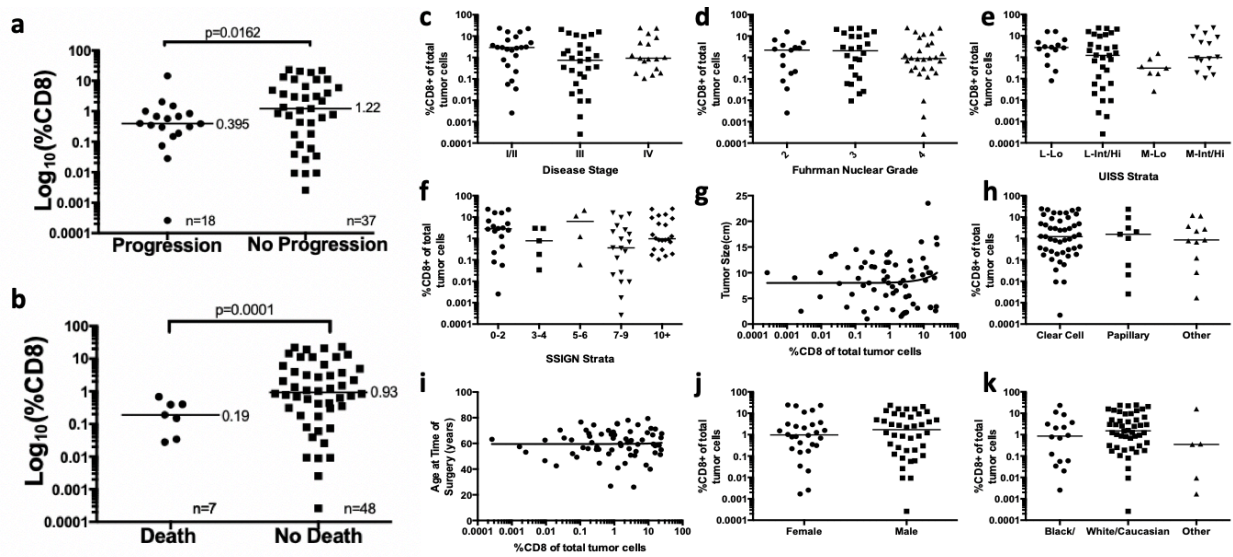


**Figure 2.3: CD8 T cell infiltration is associated with improved survival and is independent of standard risk assessment tools, tumor features, and patient demographics. (a & b)** Proportion of CD8 T cells in the tumors of patients that progress or die after surgery as compared to those without (a) disease progression or (b) death. (c) Disease stage,  $p=0.6$ , (d) Fuhrman nuclear grade,  $p=0.4$ , (e) UISS groups,  $p=0.3$ , (f) SSIGN groups,  $p=0.3$ , (g) Maximum tumor size in one dimension, in centimeters,  $R=0.01$ ,  $p=0.3$ , (h) Histologic subtype,  $p=0.7$ , (i) Patient age at the time of surgery, in years,  $R=0.001$ ,  $p=0.9$ , (j) Patient sex,  $p=0.8$ , (k) Patient race/ethnicity,  $p=0.7$ .

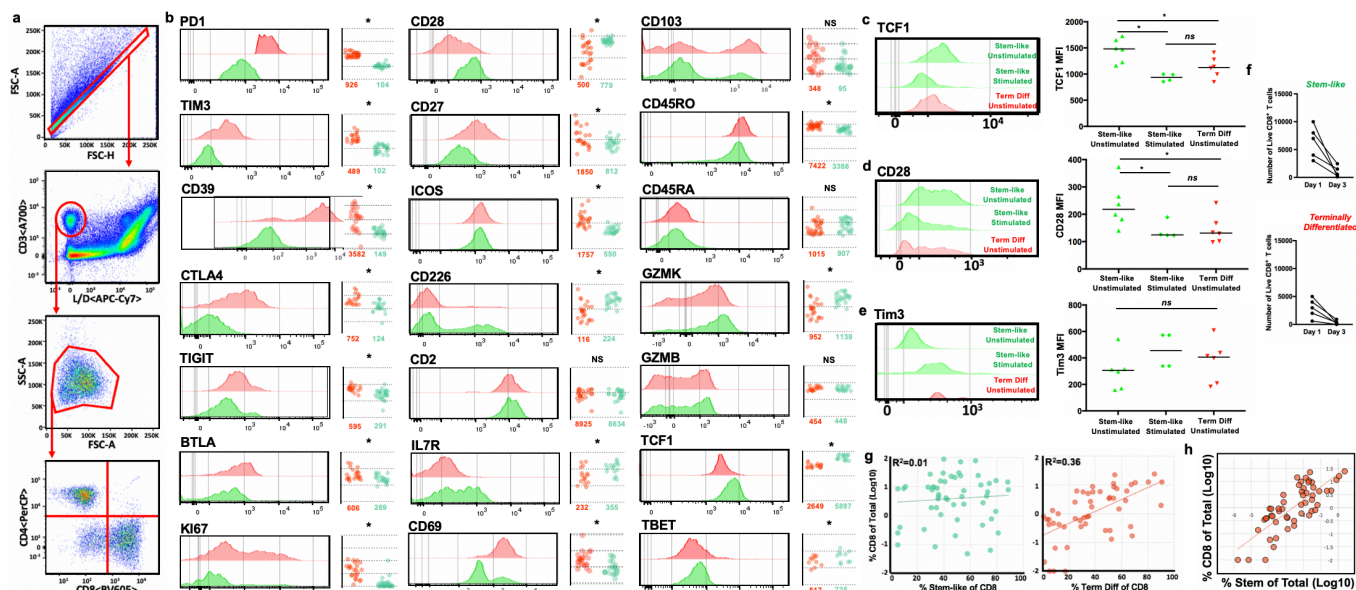


**Figure 2.4: Flow cytometry profiling and functional analysis of CD8 T cells in human RCC tumor samples.** (a) Flow cytometry gating scheme. FSC-A and FSC-H are used to select for singlets. Live (APC-Cy7 negative) CD3<sup>+</sup> events are then selected from this population of singlets. Lymphocytes are selected from this live CD3<sup>+</sup> population on the basis of FSC-A & SSC-A, and CD4<sup>+</sup> and CD8<sup>+</sup> T cell populations are selected from the lymphocyte population. (b) Expression of various molecules by stem-like (green) and terminally differentiated (red) CD8 T cells in human tumors measured by flow cytometry. (c, d, & e) Expression of TCF1 (c), CD28 (d), and Tim3 (e) as measured by flow cytometry, by stem-like and terminally differentiated CD8 T cells isolated from human kidney cancer patients (n=6) and cultured in vitro for 3 days with 10U of IL2 and with (stimulated) or without (unstimulated) anti-CD3/CD28/CD2 bead stimulation at a 1:1 ratio. (f) Number of live stem-like and terminally differentiated intratumoral CD8<sup>+</sup> T cells after 3 days of in vitro culture in IL-2 supplemented media. Live/dead staining was utilized to determine the proportion and number of live CD8 T cells by flow cytometry. (g) Composition of the CD8 T cell compartment. In 60 human kidney cancer patients, proportion of CD8 T cells that are stem-like

cells (PD1+ CD28+ Tim3-) correlates with total T cell infiltration (%CD8 T cells of total cells), while proportion of terminally differentiated cells (PD1+ Tim3+) does not. (h) Percentage of total CD8 T cells correlates with the percentage of total cells that are stem-like CD8 T cells.

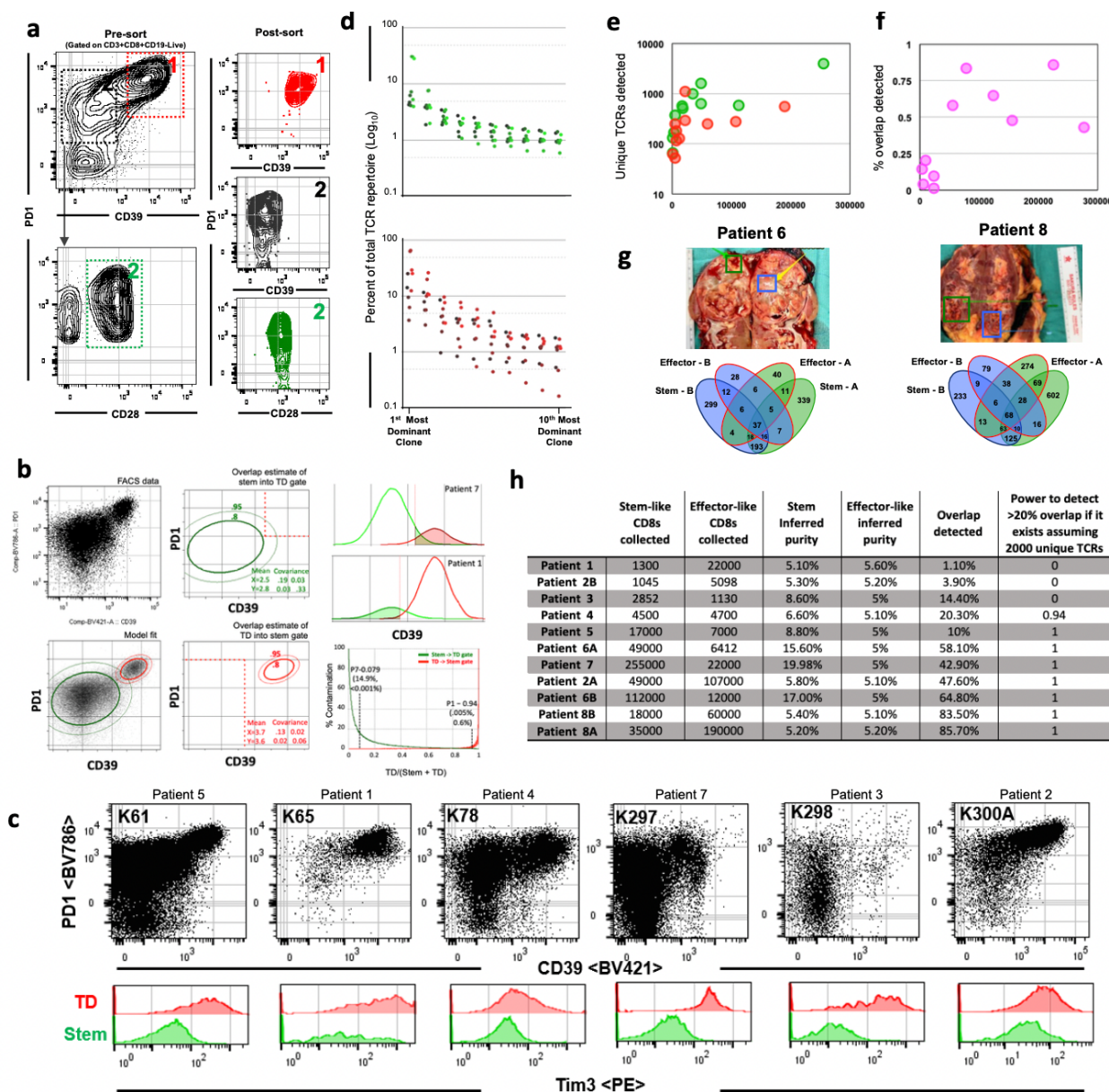


**Figure 2.5: Sorting schema and practical and statistical approach to T cell receptor analysis in RCC.** (a) Gating scheme for fluorescence activated cell sorting of cell populations for stem-like and terminally differentiated cell populations from human kidney tumors. Terminally differentiated cells (1) are PD1-High and CD39+. Stem-like cells (3) are PD1+CD39-CD28+. (b) Estimation of population overlap. PD1 and CD39 expression by flow cytometry was modeled using a 2 population Gaussian mixing model. The amount of each population falling within each

sorting gate based on the relative proportions of the populations was determined and used to calculate the if TCRs found in both populations could be accounted for by contamination. (c) Presort flow cytometry plots for patients sorted for TCR sequencing. (d) Ranking of stem-like (green) and terminally differentiated (red) TCR clones from most to 10th most dominant clone by percent of total TCR repertoire (Log10). (e) Number of unique TCR clones detected in stem-like (green) and terminally differentiated (red) cell populations as a function of number of cells collected. (f) Percent overlap detected as a function of number of cells collected. (g) Tumor samples were taken from two physically distant sites within the same tumor and stem-like and terminally differentiated cells were sorted from each and TCR sequenced. Venn diagrams illustrate unique TCRs found between stem-like populations in sites A and B, between terminally differentiated populations in sites A and B, and between location mismatched stem-like and terminally differentiated populations (e.g. stem-like-A/terminally differentiated-B, stem-like-B/terminally differentiated-A), in addition to overlap between stem-like and terminally differentiated T cell populations within a single site. (h) Table indicating the number of stem-like and terminally differentiated T cells collected, inferred purity of each population, percent overlap detected calculated by the number of TCRs detected in either sample divided by the total TCRs in both samples, and the power to detect >20% overlap (assuming 2000 unique TCRs/sample) for each patient sample.

are in contrast to reports finding that the CD39<sup>-</sup> population of TILs are unrelated to tumor antigens, and instead support a model of T cell differentiation where stem-like T cells within the tumor are the precursors to the terminally differentiated CD8 T-cell population<sup>85</sup>.

We next assessed how the composition of CD8 T cells in the tumor related to total T cells infiltration. Highly infiltrated tumors consistently had a distinct population of Tim3<sup>+</sup> cells, which resemble phenotypically exhausted CD8 T cells, while poorly infiltrated tumors rarely had these cells (Figure 2.2 K, Figure 2.4 G). The same relationship was present in prostate and bladder tumors as well, where poorly infiltrated tumors contained few TIM3<sup>+</sup> terminally differentiated cells (Figure 2.2). In poorly infiltrated tumors, the stem-like CD8 T cell population is consistently detectable at very low numbers (Figure 2.4 H) but does not appear to be induced to differentiate into the TIM3<sup>+</sup> cells (Figure 2.2 K-L, Figure 2.4 G). These data suggest that the magnitude of the T cell response within a tumor is related to the ability of many terminally differentiated cells to be generated by the stem-like TCF1<sup>+</sup> T cell population.

#### *Transcription and epigenetics of CD8 T cell subsets*

To further investigate the terminally differentiated and stem-like T cell populations in tumors, we performed RNAseq on these populations. The terminally differentiated cells expressed more checkpoint molecules and much higher levels of granzymes and perforin (Figure 2.6 A). In contrast, TCF1<sup>+</sup> stem-like CD8s had higher levels of genes involved in survival such as *IL7R* and *IL2RA* (CD25), as well as co-stimulatory molecules like *CD28*, *CD226* and *CD2* (Figure 2.6 B). We also compared these populations to stem-like and terminally differentiated CD8 T cell subsets

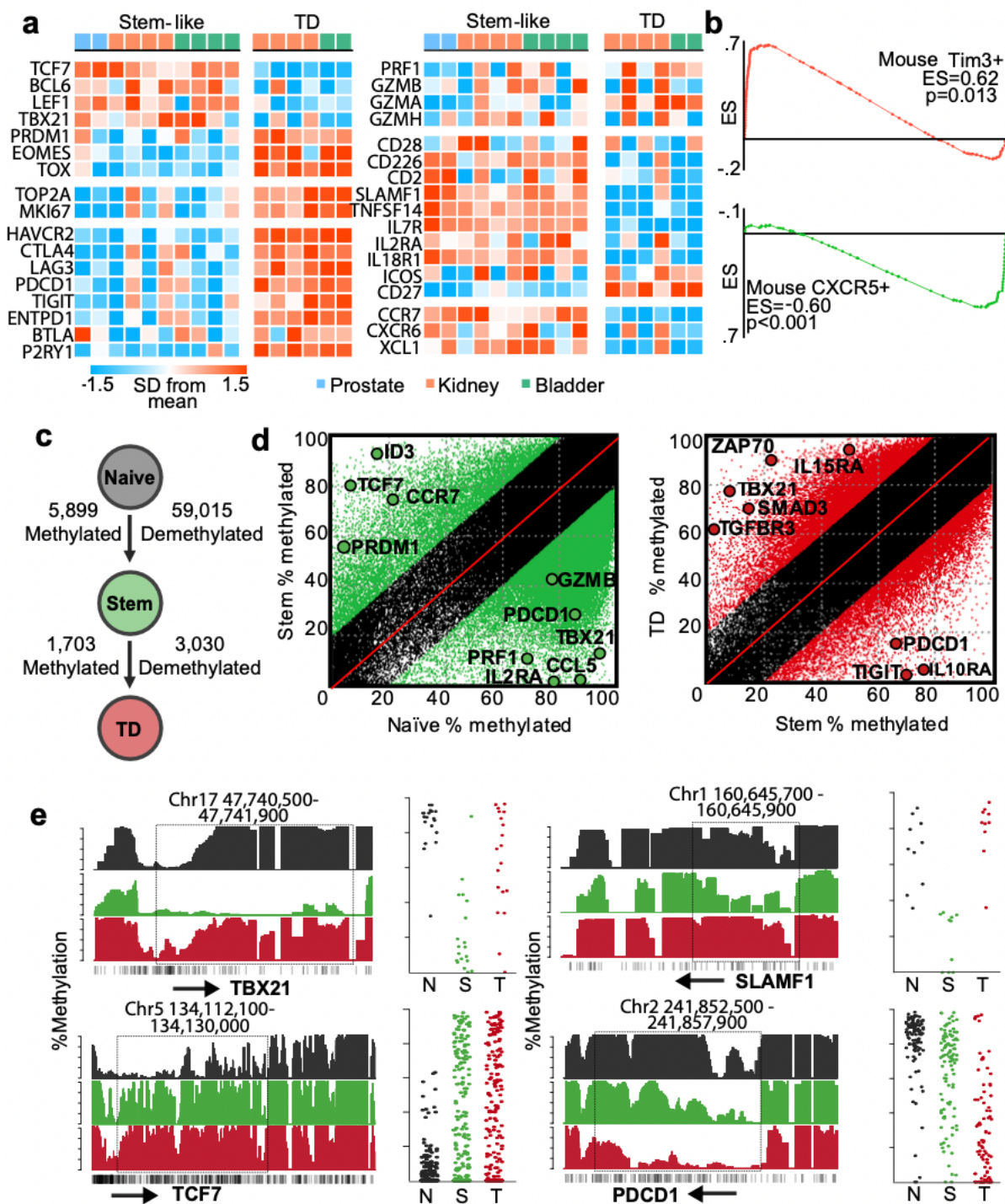


**Figure 2.6: Stem cell differentiation to the terminally differentiated state is associated with transcriptional and epigenetic changes.** a) Heatmap of transcription factors, proliferation related genes, checkpoint molecules, cytotoxic molecules, co-stimulatory molecules, survival genes, and migration and adhesion genes. Figure shows the z-scored data. b) GSEA comparison to mouse

CXCR5<sup>+</sup> and Tim3<sup>+</sup> subsets of CD8 T cells. Gene sets were created from CXCR5 stem-like and Tim3<sup>+</sup> exhausted CD8 subsets from LCMV. Plots show enrichment score against genes up-regulated (red) and downregulated (green) in mice. c) Summary of the number of epigenetic changes occurring as CD8 T cells undergo differentiation. Illustration shows the number of DNA methylation changes occurring as cells differentiate. d). Green regions show methylated and demethylated regions as cells transition from naïve to stem-like cells, and red shows these events as cells transition from stem-like to terminally differentiated. e) Specific epigenetic changes near important differentially expressed genes. Histograms show the total methylation from 0-100% in regions near important genes. Highlights show significantly differentially methylated regions. Dot-plots show the methylation of each CpG motif within this highlighted domain.

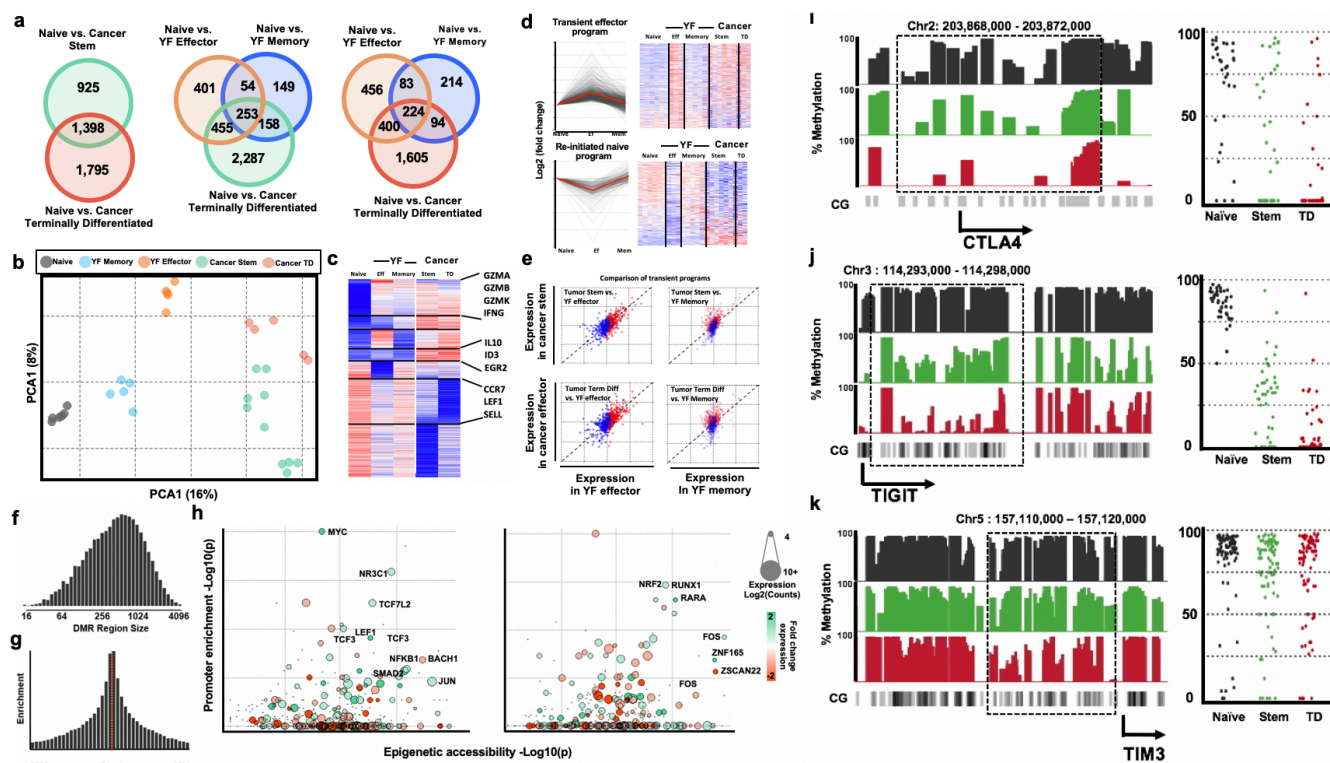


**Figure 2.7: Transcriptional and Epigenetic analysis of T cell subsets in tumors.** (a)

Comparison of differentially expressed genes between human cancer and viral specific CD8 T cell subsets. RNAseq from cancer subsets compared to RNAseq data collected from yellow fever (YF) antigen specific CD8s (GSE100745) during effector (14 days post-vaccination) and memory (4+ years post-vaccination) time points. The number of differentially expressed genes (DEG) vs. naive CD8 T cells was determined using DESeq2. Venn diagrams show number of DEG shared or unique between viral and cancer subsets. While the cancer subsets of T cells share many genes with the YF specific cells, there are also many distinct genes only expressed in cancer T cell subsets. (b) Principal component analysis of T cell subsets from cancer and viral specific CD8s, performed on genes that were differentially expressed in any group vs. naive cells. (c) DEGs were clustered using Cluster Affinity Search Technique (CAST). Clusters with greater than 5% of total genes are shown. Heat map shows z-score of averages of total genes from each group. (d) Comparison of cancer subsets

to transient effector programs found in YF specific T cells. Previously we have identified transient gene expression signatures that are expressed in YF-specific effector cells, but return to a naive state after antigen is cleared. These genes not expressed in memory or naive cells are highly expressed in both cancer subsets suggesting a similarity to an effector cell. (e) Pairwise comparison of transient effector program genes between effector and cancer subsets shows the relationship of this subset of genes re-initiated program (blue) and the transient effector program (red) compared between YF and cancer subsets. Dotted 45degree line represents equal fold change vs. a naive CD8 T cell in cancer and yellow fever cells. (f) GSEA and network analysis of pathways associated with differentiation. Gene set enrichment performed with GSEA and visualized with Cytoscape. The most significant networks are shown. Red indicates enrichment of nodes in terminally differentiated T cells, while blue shows enrichment in stem-like T cells. (g) Histogram shows the distribution of the continuous region size of DMRs. (h) Histograms show the relative frequency of DMRs within 10kb of transcription start sites. (i) Global changes in methylation. Violin plots show the distribution of total methylation within identified DMRs in naïve, stem-like, and terminally differentiated cells. (j) DMR patterns of differentiation. DMRs identified in Figure 2d were clustered using CAST. Box plots show the interquartile range and mean of DMRs in each cluster by cell type (k) Histograms show the total methylation from 0-100% in regions near important genes. Dot-plots show the methylation of each CpG motif within highlighted regions of interest. (l) Transcriptionally active transcription factors have over-represented binding in epigenetically modified regions of chromatin. Plots show the enrichment of transcription factor binding sites within differentially methylated regions in each cell type on the X-axis, and the Y-axis shows the enrichment of transcription factor binding sites within the promoters of differentially expressed genes. Color of dots represents the relative expression in stem-like (green) or terminally

differentiated (red) cells, and the size of the dot is proportional to total expression of the transcription factor.

previously described in murine chronic viral infection (LCMV)<sup>46</sup>. Gene set enrichment (GSEA) found that the genes expressed by tumor infiltrating populations were highly enriched with the analogous cell population described in LCMV (Figure 2.6 D). We compared these subsets to human effector and memory subsets, and both populations were much more similar to the effector cells than memory (Figure 2.7 A-E)<sup>86</sup>. These transcriptional data imply key functional differences between the TCF1<sup>+</sup> stem-like and Tim3<sup>+</sup> terminally differentiated T cell subsets within human tumors, and that these functions appear to be similar to what has been described in stem and terminally differentiated CD8 T cells in mice.

To understand how epigenetic mechanisms affect the different functions of these subsets, we performed whole genome DNA methylation analysis. As T cells underwent transition from naïve cells to the stem-like and terminally differentiated states, demethylation events outweighed methylation events approximately 9 to 1 (Figure 2.6 C-D, Figure 2.7 G-J). These epigenetic changes occurred near key genes involved in differentiation like *TCF7*, *TBX21*, *PDCDI* and many other checkpoint molecules (Figure 2.6 E, Figure 2.7 K) Together these data highlight that two key functional characteristics of T cells—proliferative potential and cell killing—are compartmentalized into two distinct populations, and these functions are tightly regulated by transcriptional and epigenetic mechanisms to ensure that cells perform as required.

#### *TCF1+ CD8 T cells reside in APC niches*

Our finding of a stem-like CD8 T cell population within the tumor, rather than in lymphoid tissue, is unexpected. In mouse models of chronic infection, analogous TCF1<sup>+</sup> stem-like T cells are found only in lymphoid tissue<sup>46, 67</sup>. Thus, having identified these stem-like cells in tumor tissue, we

reasoned that a lymphoid-like microenvironment within the tumor may support their survival in the tumor. We measured tumor-infiltrating antigen presenting cell (APC) populations (Figure 2.8 A). This revealed a highly significant correlation—across kidney, prostate and bladder tumors—between the presence of dendritic cells and the number of stem-like CD8 T cells in the tumor (Figure 2.8 B, Figure 2.9 H). Total macrophage percentage did not correlate with the presence of TCF1+ CD8 T cells or the number of CD8 T cells (Figure 2.8 B). We then used immunofluorescence staining to determine the spatial relationship between APCs and stem-like CD8 T cells (Figure 2.8 B, Figure 2.9 C-D). TCF1+ CD8 T cells were only found in regions with aggregations of MHC-II+ cells greater than 5 cells/10,000um<sup>2</sup> (Figure 2.8 E-F). In contrast, the TCF1- population was distributed across the tissue with no preference for APC dense zones (Figure 2.8 F). We expanded this analysis to large sections of tumor tissue and found that tumors had many regions with dense APC zones and the stem-like CD8 cells preferentially resided there (Figure 2.9 E-J). When we looked in prostate and bladder tumors, TCF1+ CD8 cells were also found in dense APC zones (Figure 2.8 G, Figure 2.9 K-L). Finally, we found a significant correlation ( $p < 0.05$ ,  $R^2 = 0.73$ ) between the number of TCF1+ CD8 T cells in a tumor and the proportion of the tumor with sufficient APC density to support stem-like cells (Figure 2.8 G). This suggests that APC dense regions serve as an intratumoral niche for stem-like CD8 T cells, which sustain the terminally differentiated T cell population and thus of the anti-tumor immune response.

We next assessed whether these antigen presenting niches were similar to tertiary lymphoid structures (TLS) previously described in other cancer types<sup>87, 88</sup>. These structures were macroscopically obvious on H&E in 5/33 patients, with densely packed mononuclear cells compartmentalized and usually found outside the tumor border (Figure 2.10 A-B). Presence of

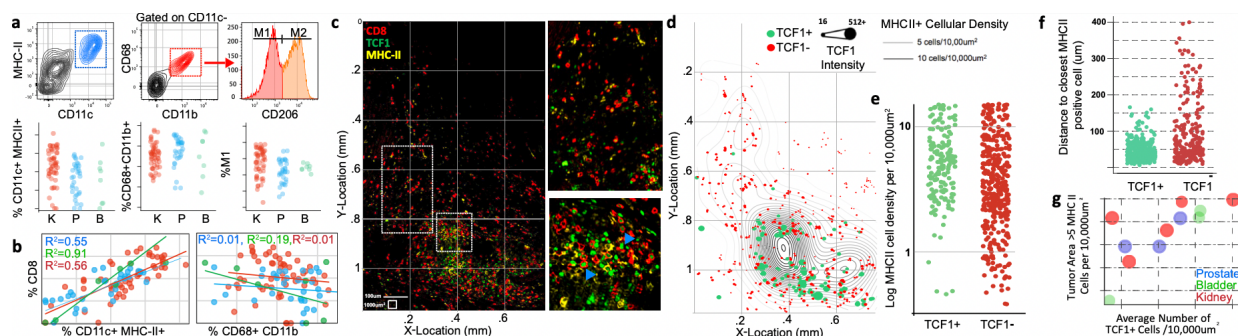


**Figure 2.8: Antigen presenting cells (APCs) form a supportive, intratumoral niche for TCF1+ stem-like CD8 T cells.** a) Identification of APC subsets in Kidney (red, n=53), Bladder (green, n=7), and Prostate tumors (blue, n=33). b) Correlation between CD8 T cells and APC populations. Percentage of total cells in the tumor that were CD8+ T cells and dendritic cells (CD11c+MHC-II+) or macrophages (CD68+CD11b+) was in patients from (a). Spearman correlation coefficient is shown. c) Immunofluorescence for MHC-II staining identifies APCs, while CD8 and TCF1 identify stem-like and terminally differentiated CD8 T cell populations in a representative kidney cancer patient. Insets show regions highlighted in the larger image. Blue arrows denote examples of TCF1+ CD8 T cells. d) Cellular spatial relationship map. After acquiring XY coordinates of MHC-II+ cells, MHC-II cellular density was calculated (number of MHC-II+ cells per 1000µm<sup>2</sup>). XY Location of CD8 T cells are overlaid with MHC-II density contour. CD8 cells were designated TCF1+/- using histo-cytometry (Extended Data Figure 6). e) MHC-II cellular density surrounding TCF1+/- subsets. MHC-II density at the corresponding XY coordinates of each CD8 T cell is shown. f) Distance between CD8 T cells and the closest MHC-II+ cell. g) Numerous regions of high MHC-II density correlates within increased number of TCF1+ cells in multiple tumor types. y-axis shows proportion of the tumor with MHC-II density >5 MHC-II+ cells/10,000µm<sup>2</sup>, with average number of TCF1+ CD8 T cells in the tumor on the x-axis.

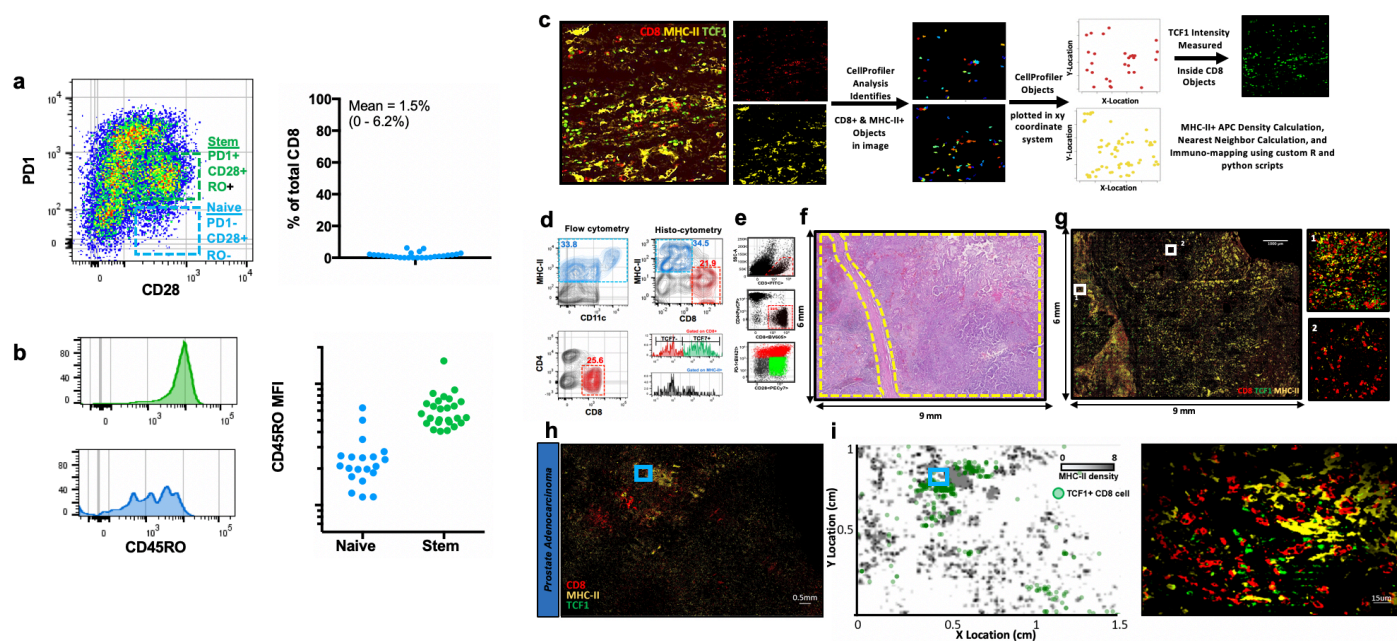


**Figure 2.9: Comparing flow cytometry and histo-cytometry methods for analysis of immune infiltrate in RCC.** (a) Flow cytometry data illustrating the number of naïve cells present intratumorally. Representative patient, left. Summary data, right. (b) Comparative amounts of CD45RO expression on naïve and stem like intratumoral CD8 T-cells. (c) Workflow for immunofluorescence imaging analysis and immuno-map creation. Single channel immunofluorescence images are imported into CellProfiler. CD8+ and MHC-II+ objects are identified in the respective channel images. The XY location of each CD8+ and MHC-II+ object is exported. The TCF1 staining intensity is measured inside the CD8+ objects. These parameters are used to calculate MHC-II+ density, measure the distance from each CD8+ object to its nearest MHC-II+ neighbor, and to finally create immuno-maps for immunofluorescence images. (d) Histo-cytometric analysis of tumor infiltrating immune populations. Location and fluorescence intensity of CD8+ and MHC-II+ cells were determined using CellProfiler. After image compensation, CD8+ and MHC-II+ cells were gated. TCF1 intensity of each cell is shown on histograms for each population below. Comparison of flow cytometry data from the same patient

sample is also shown. (e) Kidney cancer patients with high CD8 infiltration determined by flow cytometry. Patients that were determined to have high CD8 infiltration by flow cytometry were selected for analysis by immunofluorescence. (f) Hematoxylin/eosin stains of human kidney tumor. Selected slides from human kidney tumor shown in part (e) to be highly infiltrated by T cells. Regions of tumor tissue are highlighted in yellow. (g) Immunofluorescence imaging of kidney tumor. Selected tumors shown to be highly infiltrated by T cells. Tumor section was stained for MHC-II to identify antigen presenting cells, and CD8 and TCF1 to identify stem-like and terminally differentiated CD8 T cell populations. Insets shows zoomed regions highlighted in the larger image. (h) Dendritic cells populations, stem-like, and terminally differentiated CD8 T cells in three representative kidney cancer patients. (i) Cellular spatial relationship map (middle) analysis and construction conducted as in Figure 3e. (j) CD8 expression of TCF1 preferentially occurs in dense APC zones. Amount of TCF1 expressed in each CD8 T cell graphed against the density of MHC-II around each T cell (MHC-II+ cells/10,000um<sup>2</sup>). (k and l) TCF1+ CD8 T cells are localized near dense MHC-II regions in other cancers. Prostate and bladder tumors were imaged for CD8, MHCII and TCF1. Shown in (l) are regions of dense MHC-II aggregates in grey and the location of TCF1+ CD8 T cells in green.

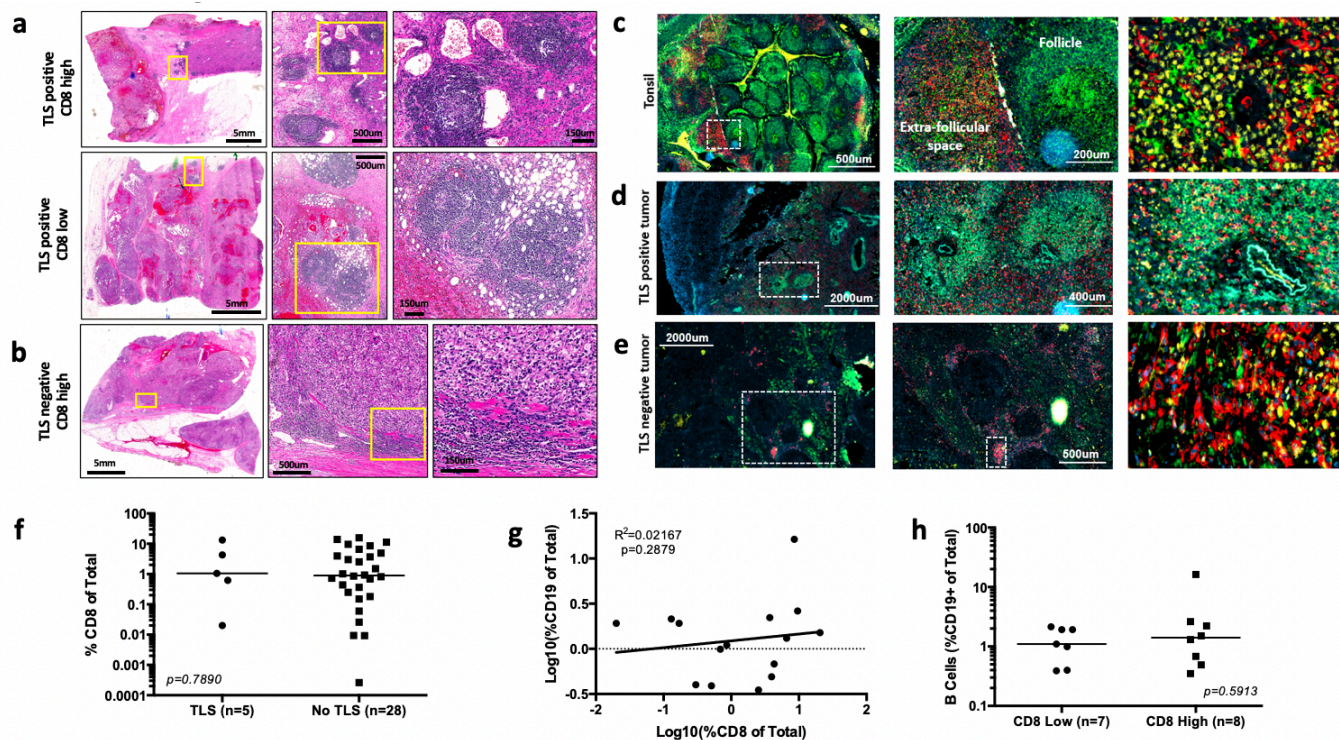


**Figure 2.10: Comparison of tertiary lymphoid structures and intratumoral antigen presenting niches in RCC tumor samples.**

(a) H&E slides highlighting tertiary lymphoid structures (TLS) in kidney tumors with high (top) and low (bottom) CD8 T cell infiltration. Yellow boxes highlight areas shown in zoomed insets. (b) H&E slide showing dense immune infiltration in a tumor with high CD8 T cell infiltration but lacking presence of TLS. Yellow boxes highlight areas shown in zoomed insets. (c) Immunofluorescence staining illustrating organizational structure of human tonsil. CD8 staining is shown in red, MHC-II in green, TCF1 in yellow, and DAPI (nuclei) in blue. White box highlights zoomed area shown in inset. Follicle and extrafollicular space shown as labeled. T cell zone shown in rightmost panel. (d) Immunofluorescence staining illustrating tumor TLS. CD8 staining is shown in red, MHC-II staining in green, and DAPI staining of nuclei in blue. White box highlights zoomed area shown in inset. Follicle and extrafollicular space shown as labeled. (e) Immunofluorescence staining illustrating dense immune infiltration in TLS negative kidney tumor. CD8 staining is shown in red, MHC-II staining in green, and DAPI staining of nuclei in blue. White box highlights zoomed area shown in inset. Follicle and extrafollicular space shown as labeled. (f) Scatter plot showing the relationship between the presence of TLS and the percentage of CD8 cells. (g) Scatter plot showing the relationship between the percentage of CD8 cells and the percentage of CD19 cells. (h) Scatter plot showing the relationship between the percentage of CD8 cells and the percentage of CD19+ B cells.

MHC-II in green, TCF1 in yellow, and DAPI in blue. White box highlights zoomed area shown in inset. Follicle and extrafollicular space shown as labeled. (f) There is no significant difference in CD8 T cell infiltration between kidney tumors with and without TLS. CD8 T cell infiltration measured by flow cytometry and shown as % CD8<sup>+</sup> of total cells. Statistical analysis resultant from Mann Whitney test is shown. (g) Lack of correlation between proportion of CD8 T cells and CD19<sup>+</sup> B cells in tumors. Linear regression results  $p = 0.6006$  with  $R^2=0.02167$ . (h) There is no significant difference in B cell infiltration between tumors with high or low CD8 T cell infiltration. B cell infiltration is shown as the %CD19<sup>+</sup> B cells of total cells. Statistical analysis resultant from Mann Whitney test is shown.

TLS did not correlate with CD8 T cell infiltration (Figure 2.10 F-H). By immunofluorescence, TLS were predominantly very densely packed MHC-II+ cells, interspersed with few CD8 T cells (Figure 2.10 D). Upon comparison to human tonsil tissue, these TLS much more closely resembled B-cell follicles, which is consistent with several other reports (Figure. 2.10 C-D)<sup>87-89</sup>. In comparison, the antigen-presenting niches populated by TCF1+ CD8 T cells were predominantly found inside the stromal barrier of the tumor (Figure 2.10 C). Interestingly, TCF1+ CD8 T cell containing these nests closely resembled the extrafollicular regions of lymphoid tissue where T cells reside—moderately densely arranged APCs packed with many TCF1+ CD8 T cells (Figure 2.10 C, E). In addition, we found a significantly higher level of blood and lymphatic endothelial cells (CD31+PDPN-, CD31+PDPN+, respectively) in tumors with CD8 infiltration, and these vessels were often closely associated with dense regions of T cell infiltration (Figure 2.11). Together these findings highlight key features of the CD8 T cell response to cancer. Regions exist in tumors that resemble a T cell zone of lymphatic tissue. These regions contain the TCF1+ CD8 T cells which seem to only reside in close proximity to APCs, and the generation of these immune niches is correlated to lymphatic and blood vessel infiltration into the tumor.

#### *Loss of APC niche during immune escape*

We next examined how the immune niche differs between patients with controlled disease after surgery compared to those whose tumors escaped immune control and rapidly progressed. We imaged large regions of tumor tissue from 26 kidney cancer patients at the time of surgery to understand how the presence of immune niches in the tumor might correlate with disease progression (see figure 2.12 A for patient characteristics). Immunofluorescence quantification of CD8 T cells tightly correlated with flow cytometry quantification of CD8 T cell infiltration (Figure

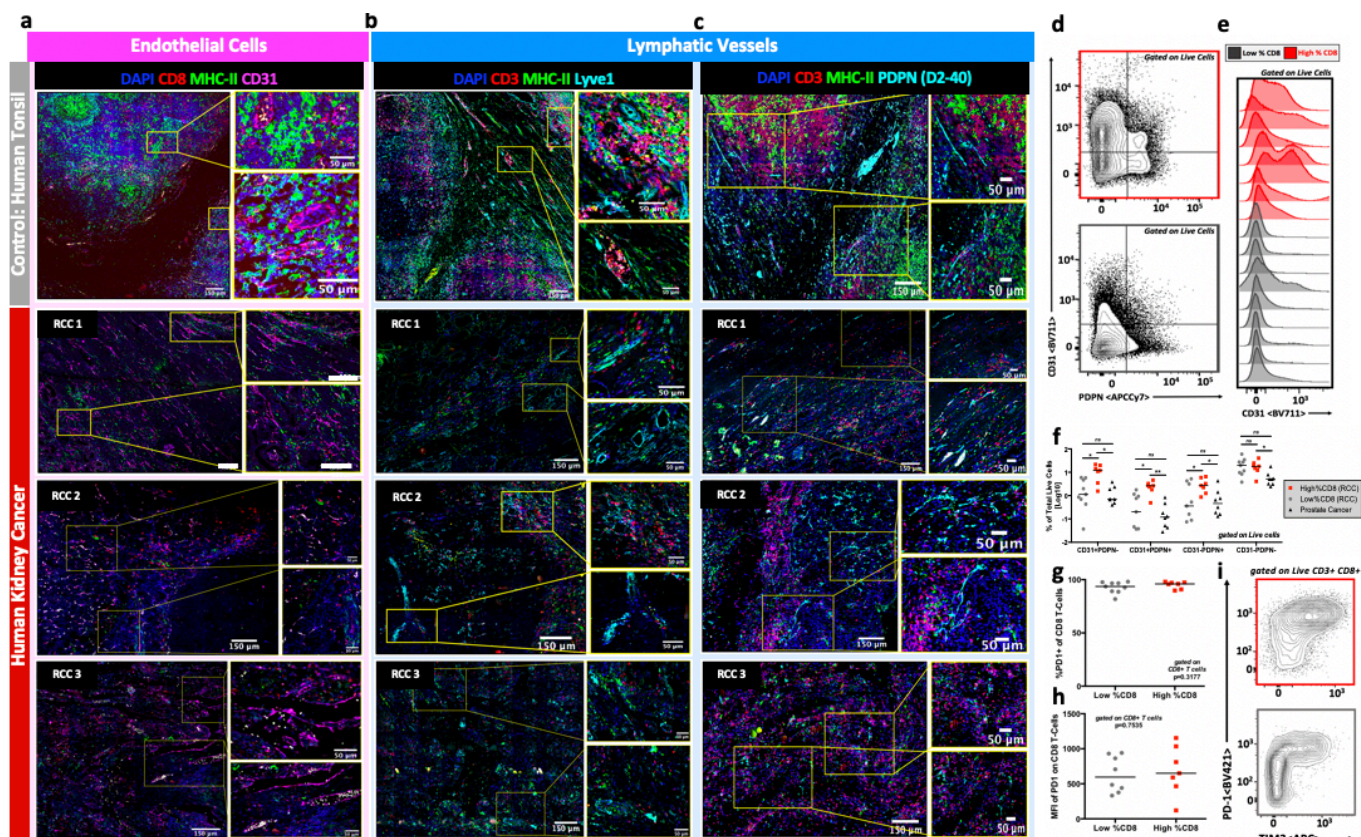


**Figure 2.11: Highly infiltrated kidney tumors are well vascularized and contain lymphatic vessels.** (a) Immunofluorescence staining of human tonsil and highly T cell infiltrated human kidney tumors showing tissue vascularization. Formalin fixed paraffin embedded tissue was stained for CD8 (T cells), MHC-II (antigen presenting cells, CD31 (endothelial cells), and DAPI (nuclei). (b and c) Immunofluorescence staining of human tonsil and highly T cell infiltrated kidney tumors showing presence of lymphatics via Lyve1 (b) and Podoplanin/D2-40 (c). Formalin fixed paraffin embedded tissue was stained for CD3 (T cells), MHC-II (antigen presenting cells, Lyve 1 or Podoplanin/D2-40 (lymphatics), and DAPI (nuclei). (d) Flow cytometry analysis shows tumor vascularization in highly (red) and poorly (gray) infiltrated kidney tumor. Tumors were stained using antibodies listed in table 2.1, collected on a Becton-Dickinson LSR-II, and analyzed using FlowJo. (e) Histogram of flow cytometry analysis showing increased CD31 staining in highly T cell infiltrated kidney tumors (red) as compared to poorly infiltrated tumors (gray).

Analysis completed as described in D. (f) Summary data of flow cytometry analysis showing differences in vascularization between highly (red) and poorly (gray) T cell infiltrated kidney tumors and prostate tumors (black). Analysis completed as described in D. (g and h) Tumor infiltrating T cells are PD1+. Flow cytometry analysis showing T cells infiltrating kidney tumors shown. In parts (d-f) are PD1+, suggesting the cells are not naïve and present due to blood contamination (g) and showing that the MFI of PD1 on tumor infiltrating T cells is not significantly different between highly (red) and poorly (gray) infiltrated tumors. (i) Representative flow cytometry plots showing PD1 and Tim3 expression on tumor infiltrated T cells in highly (red) and poorly (gray) infiltrated tumors. Populations shown are gated on live, CD3+ CD8+ cells.

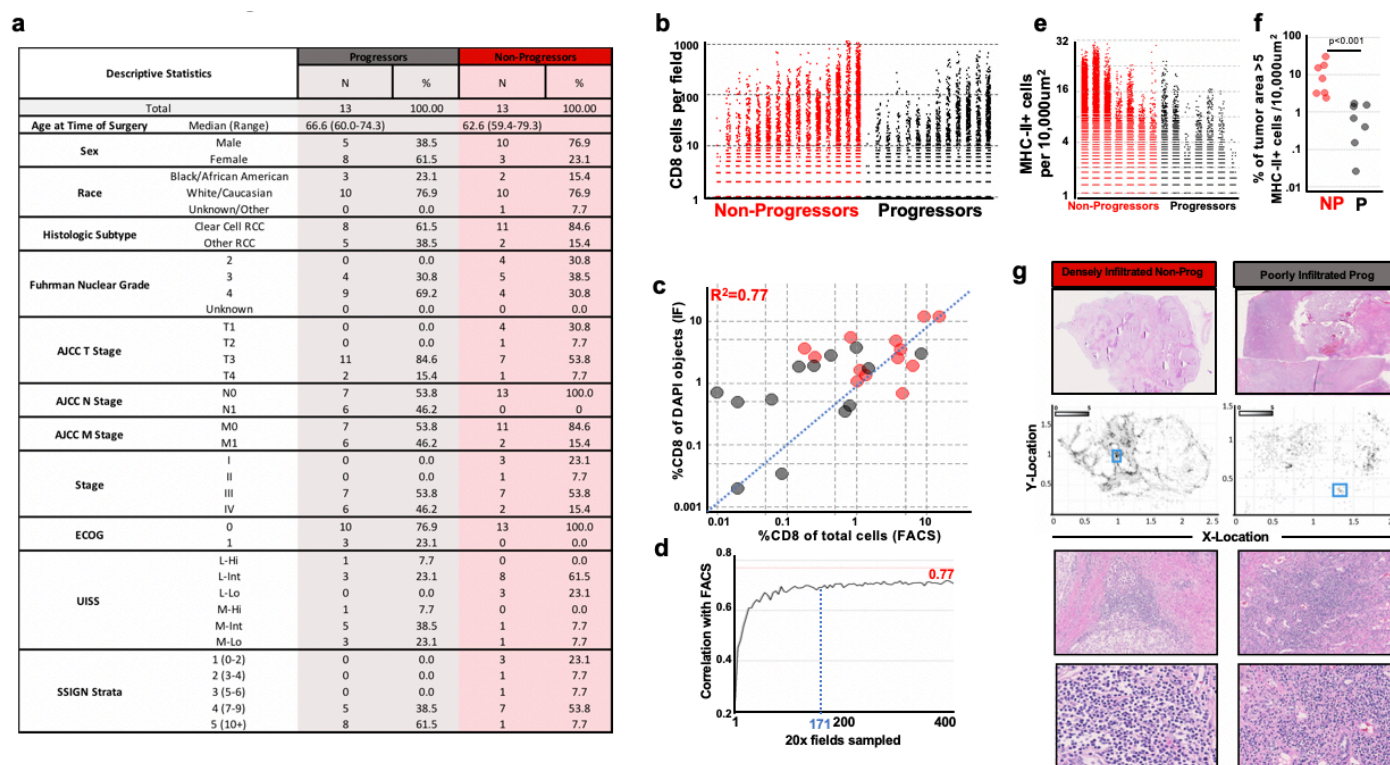


**Figure 2.12: Clinical features and clinical association of clinical outcomes with imaging-based assessment of tumor immune infiltrate.** (a) Descriptive table enumerating patient characteristic for kidney cancer patients with and without progressive disease. (b) Comparison of the number of CD8+ cells per 300um x 300um field in patients with and without progressive disease. The number of CD8+ cells per 300um x 300um field were enumerated using the methods outlined in Supplementary Figure 7. (c) The correlation between enumeration of CD8 T cells by flow cytometry and by immunofluorescence. On the x axis, CD8 T cells are measured as a proportion of total cells. On the y axis, CD8 T cells are measured as a proportion of total DAPI objects detected in the tumor section. (d) Estimated number of 20x fields of view necessary to obtain an accurate assessment of level of CD8 T cell infiltration is 171 fields of view. Increasing number of random fields of view were sampled from images and the percent of cells that were CD8 positive by IF correlated to FACS from the corresponding sample. (e) Histological comparison of kidney cancer patients shown in figure 4 – a kidney cancer patient with dense T cell

infiltration and no disease progression (red, left) and a kidney cancer patient with poor T cell infiltration and progressive disease (gray, right). (f) Comparison of the number of MHC-II+ cells per 300um x 300um field in stage III (T3N0M0) patients with and without progressive disease. The number of MHC-II+ cells per 300um x 300um field were enumerated using the methods outlined in Supplementary Figure 7. (g) Comparison of the proportion of tumor area with greater than 5 MHC-II+ cells per 10,000um<sup>2</sup> between stage III (T3N0M0) patients with and without progressive disease. Statistical analysis resultant from Mann Whitney test is shown. (h) There is no significant difference in number of fields of view sampled between patients with and without progressive disease. (i) Density of MHC-II+ APCs and CD8 T cells in densely (left) or poorly (right) infiltrated kidney tumors. x-axis shows the number of CD8+ cells/10,000um<sup>2</sup>. y-axis shows the number of MHC-II+ cells/10,000um<sup>2</sup>. Regions of predominantly MHC-II+ cells are highlighted in yellow, regions of predominantly CD8+ cells in red, and regions of shared MHC-II+ cells and CD8+ cells in green.

2.12 B-C). Across ~100,000 20x fields of view in these 26 samples, regardless of the level of CD8 infiltration in the patient, we could generally identify a few dense regions of MHC-II where TCF1+ CD8 T cells resided (Figure 2.13 A-D). Most importantly, patients with controlled disease had significantly more of these dense regions (Figure 2.13 E-F). Upon stratifying patients above or below the median MHC-II density, we found that patients with low MHC-II+ cell density experience significantly impaired progression free survival (Figure 2.14 G,  $p=0.04$ , HR= 3.157). These factors were independent of PDL1 expression in the tumor, which had no correlation to the level of CD8 or survival of patients (Figure 2.14). Importantly, when we specifically studied patients with stage III disease, ~50% of whom progress after surgery, there were >10 fold fewer immune niches in patients who progressed (Figure 2.12 E-G). Patients with progressive disease also had lower proportions of MHC-II+ dense, CD8+ dense, and shared MHC-II+ and CD8+ dense regions in their tumor (Figure 2.13 H-I, Figure 2.12 H-I), suggesting that for tumors to evade destruction by CD8 T cells, they must either prevent formation of intratumoral immune niches or find ways to destroy them.

## **2.5 Discussion.**

In this study, we sought to understand the mechanisms controlling CD8 T-cell infiltration into human tumors. We found tumor infiltrating T cells are comprised of two functionally distinct subsets, a TCF1+ stem-like CD8 T cell population, and their progeny, a clonally related terminally differentiated population that express high levels of checkpoint molecules. These terminally differentiated cells fit the traditional definition of an exhausted CD8 T-cell; they do not proliferate in response to re-stimulation and express high levels of checkpoint molecules. However, the presence of this terminally differentiated cell population positively correlates with total number of

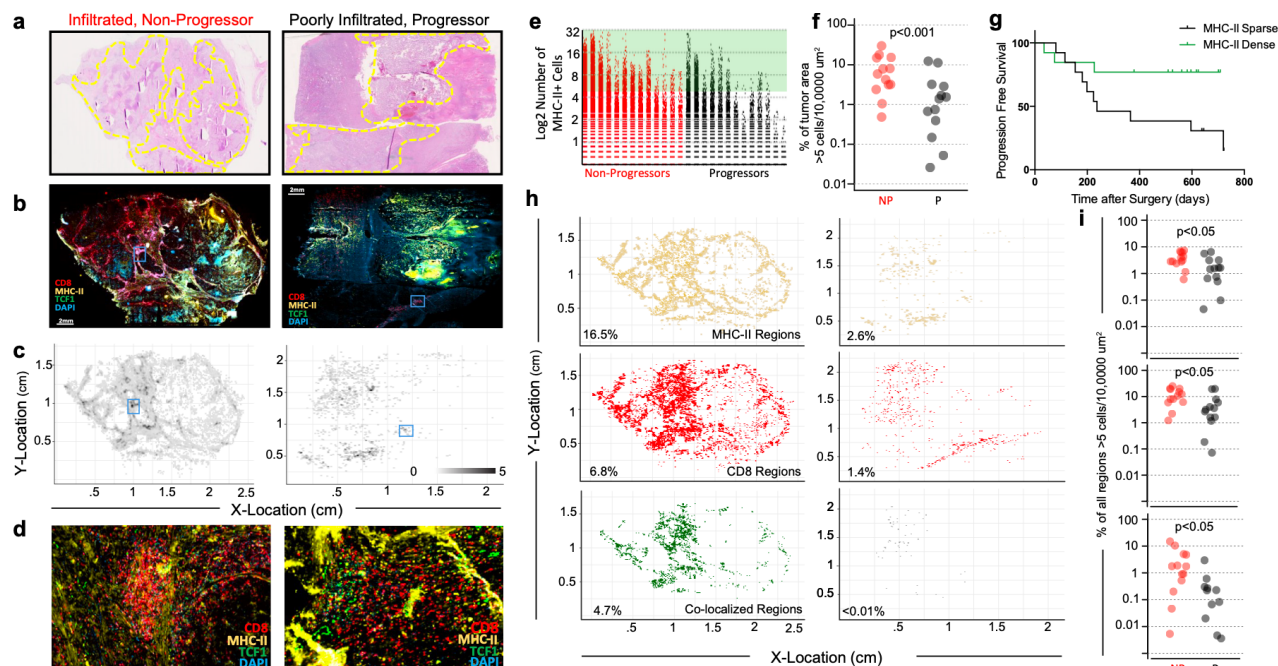


**Figure 2.13: Loss of APC niche is associated with impaired CD8 T cell response and disease progression.** a-d) Patients with dense T cell infiltration and no disease progression (red, left) and one with poor T cell infiltration and progressive disease (gray, right). a) H&E whole slide images. Tumor is outlined in yellow. b) Whole slide immunofluorescence images. MHC-II (yellow), TCF1 (green), CD8 (red) and DAPI (blue) c) Immunomap of APC density in tumors from (b) constructed as in Figure 3 & Extended Data Figure 7. d) Insets show highlighted regions from (b & c), illustrating regions of high MHC-II+ density and stem-like T cell infiltration in kidney tumors. e) Comparison of the number of MHC-II+ cells per 300um x 300um field in patients with (n=13) and without (n=13) progressive disease. f) Comparison of the proportion of tumor area with >5 MHC-II+ cells/10,000um<sup>2</sup> between patients with and without progressive disease. Mann Whitney test result is shown. g) Patients with high MHC-II+ cell density had improved progression free survival. Log-rank statistical analysis yields p=0.04 & HR=3.226. h) Immunomaps illustrating regions of MHC-II+ cell density (yellow), CD8+ cell density (red), or shared density (green) in tumors from (h). i) From top to bottom: Patients without progressive disease have more areas

where the density of MHC-II+ cells (i), CD8+ cells (ii), or both MHC-II+ cells and CD8+ cells (iii) exceeds 5 cells/10,000 $\mu\text{m}^2$ .

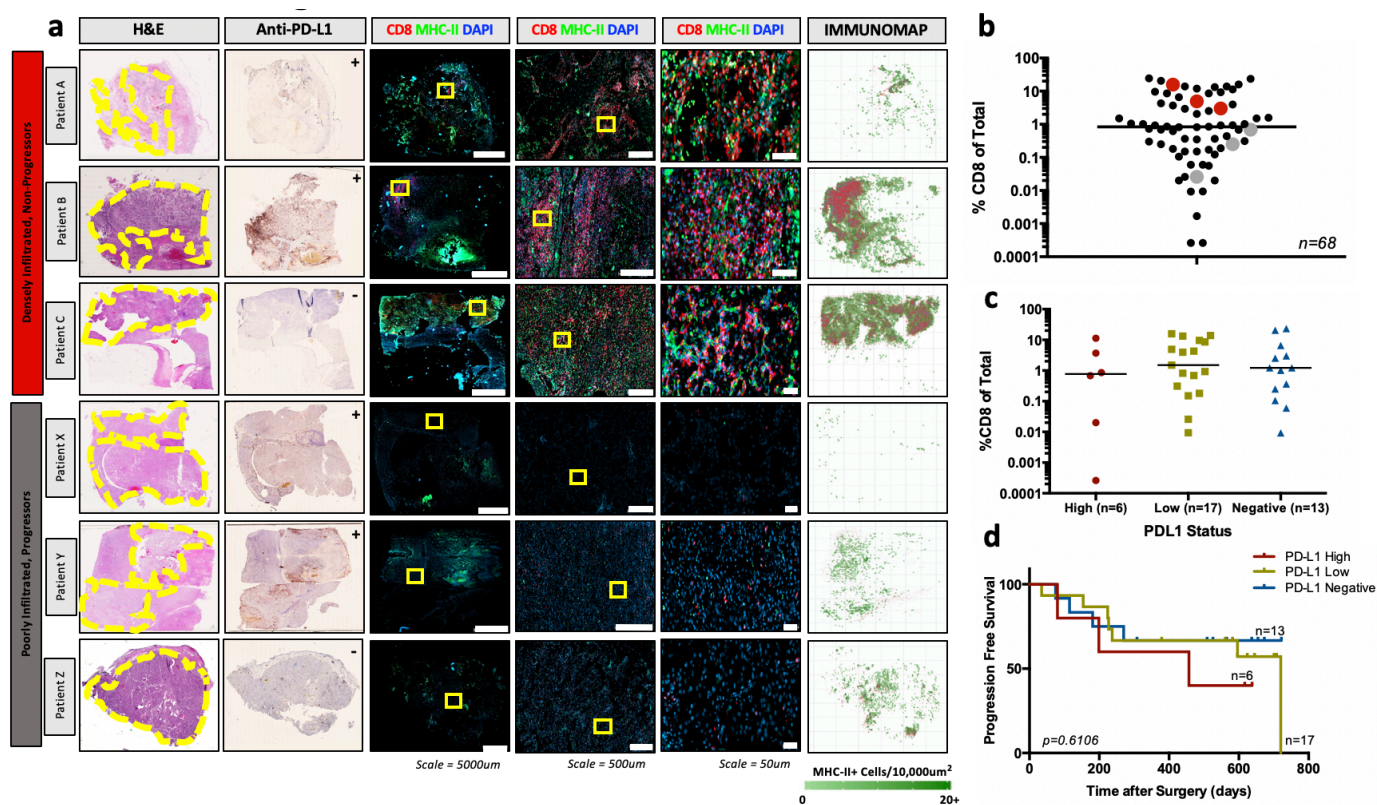


**Figure 2.14: PDL1 status is not associated with CD8 T cell infiltration in human RCC tumor**

**samples.** (a) Representative patients with densely infiltrated and poorly infiltrated kidney tumors whose disease has not progressed or has progressed, respectively. Whole slide scans are shown for H&E, anti-PD-L1, and immunofluorescence (CD8, MHC-II, DAPI) stains, with zoomed insets of immunofluorescence data. Yellow circles highlight the location of tumor tissue on the H&E slide. Yellow boxes highlight the areas shown in the zoomed insets of immunofluorescence images. Immunofluorescence data is quantitatively analyzed and mapped to show the density of MHC-II+ cells and the x-y location of CD8+ T cells in the rightmost panel. Anti-PD-L1 scans are marked as ++ (positive-high), + (positive-low), or - (negative), as scored by board-certified pathologists. (b) Patients in (A) are highlighted in red (highly infiltrated, non-progressors) and gray (poorly infiltrated, progressors) to show the %CD8 T cell infiltration by flow cytometry. (c) PD-L1 staining was scored by board-certified pathologists as positive-high, positive-low, and negative. There is no significant difference between the percent CD8 T cell infiltration amongst these

categories by ANOVA with Holm-Sidak correction. (d) Progression free survival for patients with positive-high (PD-L1 High), positive-low (PD-L1 Low), and negative (PD-L1 negative) kidney tumors. There is no significant difference in progression free survival between the groups by Mantel-Cox Logrank test ( $p=0.6106$ ) or by Logrank test for trend ( $p=0.3374$ ).

tumor infiltrating T cells and protection from disease progression. These observations are not well explained by a model of T-cell exhaustion where continuous antigen exposure leads to accumulation of checkpoint molecules, resulting in a decline of the T-cell response. Based on the functional characteristics we defined in these two cell populations and on the clonal relationship between stem-like and terminally differentiated cells, we propose that the stem-like CD8 T-cell acts as a precursor to generate a terminally differentiated effector population, which is in agreement with other recent studies<sup>44, 45, 47, 48, 68, 84</sup>. In this model, the stem-like cells require a region within the tumor that resembles the T-cell zone of secondary lymphatic tissues, made up of dense areas of antigen presenting cells. An unanswered question in this model is how stem-like CD8s originate in the tumor. Recent work by others have found that CD8 T-cells in tissue draining lymph nodes are transcriptionally and phenotypically similar to the stem-like CD8 T-cell described chronic LCMV infection, suggesting this may be the source of the stem-like cells in tumors<sup>90</sup>.

Based on this model, we propose that the decline of the T-cell response in human cancer is not caused by accumulation of checkpoint-expressing exhausted CD8 T-cells, or over-expression of PDL1 in the tumor, but by the failure of stem-like CD8 T cells to be sufficiently stimulated by an antigen presenting cell niche to continuously produce terminally differentiated CD8 T-cells in the tumor. Furthermore, the scarcity of these niches in tumors that rapidly progress after surgery suggests that tumors may be interfering with the formation or continued maintenance of immune niches and that this may be a novel mechanism of immune evasion requiring further investigation.

## **2.6 Materials & Methods.**

**Sample Collection, Preparation, and Storage:** Patients were recruited in accordance with an

approved IRB protocol, and all patients provided informed consent. Patient tumor samples were collected immediately after undergoing partial or radical nephrectomy or prostatectomy or undergoing transurethral resection of a bladder tumor (TURBT). Samples for flow cytometric analysis were harvested in Hank's Balanced Salt Solution, minced into small pieces, digested using Liberase enzyme cocktail, and homogenized using a MACS Dissociator. Single cell suspensions were obtained, RBC ACK lysed, and stored at  $-80^{\circ}\text{C}$  in freezing media for batch analysis. Samples for immunofluorescence analysis were formaldehyde fixed and embedded in paraffin blocks by Emory Pathology. Unstained and hematoxylin/eosin-stained sections of FFPE blocks were obtained from Emory Pathology.

**Statistical analysis:** Patients were selected to have at minimum 365 days of follow up. Follow up time was calculated as the number of days from the date of surgery to an event or to censorship. Progression and death were classified as events. Patients who had not progressed or are not deceased were censored, and the number of days is calculated from the date of surgery to May 9, 2018. Statistical analysis was conducted using GraphPad Prism or using SAS Version 9.4 and SAS macros developed by the Biostatistics and Bioinformatics Shared Resource at Winship Cancer Institute. The significance level was set at  $p < 0.05$ . Descriptive statistics for each variable were reported. The univariate association with %CD8 was carried out by ANOVA/Kruskal Wallis test for categorical covariates and by Pearson correlation coefficient for numerical covariates. The univariate association of each covariate with PFS was tested by proportional hazard model with hazard ratio and its 95% confidence interval being reported. We examined a possible non-linear relationship between a continuous %CD8 and PFS through a martingale residual plot and identified an optimal cutoff value of %CD8 that maximizes the separation between the two groups by a bias

adjusted log rank test<sup>91, 92</sup>. The method enables the estimation and evaluation of the significance of the cutoff value and also is adjusted for the bias created by the data driven searching process. The optimal cutoff value was found to be 2.2% (Figure 2.1 B-C). Using this same 2.2% cutoff for CD8 infiltration in patients with more aggressive, non-metastatic disease (T3N0M0), less CD8 T cell infiltration predicted a 6-fold more rapid progression (Figure 2.1 D). CD8 T cell infiltration also significantly predicted progression amongst patients categorized as high-risk by a conventional prognostic scoring system (SSIGN) (Figure 2.1 E).

**Flow Cytometry:** Single cell suspensions from human tumors were stained with antibodies listed in Table 2.1. Live/dead discrimination was performed using fixable Near-IR Dead Cell Stain Kit (Invitrogen). Samples were acquired with a Becton-Dickinson LSRII and analyzed using FlowJo. For intracellular staining, cells were fixed and permeabilized using the FOXP3 Transcription Factor Staining Buffer Set (eBioscience).

**Proliferation assays:** CD8 T-cells subsets were sorted from tumors and labeled with Cell trace violet (Thermo) according to manufacturer's instruction. Cells were incubated with anti-CD3/anti-CD28 T cell activation beads (Miltenyi) at a ratio of 1 bead to 2 T-cells in U-bottom plates. Ten U/ml of human IL2 (Peprotech) was included in culture media (RPMI + 10% FBS). After 4 days, cells were analyzed by flow cytometry for proliferation and expression of various proteins. Proliferation index was assessed using FlowJo.

***In vitro* assays:** Stem-like and terminally differentiated CD8 T-cells were sorted from human tumors and incubated with T-cell culture media (RPMI + 10%FBS) supplemented with human IL-

2 (10 IU/ml) in U-bottom plates. After 3 days, cells were analyzed by flow cytometry for expression of various proteins.

**TCR Sequencing:** Single cell suspensions from human tumors were stained with antibodies listed in Table 2.1. Live/dead discrimination was performed using fixable Near-IR Dead Cell Stain Kit (Invitrogen). Populations of interest were isolated using a Becton-Dickinson FACS Aria II Cell Sorter. Gating is shown in Figure 2.5 A & C. DNA was isolated using a Qiagen AllPrep DNA/RNA Micro Isolation Kit. TCR sequencing was performed by Adaptive Biotechnologies Immunoseq technologies. TCR Sequencing analysis was performed using custom R scripts. The number of TCRs detected and degree of overlap detected was highly subject to the number of cells collected, highlighting the need to sufficiently sample the pools of cells to accurately understand the clonal relationship between them (Figure 2.5 E-F).

To determine if there was significant overlap between populations, we first calculated the contamination of each population with the other so we could determine if overlap in TCRs could be explained by the contamination rate. To determine the overlap between the stem and terminally differentiated cells due to biological and technical variance, flow cytometry data was fit using an EM mixing model<sup>93</sup>. The characteristics of these fitted models are shown in Figure 2.5 B. Shown on the plot are 80% and 95% confidence intervals for each population and the approximate position of gates used to sort populations. We then placed gates where we had for the sort and asked the question of what proportion of the cells in that gate were derived from the target and contaminating population. This contamination rate is highly subject to the ratio of the two populations. In our 2 most extreme patients shown in E, if 93% of the cells are the stem-like population, the

contamination rate in the TD population is as high as 14%.

Figure 2.5 B shows how the purity changes as the ratio of stem to terminally differentiated cells changes. The two most extreme samples are highlighted on the figure to show what the inferred proportion of each population is in the sorted cells. In addition, we added 5% to this number for each sample to account for additional contamination from the sorting procedure. The summary of this analysis is included in Figure 2.5 H.

To identify significance of TCR overlap we used the purity calculated for each patent we tested if

$$P(X \leq 10) = \sum_{i=0}^{10} \binom{1000}{i} 0.01^i \cdot (1 - 0.01)^{1000-i}$$

the relative frequency of each TCR could be explained by contamination. For each specific TCR that was detected in both populations, we tested two hypotheses. Firstly, can the number of a particular TCR in the stem-like population be accounted for by contamination from the TD cell population, and conversely, can the same TCR in the TD population be accounted for by contamination from the stem-like population. This was achieved by assuming each TCR detected in a sample was a Bernoulli trial with a probability of occurring equal to the expected frequency of the TCR due to contamination. For example, we assumed that if a TCR was found at a frequency of 10% in the stem population, and the inferred overlap into the TD was 10%, it would contaminate the terminally differentiated cells at a frequency of 1%. If we collected 1000 total TCRs for a particular sample, and detected 10 of this specific TCR, the probability of detecting at least this many TCRs due to this 1% contamination rate would be given by:

The general formula for testing if the overlap in the terminally differentiated population is caused by contamination from the stem-like cells is given by:

$$P(X \leq k) = \sum_{i=0}^k \binom{n}{i} p^i (1-p)^{(n-i)}$$

Where:

k = number of the specific TCR detected in the terminally differentiated population

p = frequency of the specific TCR in the stem population x contamination rate

n = total number of TCRs detected in a sample

We applied this analysis to every TCR collected that had overlap detected and tested the converse hypothesis that the fraction of stem-like TCRs detected could be accounted for by contamination from the terminally differentiated cells. If both tests were under 0.05, we rejected their hypothesis that the overlap was caused by contamination. Figure 1L highlights the proportion of TCRs in each sample that meet these criteria. The supplementary table (Figure 2.5 H) provided has these values used for every TCR and the p-value calculated.

To identify significance of TCR overlap we assumed 90% purity and conducted a Fisher Exact test to test the hypothesis that the TCR overlap we detected could be explained by this contamination rate. To determine the probability that an overlap could have been detected given the number of cells recovered, we fit an exponential distribution of the observed stem- and effector- TCR clone frequency (Shown in Figure 2.5 B). We then used a bootstrapping approach to

randomly sample the same number of TCRs from these two distributions as cells we had collected. We repeated this 1000 times. If a 20% overlap was not detected at least 80% of the time, the sample was considered underpowered to detect an overlap. Analysis of the TCRs found that the TCR repertoires showed a high degree of immunodominance, where the ten most dominant clones account for 55% of the terminally differentiated repertoire and for 31% of the stem-like repertoire, indicating an expansion against a narrow range of antigens in the tumors (Figure 2.5 D).

**RNA sequencing and analysis:** RNA was isolated from FACS sorted cells using QIAGEN All-prep kit. RNA was prepared using Contech SmartSeq2 (Bladder samples) or Nugen Ovation (Prostate, Kidney samples) library prep kits. Prostate and Kidney samples were sequenced at HudsonAlpha on a HiSeq25000, Bladder samples were sequenced at the Emory Yerkes Genomics Core on a HiSeq1000. Data was normalized and differential expression of genes identified using DESeq2<sup>94</sup>. Raw fastq files and analysis of RNAseq is uploaded to GEO under identifier GSE140430.

**DNA-methylation analysis:** Whole genome DNA methylation was performed using the Illumina TruSeq DNA Methylation Kit. Sequence data was aligned using Bismark<sup>95</sup>, and data was analyzed using custom R and Python scripts which are available upon request. Briefly, individual significantly differentially methylated CpG motifs were identified by Fisher exact test. Continuous regions of differentially methylated CpGs were identified by finding regions were at least 6 out of 10 CpGs in a continuous stretch were differentially methylated. These regions were then collapsed and analyzed as single ‘differentially methylated regions’ (DMRs). Differentially expressed regions were identified as those that had a p value less than  $1 \times 10^{-4}$  by fisher exact test and were at

least 20% different to the comparison sample. Transcription factor binding enrichment analysis was also conducted, identifying TCF4, TCF7L2, and MYC as enriched in the stem-like cells and E2F, NRF2, and SP1 in the terminally differentiated cells (Figure 2.7 L). Whole genome DNA methylation data is uploaded to GEO under identifier GSE140430.

**Deparaffinization & Antigen Retrieval:** Sections were deparaffinized in successive incubations with xylene and decreasing concentrations (100, 95, 75, 50, 0%) of ethanol. Antigen retrieval was achieved using either (a) Abcam 100x Citrate Antigen Retrieval Buffer (pH=6.00) for 20 minutes at 100°C, followed by 20 minutes at ambient temperature or (b) Abcam 100x TrisEDTA Antigen Retrieval Buffer (pH=9) heated to 115°C under high pressure. Sections were then washed in either (a) a solution of 10mM glycine and 0.2% sodium azide in phosphate buffered saline or (b) PBS + 0.1% Tween20 before antibody staining.

**Immunofluorescence Antibody Staining:** Sections were blocked for 15-30 minutes with a 5% goat serum, 1% bovine serum albumin blocking solution containing (a) 10mM glycine and 0.2% sodium azide or (b) PBS + 0.1% Tween20. Sections were then stained with appropriate primary and secondary antibodies. Primary antibodies were used at a concentration of 1:100 and incubated for 1 hour at room temperature. Secondary antibodies were used at a concentration of 1:250 and incubated for 30 minutes at room temperature. Detailed information about antibodies used is listed in Table 2.2.

**PD-L1 Staining & Scoring:** FFPE slides for 45 patients were stained using Agilent Biotechnologies PD-L1 IHC (clone 22C3 pharmDx) Staining Kit by Emory Pathology

Laboratories. Clinical-grade scoring of PD-L1 status was performed by two board-certified pathologists at Emory University Hospital. Slides with 1-49% of tumor cells expressing PD-L1 were scored 'positive-low,' slides with 50+% of tumor cells expressing PD-L1 were scored 'positive-high,' and slides with <1% of tumor cells expressing PD-L1 were scored 'negative.'

**Image Capture & Analysis:** We selected a fluorophore panel which allowed for simultaneous visualization of three targets and a nuclear stain (DAPI). For images shown in Figure 3, we utilized a Leica SP8 confocal microscope with a motorized stage for tiled imaging, and a 40X, 1.3NA, 0.24mm WD oil immersion objective was used, allowing for highly resolved, smoothly tiled images. Fluorophores were excited with the 496, 561, and 594 laser lines or with a multiphoton Coherent Chameleon Vision II laser, tuned to 700nm (DAPI). Emission-optimized wavelength ranges informed specific detector channels, which were used to detect fluorescence. Leica LASX software was utilized to create a maximum projection image, allowing us to obtain large tiled images regardless of a varying focal plane across each tissue section. For images shown in Figure 4, we utilized a Zeiss Z.1 Slide Scanner equipped with a Colibri 7 Flexible Light Source. Zeiss ZenBlue software was utilized for post-acquisition image processing. For brightfield imaging, slides were scanned using a Hamamatsu's Nanozoomer slide scanner.

CellProfiler, a free, open-source software for image analysis, was used for subsequent image manipulations. CellProfiler was used to define 'primary objects' within images, based upon user-defined parameters (diameter, fluorescence intensity, object clumping, etc.). We used this technique to define DAPI 'primary objects' (i.e., all cells) and MHC+ 'primary objects' (i.e., defining antigen presenting cells). We also used this technique to define CD8+ 'primary objects,'

which we then used to create ‘secondary objects’ by extending the border of each object by 1 pixel in all directions. These CD8+ ‘secondary objects’ were used to define CD8+ T-cells. Detailed review of parameters used to MHC-II+ antigen presenting cells and CD8+ T-cells can be found in Table 2.3. We then used CellProfiler to measure the intensity of TCF1 staining intensity in each CD8+ T-cell object. Data exported from the CellProfiler pipeline included xy location of CD8+ objects, MHC-II+ objects, and mean intensity of TCF1 staining in CD8+ T-cell objects. The remainder of image analysis was carried out using custom R and python scripts. MHC-II density and distance to nearest MHC-II+ neighbor were calculated in custom python scripts.

In order to determine the area of tissue necessary to be sampled to obtain an accurate and quantitative assessment of the CD8 T cell infiltration into tumors, large slide scanned images were dissected into areas the approximate size of a 20x field of view. Increasing number of random fields of view were sampled from images and the percent of cells that were CD8 positive by IF correlated to FACS from the corresponding sample. The estimated number of 20x fields of view necessary to obtain an accurate assessment of level of CD8 T cell infiltration is 171 fields of view (Figure 2.12 D). Histo-cytometric analysis approach employed similar to that in<sup>96</sup>.

## **2.7 Acknowledgements**

This work was supported by funding from the Prostate Cancer Foundation, Swim Across America, the James M. Cox Foundation and James C. Kennedy, pilot funding from the Winship Cancer Institute supported by The Dunwoody Country Club Senior Men’s Association, and NCI grants 1-R00-CA197891 (Kissick) and U01-CA113913 (Sanda). We recognize Adaptive Biotechnologies

for providing laboratory services as a part of an educational grant award. We would like to acknowledge The Yerkes NHP Genomics Core which is supported in part by NIH P51 OD011132, the Emory Flow Cytometry Core (EFCC) supported by the National Center for Georgia Clinical & Translational Science Alliance of the National Institutes of Health under award number UL1TR002378, the Intramural Research Program of the NIH, National Cancer Institute, and the Emory University Integrated Cellular Imaging Microscopy Core of the Winship Cancer Institute of Emory University and NIH/NCI under award number, 2P30CA138292-04.

## 2.8 Tables

**Table 2.1: Flow Cytometry Antibodies**

Target	Clone	Fluorophore	Supplier
CD8a	RPA-T8	BV-605	Biolegend
CD4	OKT4	PerCP	Biolegend
CD3	UCHT1	FITC	Biolegend
CD3	HIT3a/OKT3/SK7	AF-700	Biolegend
CD45RO	UCHL1	BV-785/BV-650	Biolegend
CD45RA	HI100	BV-510/BV-785	Biolegend
PD1	EH12.2H7	BV-785/BV-421	Biolegend
Tim3	F38-2E2	PE	Biolegend
Tim3	344823	APC	R&D
CTLA4	L3D10	PE-TR	Biolegend
TIGIT	MBSA43	APC	eBioscience
Ki67	B56	AF-647	eBioscience
TCF1	C6309	FITC/PE	Cell Signaling
CD28	CD28.2	PE-Cy7	eBioscience
CD39	A1	BV-421	Biolegend
CD244	C1.7	PE-Dazzle	Biolegend
CD11b	ICRF44	BV-605	Biolegend
CD11c	3.9	APC	Biolegend
CD68	Y1/82A	FITC	Biolegend
MHC-II (HLA-DR)	L243	BV-421	Biolegend
CD206	15-2	BV-421	Biolegend
CD31	WM59	BV-711	Biolegend
Podoplanin	NC-08	APC/Fire750	Biolegend
CD69	FN50	BV510	Biolegend
CD103	BER-ACT8	PE-Dazzle	Biolegend

**Table 2.2: Immunofluorescence Antibodies**

Target	Antibody Type	Clone	Concentration	Secondary Antibody	Concentration
MHC-II (HLA-DR, DP, DQ)	Mouse IgG2a	Tu39	1:100	Goat anti-mouse IgG2a A488	1:250
TCF1	Rabbit	C63D9	1:100	Goat anti-rabbit A555	1:250
CD8	Mouse IgG1	C8/144B	1:100	Goat anti-mouse IgG1 A594	1:250
CD3	Rabbit	Polyclonal	1:100	Goat anti-rabbit A555	1:250
Lyve1	Mouse IgG1	537028	1:100	Goat anti-mouse IgG1 A647	1:250
CD31	Rabbit	Polyclonal	1:100	Goat anti-rabbit A555	1:250
Podoplanin	Mouse IgG1	D2-40	1:100	Goat anti-mouse IgG1 A647	1:250

Table 2.3: CellProfiler Primary Object Parameters

	CD8 'Primary Objects'	MHC-II 'Primary Objects'	DAPI 'Primary Objects'
Diameter of object, in pixel units (min, max)	10, 40	8, 50	8, 25
Discard objects outside diameter range?	Yes	Yes	Yes
Discard objects touching border of image?	Yes	Yes	Yes
Threshold strategy	Global	Global	Global
Threshold method	Manual	Manual	Min cross entropy
Method to distinguish clumped objects	Intensity	Intensity	Intensity
Method to draw dividing lines between clumped objects	Intensity	Intensity	Intensity
Automatically calculate size of smoothing filter for de-clumping?	Yes	Yes	Yes
Automatically calculate minimum allowed distance between local maxima?	Yes	Yes	Yes
Speed up by using lower-resolution image to find local maxima?	Yes	Yes	Yes
Fill holes identified objects?	After both thresholding and de-clumping	After both thresholding and de-clumping	After both thresholding and de-clumping
Handling of objects if excessive number of objects identified?	Continue	Continue	Continue
Secondary object defined?	Yes, defined by distance (1 pixel)	Yes, defined by distance (1 pixel)	Yes, defined by distance (1 pixel)

## **Chapter 3: Stem-like CD8 T cells are present in intra-tumoral immune niches in diverse tumor types**

### **3.1. Author's Contribution and Acknowledgement of Reproduction.**

This chapter contains sections of unpublished data and a section that is reproduced with minor edits from Figure 3 of Carla Calagua<sup>1</sup>, Miriam Ficial<sup>2,3</sup>, Caroline S Jansen<sup>4</sup>, Taghreed Hirz<sup>5,6,7</sup>, Luke Del Balzo<sup>4</sup>, Scott Wilkinson<sup>8</sup>, Ross Lake<sup>8</sup>, Anson T Ku<sup>8</sup>, Olga Voznesensky<sup>1</sup>, David B Sykes<sup>3,5,6,7</sup>, Philip J Saylor<sup>3,7</sup>, Huihui Ye<sup>9</sup>, Sabina Signoretti<sup>2,3,10</sup>, Haydn Kissick<sup>4</sup>, Adam G Sowalsky<sup>8</sup>, Steven P Balk<sup>3,11</sup>, David J Einstein<sup>3,11</sup>, A Subset of Localized Prostate Cancer Displays an Immunogenic Phenotype Associated with Losses of Key Tumor Suppressor Genes. *Clin Cancer Res*, 2021 Sep 1;27(17):4836-4847. doi: 10.1158/1078-0432.CCR-21-0121.

For the reproduced work, C.S.J., H.K., S.P.B, and D.J.E conceived and designed the study and composed the manuscript sections. C.S.J. and H.K. designed experiments. C.S.J. and L.D.B. performed immunofluorescence slide staining. C.S.J., S.W., R.L. and A.G.S. optimized and performed immunofluorescence slide scanning. C.S.J. and H.K. developed quantitative immunofluorescence techniques and performed quantitative analysis of immunofluorescence data. All authors reviewed the manuscript.

#### Affiliations:

1. Division of Medical Oncology, Department of Medicine, Beth Israel Deaconess Medical Center, Boston, Massachusetts. 2. Department of Pathology, Brigham and Women's Hospital, Boston,

Massachusetts. 3. Harvard Medical School, Boston, Massachusetts. 4. Department of Urology, Emory University, Atlanta, Georgia. 5. Center for Regenerative Medicine, Massachusetts General Hospital, Boston, Massachusetts. 6. Harvard Stem Cell Institute, Harvard University, Cambridge, Massachusetts. 7. Division of Hematology-Oncology, Department of Medicine, Massachusetts General Hospital, Boston, Massachusetts. 8. National Cancer Institute, Bethesda, Maryland. 9. Department of Pathology, University of California, Los Angeles, Los Angeles, California. 10. Department of Oncologic Pathology, Dana-Farber Cancer Institute, Boston, Massachusetts. 11. Division of Medical Oncology, Department of Medicine, Beth Israel Deaconess Medical Center, Boston, Massachusetts.

### **3.2 Introduction.**

As more and more is learned and appreciated about the importance of the anti-tumor immune response<sup>27-45, 52-54</sup>, a significant question has emerged—what realities of this response are unique to certain tumor types and what aspects of the response are globally applicable, holding true in a variety of tumors, tissues, and histologies? Accordingly, after having extensively characterized the anti-tumor T cell response in renal cell carcinoma and defined the importance of careful intratumoral organization of this response<sup>43</sup>, we sought to test the hypothesis that this same phenomenon—the presence of TCF1+ stem-like CD8 T cells in dense antigen presenting immune niches—also supports the anti-tumor immune response in other tumor types. Our initial study had looked most extensively at renal cell carcinoma, but also considered a small number of bladder and prostate tumor samples, in which it appeared that these TCF1+ stem-like T cells were present, and similarly residing in antigen presenting immune niches. This observation further encourages investigation into the trans-tumor type applicability of this immunobiology.

We were particularly interested in examining the tumor immune microenvironment in prostate cancers, as prostate cancer is classically considered to be “immunologically cold” and specifically lacking significant CD8 T cell infiltration<sup>43, 97, 98</sup>. However, while it is true that prostate cancers tend to be largely lacking in lymphocytic infiltration, there are a subset of tumors that exhibit significant immune infiltration<sup>97</sup>. Furthermore, we wondered if the presence of stem-like T cells in intratumoral immune niches may represent a specific feature of this particular immunogenic subset of prostate cancers, enabling the higher levels of immune infiltration observed in this subset.

Similarly, we were also interested in specifically investigating the landscape of the immune response in brain metastases, given that the brain had classically been considered a more immune privileged site, but has more recently has been shown (1) to harbor a functional lymphatic vessel system and (2) that both primary and metastatic intracranial malignancies have variable intensities of immune infiltration<sup>99-102</sup>. Accordingly, we wondered if TCF1+ stem like CD8 T cells would be present in brain metastases and if they would be present in immune niches as in other tissues. Furthermore, the investigation of brain metastases would allow for discernment of whether this biology is present in tumors from diverse tissue origins (e.g., breast cancer, melanoma, and lung cancer) and to probe what the effect of radiation therapy might be on the presence of these immune niches.

In sum, the goal of this work was to investigate whether TCF1+ stem-like CD8 T cells were present and residing in dense antigen presenting immune niches in a diversity of tumor types—in immunogenic prostate cancers and in brain metastases of several different histologies. The findings

of these investigations shed light and interest on understanding what tenets of the biology of the anti-tumor immune response, and particularly of the organization of this response, are broadly translatable across cancers, and what aspects may be unique to individual tumor types.

### 3.3 Results.

#### *Stem-like, exhausted progenitor CD8 T cells are present in intratumoral immune niches in immunogenic prostate cancers*

In murine models of chronic viral infection, the T-cell response is known to be maintained by a progenitor-type cell that expresses the transcription factor TCF1 and resides predominantly in the lymphoid tissue<sup>46</sup>. Interestingly, a number of studies reported the identification of analogous CD8+TCF1+ exhausted progenitor T lymphocytes directly in tumor tissue<sup>44, 48, 64</sup>, and we previously observed these cells in close proximity to MHC-II+ APCs. These aggregated TCF1+ T cells and MHC-II+ APCs form intratumoral APC niches<sup>43</sup>, which closely resemble the T-cell zone of lymphoid tissue, suggesting that these niches may support TCF1+ stem-like cell survival by analogous mechanisms to those in the lymphoid tissue. Previous studies examined these TCF1+ T cells and this pattern of immune organization in predominantly classically immunogenic tumor types, with a small subset of analysis in unselected prostate cancer.

Here, we identified intratumoral APC niches in immunogenic prostate cancer (Figure 3.1 A–D). As in prior work, APC niches are defined as areas within tumor tissue with MHC-II+ cells and CD8+TCF1+ T cells identified in the same 100 × 100 μmol/L area. These niches were present in the described immunogenic prostate cancer cohorts, as well as in two MSI-H prostate cancer cases

(one RP specimen, one biopsy from a patient with mCRPC at time of resistance to PD-1 blockade after initial response), and the percentage of tissue with these APC niches was not significantly different when comparing the immunogenic prostate cancer cohorts to MSI-H cases ( $P = 0.15$ ; Figure 3.1 E). These findings are consistent with the conclusion that these tumors are eliciting immune responses, although the extent to which this is predictive of responsiveness to ICI remains to be determined. The percentage of tumor tissue occupied by APC niches loosely correlated with amount of infiltrating MHC-II+ cells ( $R^2 = 0.18$ ,  $P = 0.065$ ; Figure 3.1 F) and more tightly correlated with the number of infiltrating CD8+ and TCF1+ TILs ( $R^2 = 0.57$ ,  $P = 0.0001$  for both comparisons; Figure 3.1 G and H), further supporting the role of these APC niches in maintaining the tumor T-cell response.

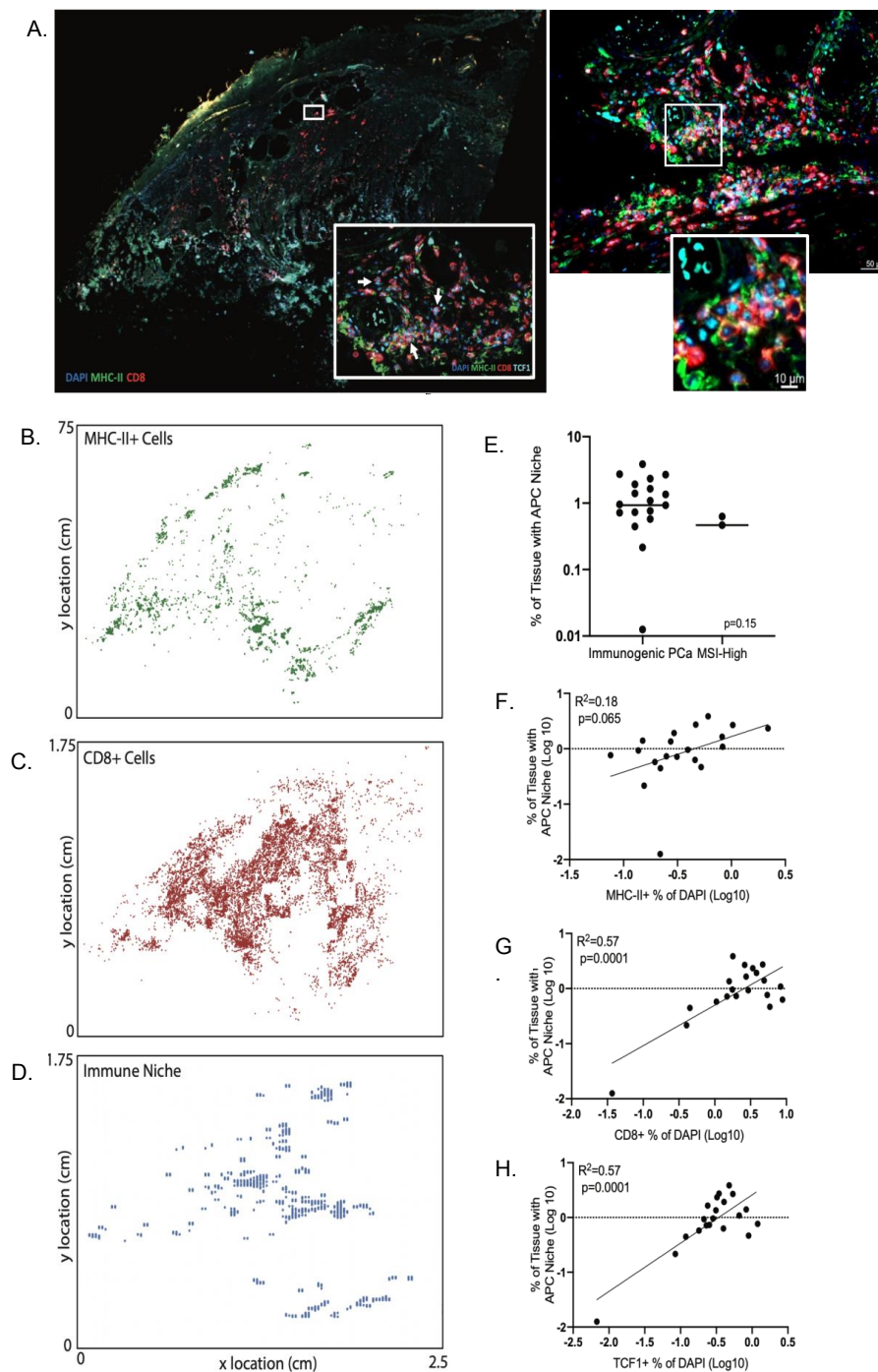


**Figure 3.1. Evaluation of antigen-presenting cell (APC) niches within PCa cases.** (A) Sample multiplex immunofluorescence image showing MHC II and CD8 expression. The left inset is expanded on the right, with an additional high-power view in the right inset. (B-D) Spatial analysis of individual cell populations and areas defined as APC immune niches (presence of both MHC-

II+ and TCF1+ cells). (E) Percentage of tissue with APC niches by tissue cohort. (F- H) Correlation of percentage of tissue with APC niches with MHC-II+ Cells (F), CD8+ TILs (G), and TCF1+ TILs (H).

*Investigating the immune landscape in brain metastases*

Having identified TCF1<sup>+</sup> stem-like CD8 T cells present in both renal cell carcinoma and immunogenic prostate cancers, we were next interested to see if these cells might also be present in additional tumor histologies, as well as in unique tissue locations, such as brain metastases. Accordingly, we examined a cohort (cohort 1) of 115 archived, FFPE samples of brain metastases from patients with melanoma, breast cancer, or non-small cell lung cancer by immunofluorescence and a cohort (cohort 2) of 13 intraoperative tumor samples from patients with assorted tumor types by flow cytometry. Each cohort contained patients who had and had not received radiation therapy prior to tumor resection.

We performed multiplex immune fluorescence staining on the cohort of FFPE samples, accompanied by high resolution, whole slide scanning, and subsequent quantitative analysis. This approach allows for extraction of quantitative measures from whole slide immunofluorescence images. With this approach, the x, y location of each cell is measured, cell types are classified, and the intensity of each stained marker within each cell is quantified. This technique also allows accurate quantification of the patterns of aggregation of different cell types within tissue, as well as measurement of cell type density. Steps through this approach are featured in Figure 3.2, where adjacent slide scans show (Figure 3.2 A) an H&E stain and (Figure 3.2 B) an immunofluorescence stain of a brain metastasis sample. In (Figure 3.2 C), the result of this quantitative approach is shown where the immunofluorescence image is reproduced in digitized form, where green dots represent MHC-II<sup>+</sup> APCs, red dots represent CD8<sup>+</sup> T cells, and blue dots represent all other cell nuclei. The inset panel shows immunofluorescence (left) and digitization (right), illustrating the fidelity of this quantification method to the native immunofluorescence data. In Figure 3.2 D, the

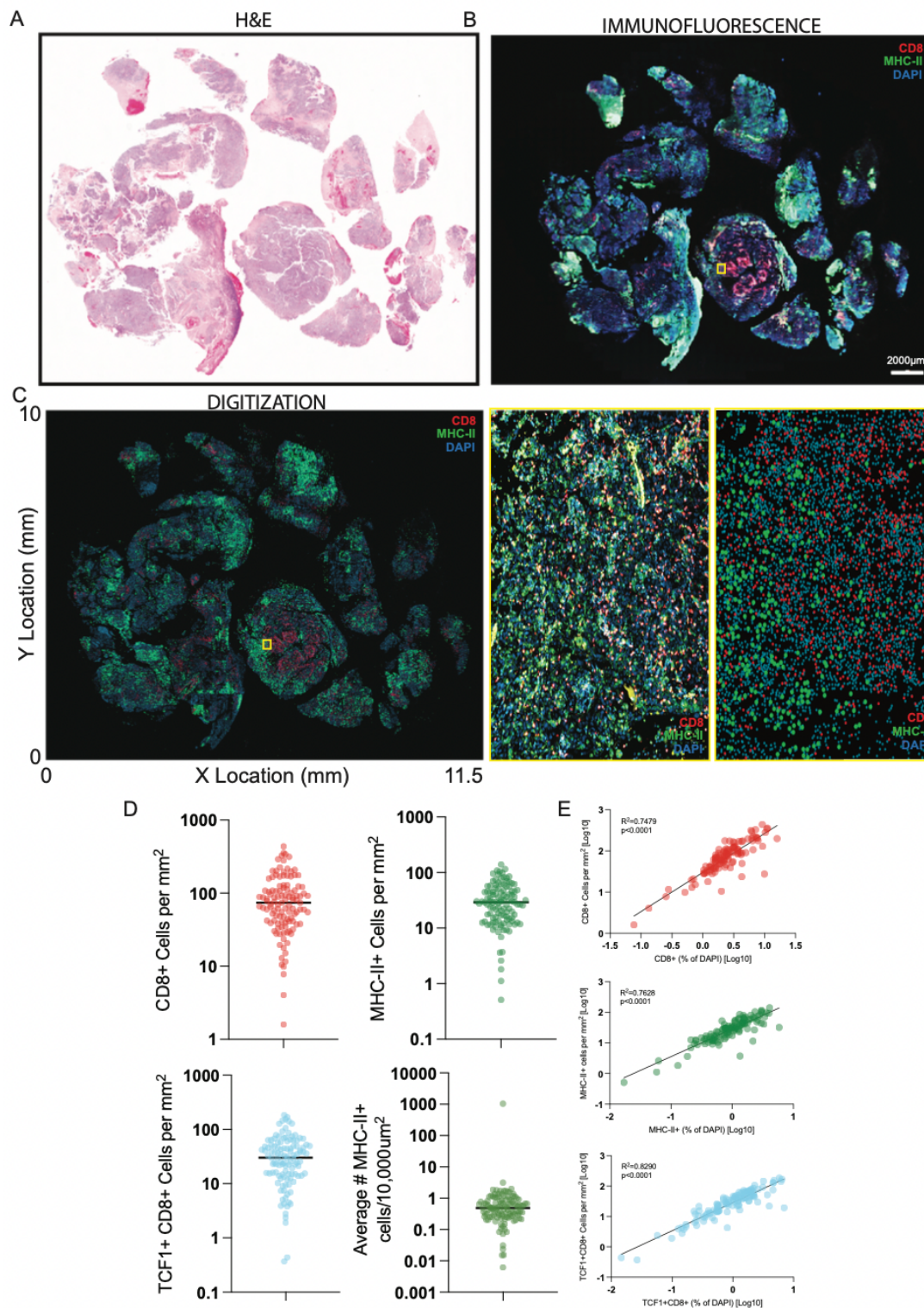


**Figure 3.2: Multiplex, quantitative immunofluorescence imaging analysis of human brain metastasis samples. (A) Brain metastasis sample stained with hematoxylin & eosin and brightfield**

scanned. (B) Brain metastasis sample immunofluorescence stained for CD8, MHC-II, and counter stained with DAPI and fluorescence-scanned. (C) Digitization of whole slide sample shown in B (left), with zoomed inset comparing immunofluorescence (middle) to digitization (right). (D) Quantification of CD8+, MHC-II+, and TCF1+ CD8+ cells present in brain metastasis samples, as well as local MHC-II+ cellular density, as measured by calculating the average number of MHC-II+ cells per  $10,000\mu\text{m}^2$ . (E) Internal consistency of multiple quantification methods, where there is concordance between quantifying infiltrating immune cells per  $\text{mm}^2$  or as a percentage of DAPI+ cells for CD8+ cells, MHC-II+ cells, and TCF1+CD8+ cells.

result of this digitization and quantification across the entire cohort is shown, where the number of CD8<sup>+</sup> T cells, TCF1<sup>+</sup> stem-like CD8<sup>+</sup> T cells, and MHC-II<sup>+</sup> cells are quantified, along with the density of MHC-II<sup>+</sup> cells. Furthermore, the fidelity of this method is demonstrated by showing concordance between multiple quantification methods (per mm<sup>2</sup> vs. as a percentage of all DAPI nuclei).

*Stem-like CD8 T cells are present in brain metastases from patients with melanoma, breast cancer, and non-small cell lung cancer, with or without exposure to radiation therapy*

We utilized these FFPE and intraoperative sample cohorts to examine the immune infiltrate present in these brain metastases. By immunofluorescence, we were able to identify TCF1<sup>+</sup> stem-like CD8 T cells present in brain metastases (Figure 3.3 A). These TCF1<sup>+</sup> stem-like CD8 T cells were present in all brain metastases samples, regardless of exposure to radiation therapy (Figure 3.3 B, C). MHC-II<sup>+</sup> cells were also identified in all samples, regardless of exposure to radiation therapy (Figure 3.3 A-C).

We also found that the presence of the TCF1<sup>+</sup> stem-like CD8 T cells paralleled the total CD8 T cell infiltration into the tumor. More specifically, while the proportion of CD8 T cells that are TCF1<sup>+</sup> stem-like cells did not correlate with the overall T cell response (Figure 3.3 D), the amount of TCF1<sup>+</sup> CD8 T cells (measured per mm<sup>2</sup> or as a proportion of all DAPI<sup>+</sup> cells) strongly correlated with the total CD8 T cell response (measured per mm<sup>2</sup> or as a proportion of all DAPI<sup>+</sup> cells), suggesting that, similar to what we have described in renal cell carcinoma, TCF1<sup>+</sup> stem-like CD8 T cells are vital for maintaining the anti-tumor T cell response (Figure 3.3 E). Importantly, this relationship was true in irrespective of radiation treatment status (Figure 3.3 F).

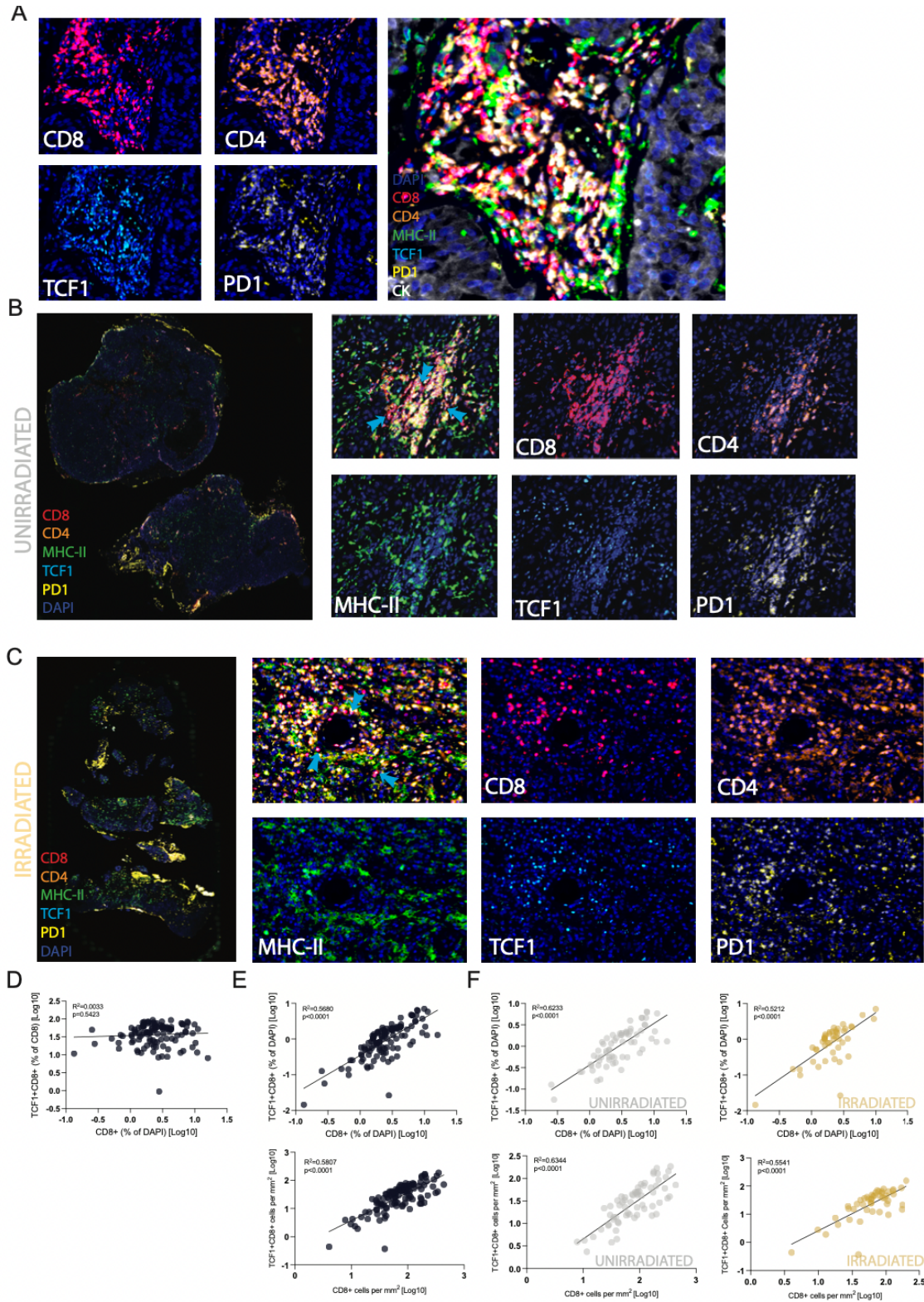


**Figure 3.3: TCF1+ stem-like CD8 T cells are present in brain metastases in both irradiated and unirradiated samples. (A) Immunofluorescence staining of a brain metastasis sample**

revealing the presence of immune infiltrate, including TCF1+ CD8+ cells. Inset shows CD8 + DAPI, CD4 + DAPI, TCF1 + DAPI, and PD1 + DAPI, while merged image shows CD8, CD4, MHC-II, TCF1, PD1, and DAPI stains. (B&C) Immunofluorescence staining of an unirradiated brain metastasis (B) and an irradiated brain metastasis (C). Whole slide scan (left) shows CD8, CD4, MHC-II, TCF1, PD1, and DAPI stains. Insets show MHC-II + DAPI, CD8 + DAPI, CD4 + DAPI, TCF1 + DAPI, and PD1 + DAPI, while merged image shows CD8, CD4, MHC-II, TCF1, PD1, and DAPI stains and demonstrates the presence of TCF1+ CD8+ cells with blue arrows. (D) Lack of correlation between the abundance of infiltrating CD8+ cells and the proportion of CD8+ cells that are TCF1+.  $R^2=-0.0033$ ,  $p=0.5423$ . (D) Correlation between the abundance of infiltrating CD8+ cells and the abundance of TCF1+ CD8+ cells, both per  $\text{mm}^2$  (top,  $R^2=0.5680$ ,  $p<0.0001$ ) or as a percentage of DAPI+ cells (bottom,  $R^2=0.5807$ ,  $p<0.0001$ ). (E) Correlation between the abundance of infiltrating CD8+ cells and the abundance of TCF1+ CD8+ cells in both irradiated (left) and unirradiated (right) samples, both per  $\text{mm}^2$  (top, irradiated:  $R^2=0.6233$ ,  $p<0.0001$ , unirradiated:  $R^2=0.5212$ ,  $p<0.0001$ ) or as a percentage of DAPI+ cells (bottom, irradiated:  $R^2=0.6344$ ,  $p<0.0001$ , unirradiated:  $R^2=0.5541$ ,  $p<0.0001$ ).

We were also able to identify TCF1<sup>+</sup> stem-like CD8 T cells in intraoperative tumor samples by flow cytometry. A sample gating strategy for identification of these cells is shown in Figure 3.4 A, and the presence of TCF1<sup>+</sup> stem-like CD8 T cells, as well as Tim3<sup>+</sup> terminally differentiated CD8 T cells, are shown in Figure 3.4 B. Similar to what we have described in renal cell carcinoma, these stem-like cells have higher expression of TCF1 and the costimulatory molecule CD28, while the terminally differentiated cells have higher expression of checkpoint and effector molecules like PD1, Tim3, CD39, and Granzyme B, and both cell populations express the activation markers CD39 and HLA-DR, as well as the marker PD1, indicating their status as antigen-experienced cells (Figure 3.4 C).

Importantly, these cell populations were identifiable in both irradiated and unirradiated samples, as highlighted in Figure 3.5, which shows PD1<sup>+</sup> Tim3<sup>+</sup> CD39<sup>+</sup> terminally differentiated CD8 T cells in red, and PD1<sup>+</sup> TCF1<sup>+</sup> CD28<sup>+</sup> stem-like CD8 T cells in green. Importantly, the phenotype of these cell populations remains concordant between irradiated and unirradiated samples, where stem-like T cells express lower levels of checkpoint and effector molecules, but higher levels of TCF1 and costimulatory molecules, than do their terminally differentiated counterparts (Figure 3.6 A, B).

*Stem-like CD8 T cells in brain metastases reside in antigen-presenting immune niches, which sustain the anti-tumor T cell response in brain metastases and are associated with improved local control*

After having identified these TCF1<sup>+</sup> stem-like CD8 T cells in brain metastases, we next wondered if they preferentially resided in dense antigen presenting “immune niches,” as we had found in

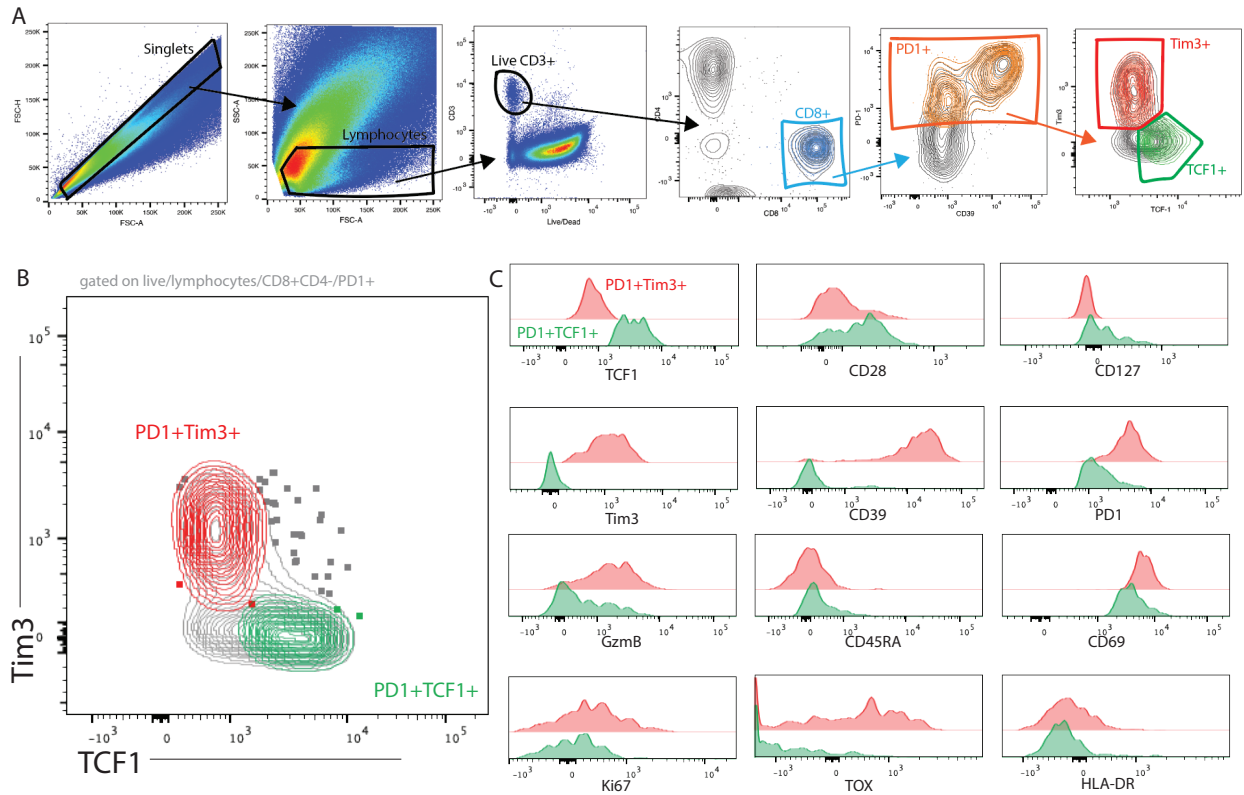


**Figure 3.4: Flow cytometry identification of TCF1+ stem-like CD8 T cells and Tim3+ terminally differentiated CD8 T cells in brain metastases. (A) Flow cytometry gating strategy for identifying TCF1+ stem-like CD8 T cells and Tim3+ terminally differentiated CD8 T cells in brain metastases. (B) Flow cytometry plot showing TCF1+ stem-like CD8 T cells (green) and Tim3+ terminally differentiated CD8 T cells (red), (C) Flow cytometry-based measurement (mean fluorescence intensity) of selected phenotypic markers on TCF1+ stem-like CD8 T cells (green) and Tim3+ terminally differentiated CD8 T cells (red).**

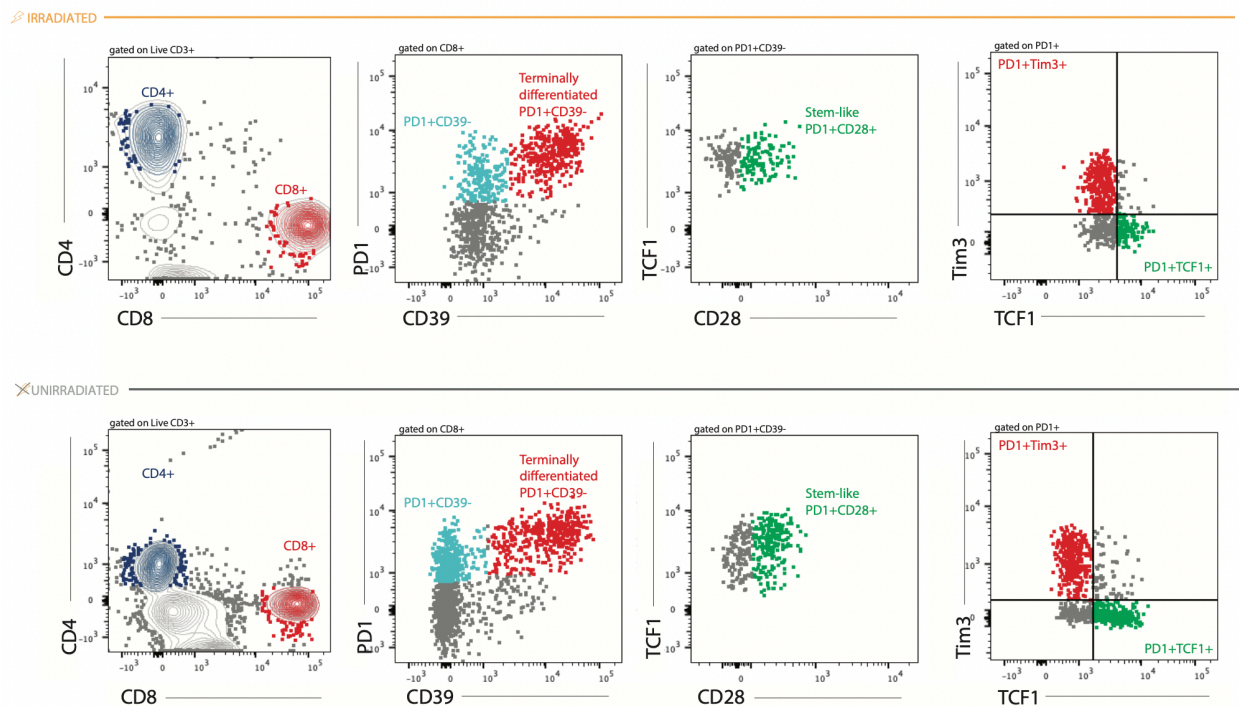


**Figure 3.5: Flow cytometry comparison of T cell infiltration in irradiated (top) and unirradiated (bottom) brain metastasis samples.** From left to right, plot 1 (leftmost) is gated singlet/live/CD3+ cells and shows CD4 (blue) and CD8 (red) T cells, plot 2 (left of center) is gated on singlet/live/CD3+ CD8 T cells and shows PD1+CD39- CD8 T cells (cyan) and PD1+CD39+ terminally differentiated CD8 T cells (red), plot 3 (right of center) is gated on singlet/live/CD3+/CD8+/PD1+CD39- cells and shows TCF1+ CD28+ stem-like CD8 T cells (green), and plot 4 (rightmost) is gated on singlet/live/CD3+/CD8+/PD1+ cells and shows Tim3+ terminally differentiated CD8 T cells (red) and TCF1+ stem-like CD8 T cells (green).

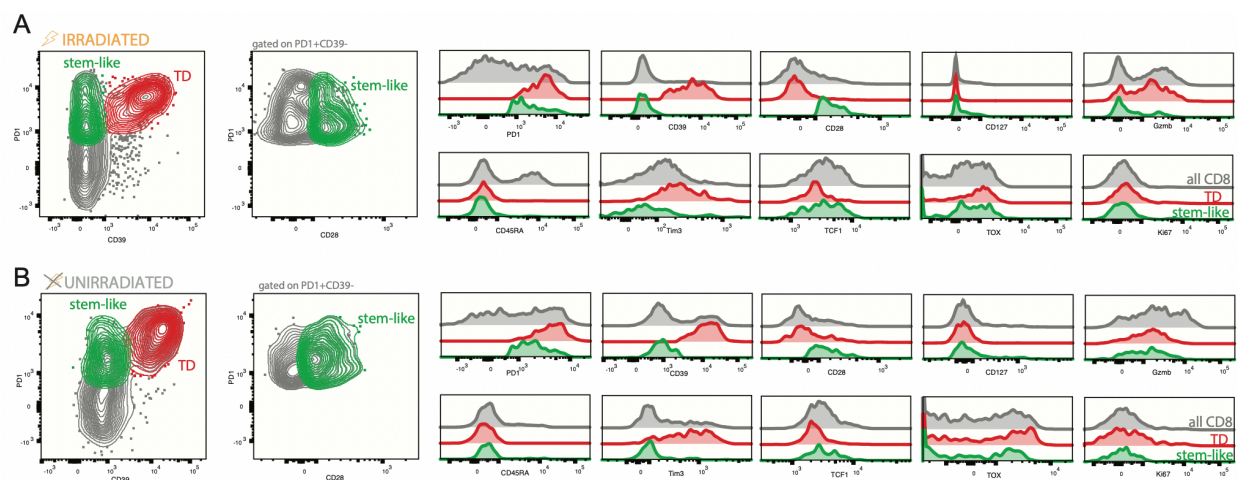


**Figure 3.6: Flow cytometry comparison of the phenotype of stem-like and terminally differentiated CD8 T cells in irradiated (A) and unirradiated (B) brain metastasis samples.**

Leftmost flow cytometry plot is gated on singlet/live/CD3+ CD8 T cells. The flow cytometry plot to the right is gated on singlet/live/CD3+/PD1+CD39- CD8 T cells. On these plots, PD1+TCF1+ stem-like CD8 T cells are shown in green, whereas PD1+CD39+ terminally differentiated cells are shown in red. Histograms demonstrating the mean fluorescence intensity of selected phenotypic markers on stem-like and terminally differentiated CD8 T cells in both irradiated and unirradiated brain metastases are shown to the right.

renal cell carcinoma and in immunogenic prostate cancers. Using quantitative analysis of whole slide immunofluorescence imaging (Figure 3.7 A), we construct “immunomaps” to map the patterns of immune cell infiltration and aggregation in tumors. In Figure 3.7 B, we show MHC-II<sup>+</sup> cellular density with a gray contour map, overlaid with the x, y location of TCF1<sup>+</sup> stem-like CD8 T cells in green and all other CD8 T cells in red, illustrating how stem-like cells preferentially reside in areas of highest antigen presenting cell (MHC-II<sup>+</sup> cell) density. Furthermore, when we measure the distance between each CD8 T cell and its nearest antigen presenting (MHC-II<sup>+</sup>) cell neighbor, we find that TCF1<sup>+</sup> cells, on average, reside closer to their nearest APC neighbors than do TCF1<sup>-</sup> cells (Figure 3.7 C), again reinforcing the tenet that TCF1<sup>+</sup> stem-like CD8 T cells preferentially reside in dense antigen presenting immune niches in tumors.

Additionally, when we examine these phenomena across our entire cohort, we see that MHC-II<sup>+</sup> cellular infiltration/density correlates with both overall CD8 T cell infiltration, as well as specific TCF1<sup>+</sup> CD8 T cell infiltration (Figure 3.7 D), underscoring the importance of the cooperation between these cell types in maintaining the anti-tumor immune response. This is further illustrated in Figure 3.8, where we demonstrate a side-by-side comparison of highly and poorly infiltrated brain metastases. In a highly infiltrated brain metastasis (left), there is significant CD8 T cell infiltration (red), including TCF1<sup>+</sup> stem-like cells (green), as well as significant MHC-II<sup>+</sup> cell infiltration (gray). Importantly, the highly infiltrated brain metastasis also contains many areas of immune niches (blue), which are defined as local cellular neighborhoods which harbor both TCF1<sup>+</sup> stem-like CD8 T cells and MHC-II<sup>+</sup> antigen presenting cells. On the contrary, in a poorly infiltrated brain metastasis (right), there are many fewer areas of T cell infiltration, of MHC-II<sup>+</sup> antigen presenting cell infiltration, and critically, many fewer areas occupied by these immune

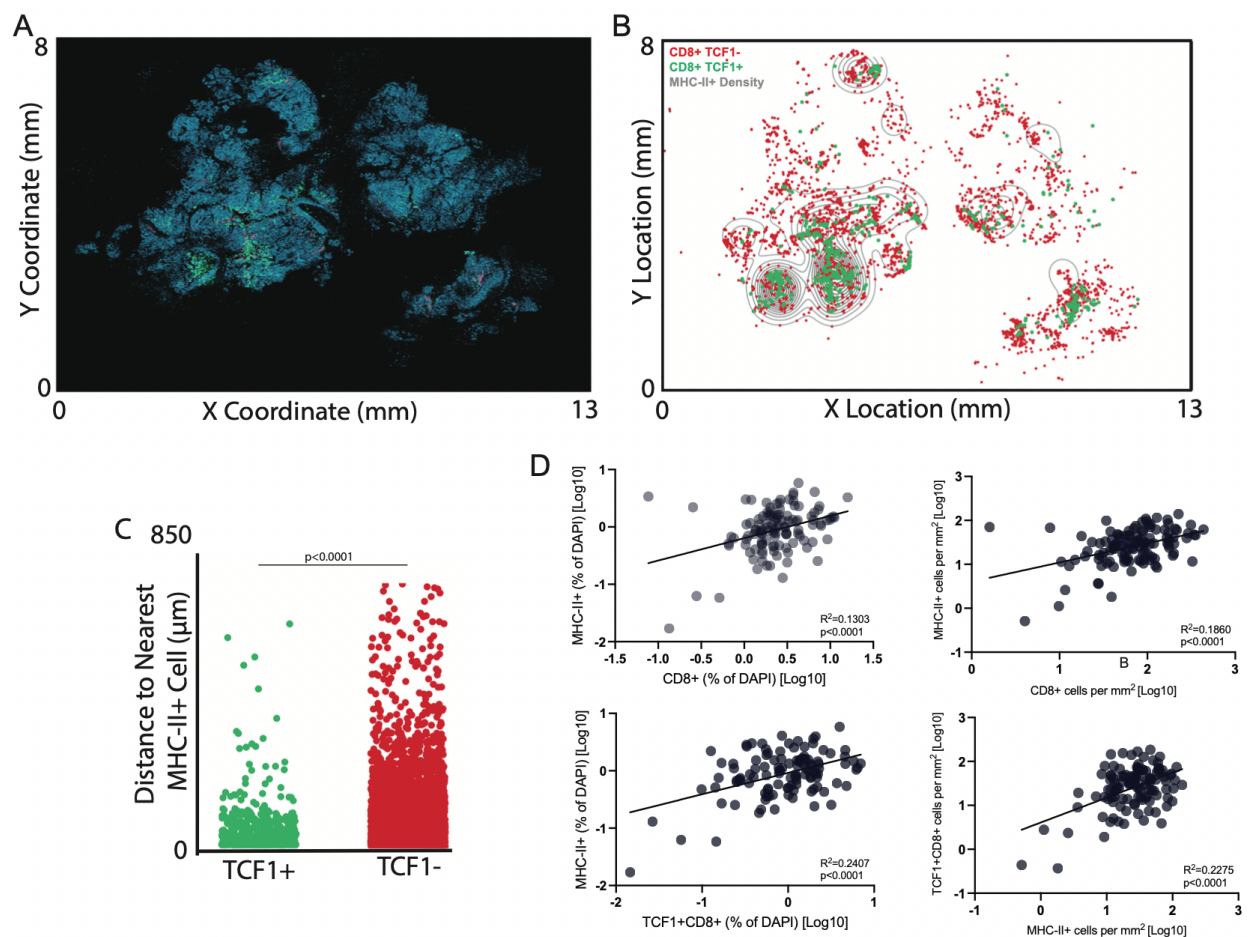


**Figure 3.7: TCF1+ stem-like CD8 T cells reside in dense antigen presenting immune niches in brain metastases.** (A) Digitization of whole slide scan of a brain metastasis sample immunofluorescence stained for MHC-II, TCF1, and CD8 and counterstained with DAPI. (B) Immunomap of the sample shown in (A), where the gray contour illustrates the MHC-II+ cell density, which is overlaid the x,y location of TCF1+ CD8+ cells in green and TCF1- CD8+ cells in red. (C) Measurement of the distance between each CD8+ cell identified in the sample shown in A & B and its nearest MHC-II+ cell neighbor, broken down between TCF1+ and TCF1- CD8+ cells. TCF1+ CD8+ cells are on average significantly closer ( $p < 0.0001$ ) to their nearest MHC-II+ cell neighbors than their TCF1- CD8+ counterparts. (d) Correlation between CD8+ cell infiltration and MHC-II+ cell infiltration (top left, as measured a percentage of DAPI+ cells:  $R^2=0.1303$ ,

$p < 0.0001$ , top right, as measured per  $\text{mm}^2$ :  $R^2 = 0.1860$ ,  $p < 0.0001$ ) and specifically between TCF1+ CD8+ cell infiltration and MHC-II+ cell infiltration (bottom left, as measured a percentage of DAPI+ cells:  $R^2 = 0.2407$ ,  $p < 0.0001$ , bottom right, as measured per  $\text{mm}^2$ :  $R^2 = 0.2275$ ,  $p < 0.0001$ ).

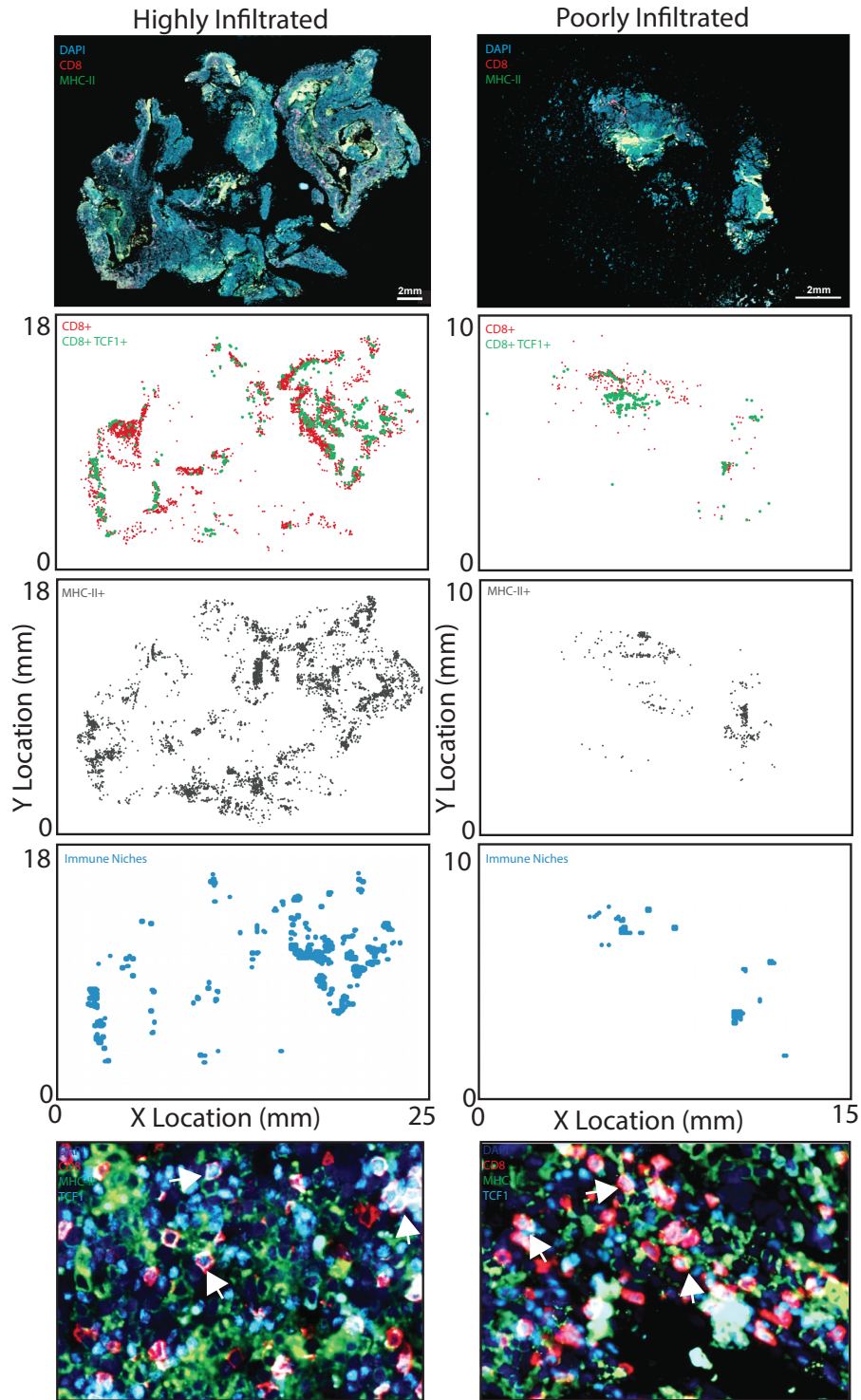


**Figure 3.8: Comparison between highly (left) and poorly (right) infiltrated brain metastases samples, from top to bottom:** At top, a whole slide scan of a brain metastasis sample

immunofluorescence stained for MHC-II, TCF1, and CD8 and counterstained with DAPI is shown. Next from the top is shown a set of three immunomaps, with (1) the x,y location of CD8 T cells shown in red, with the location of TCF1+ CD8 T cells overlaid in green, (2) the x,y location of MHC-II+ cells in green, and (3) the local cellular neighborhoods (approximately  $10,000\mu\text{m}^2$ ) occupied by immune niches (blue), which are defined by areas where both TCF1+ CD8 T cells and MHC-II+ cells associate. At bottom, zoomed insets of whole slide scan of a brain metastasis sample immunofluorescence stained for MHC-II, TCF1, and CD8 and counterstained with DAPI are shown, with TCF1+ stem-like CD8 T cells highlighted with white arrows.

niches. This remains true at the cohort level, where we see that CD8 T cell infiltration (Figure 3.9 A), including specific TCF1+ stem-like CD8 cell infiltration (Figure 3.9 B), and MHC-II+ antigen presenting cell infiltration (Figure 3.9 C) correlate with the proportion of the tumor tissue occupied by these immune niches, further demonstrating the critical importance of the presence and abundance of these immune niches in maintaining a robust anti-tumor immune response.

Perhaps most importantly, we find that patients with a high proportion of TCF1+ stem-like CD8 T cells or patients with a higher proportion of tumor tissue occupied by immune niches have improved local control of brain metastases (Figure 3.9 D, E). This is not only consistent with our findings in renal cell carcinoma, where the presence of a strong anti-tumor immune response was associated with improved progression free survival, but also demonstrates the clinical relevance of the immunobiology we have described, whereby the ability of these intratumoral immune niches to contribute to a sustained, productive antitumor immune response promotes improved clinical outcomes for patients.

#### *Intratumoral immune niches persist in brain metastases despite radiation therapy*

While TCF1+ stem-like CD8 T cells were present and residing in antigen presenting dense immune niches in both irradiated and unirradiated brain metastases (Figure 3.10 A, B), we wondered if there might be more granular differences in the components of this antitumor immune response, resultant from exposure to radiation therapy, even if the more global tenets of the response remain intact. Interestingly, when we compared our irradiated and unirradiated cohorts, we found that the overall CD8 T cell response and the TCF1- CD8 T cell response were attenuated in the irradiated samples, whereas the MHC-II+ cell infiltration and the specific TCF1+ stem-like CD8 T cell

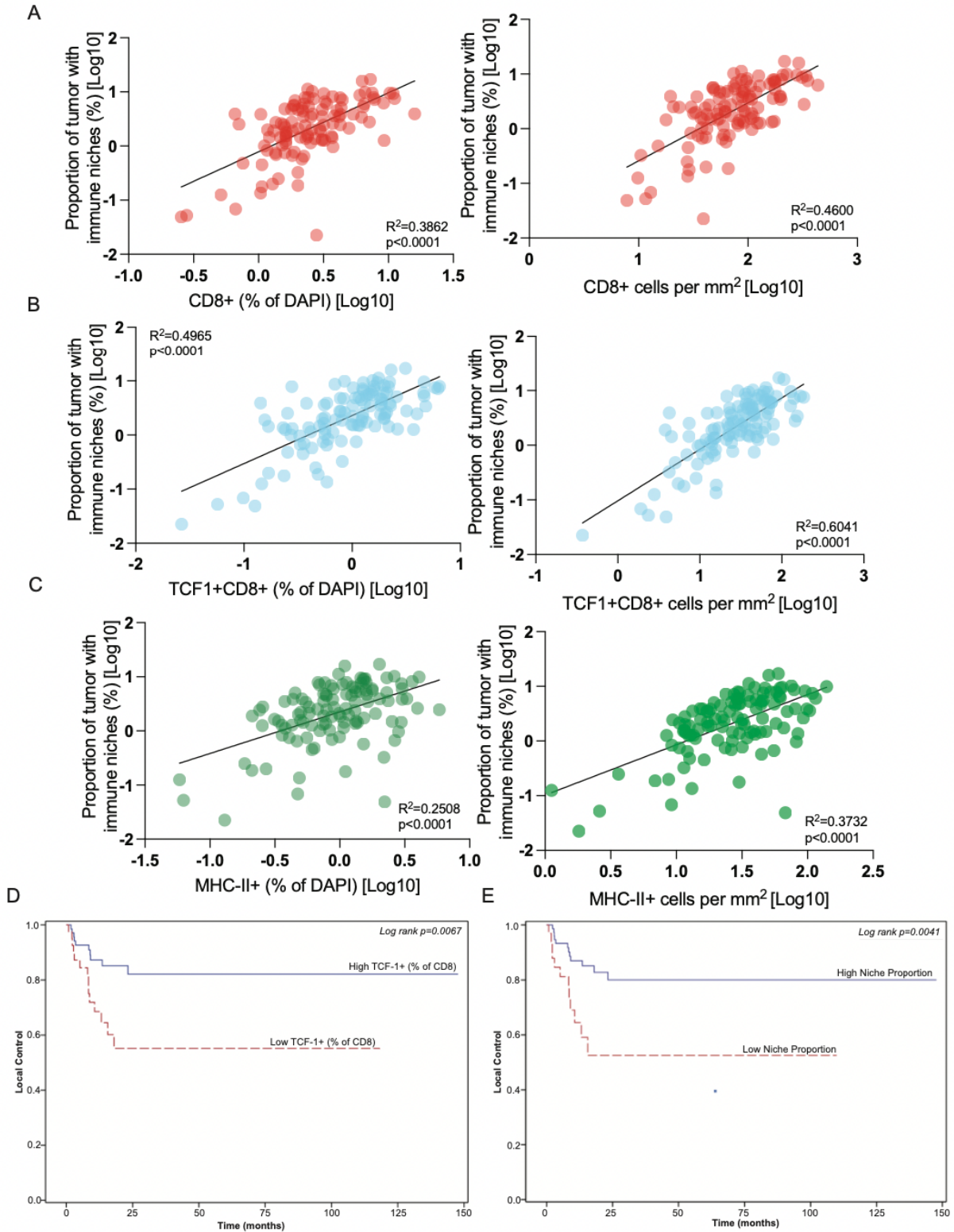


**Figure 3.9: Higher levels of TCF1+ stem-like CD8 T cells and higher proportions of intratumoral immune niches in brain metastases are associated with improved local control.**

(A) Correlation of the proportion of the tumor occupied by immune niches with the CD8+ cell infiltration (left, as measured a percentage of DAPI+ cells:  $R^2=0.3862$ ,  $p<0.0001$ , right, as measured per  $\text{mm}^2$ :  $R^2=0.4600$ ,  $p<0.0001$ ). (B) Correlation of the proportion of the tumor occupied by immune niches with specifically TCF1+ CD8+ cell infiltration (left, as measured a percentage of DAPI+ cells:  $R^2=0.4965$ ,  $p<0.0001$ , right, as measured per  $\text{mm}^2$ :  $R^2=0.6041$ ,  $p<0.0001$ ). (C) Correlation of the proportion of the tumor occupied by immune niches with the MHC-II+ cell infiltration (left, as measured a percentage of DAPI+ cells:  $R^2=0.2508$ ,  $p<0.0001$ , right, as measured per  $\text{mm}^2$ :  $R^2=0.3732$ ,  $p<0.0001$ ). (D) Kaplan-Meier curves demonstrating clinical outcomes analysis, where patients with higher TCF1+ (% of CD8, left,  $p=0.0067$ ) or a higher immune niche proportion (right,  $p=0.0041$ ) have improved local control of brain metastases.

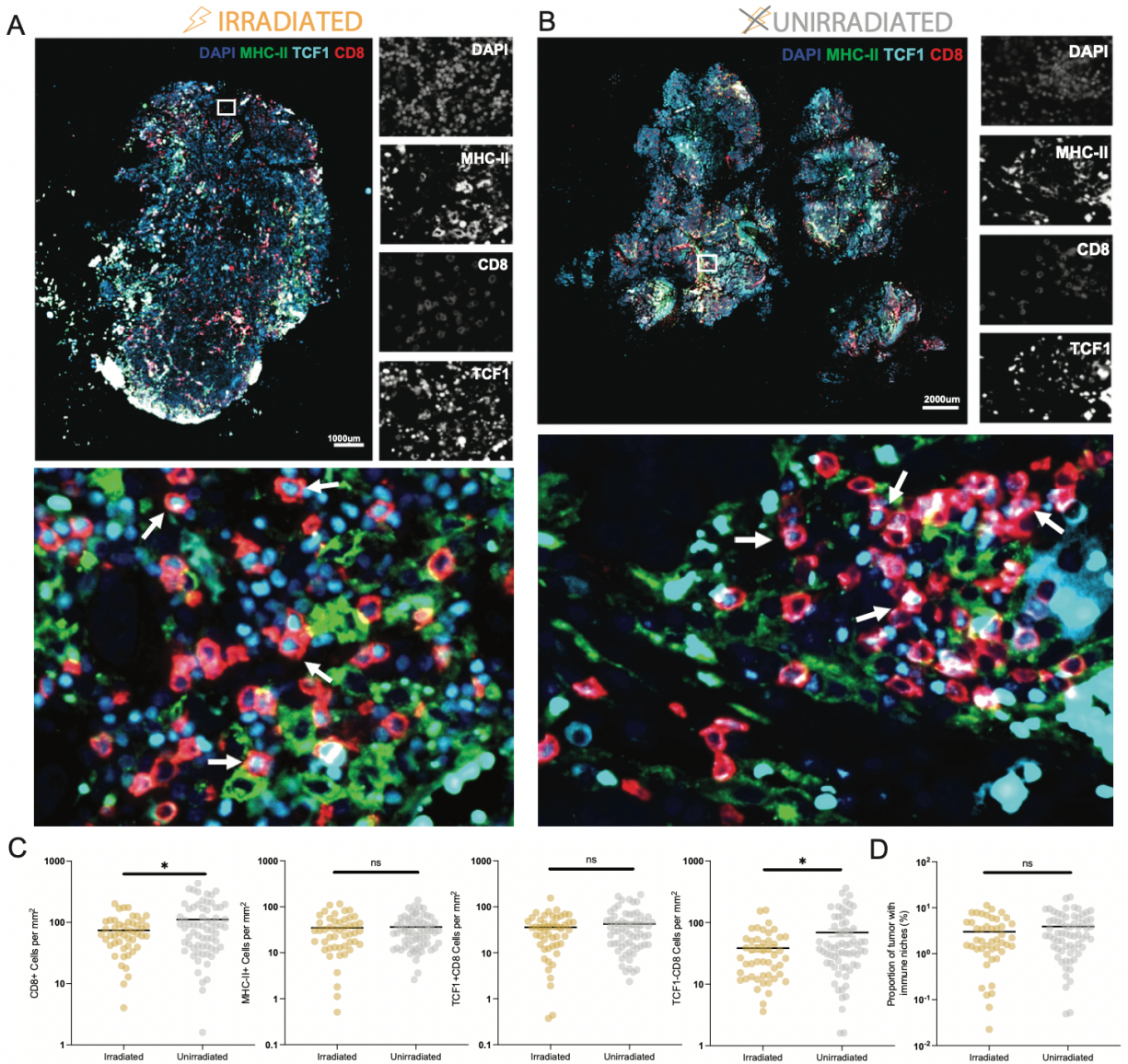


**Figure 3.10: Exposure to radiation therapy attenuates the CD8 T cell response, but TCF1+ stem-like cells, MHC-II+ cells, and immune niches persist.** (A) A whole slide scan of an irradiated brain metastasis sample immunofluorescence stained for MHC-II, TCF1, and CD8 and counterstained with DAPI is shown. Inset shows CD8, TCF1, MHC-II, and DAPI while merged image shows CD8, MHC-II, TCF1, and DAPI stains, with white arrows indicating selected examples of TCF1+ stem-like CD8 T cells. (B) A whole slide scan of an unirradiated brain metastasis sample immunofluorescence stained for MHC-II, TCF1, and CD8 and counterstained

with DAPI is shown. Inset shows CD8, TCF1, MHC-II, and DAPI while merged image shows CD8, MHC-II, TCF1, and DAPI stains, with white arrows indicating selected examples of TCF1+ stem-like CD8 T cells. (C) Comparison of CD8+ cells per mm<sup>2</sup> (p=0.0155), MHC-II+ cells per mm<sup>2</sup> (p=0.7759), TCF1+CD8+ cells per mm<sup>2</sup> (p=0.3403), and TCF1-CD8+ cells per mm<sup>2</sup> (p=0.0112), between irradiated (gold) and unirradiated (gray) samples. (D) Comparison of the proportion of tumor tissue occupied by immune niches between irradiated (gold) and unirradiated (gray) samples, (p=0.1500).

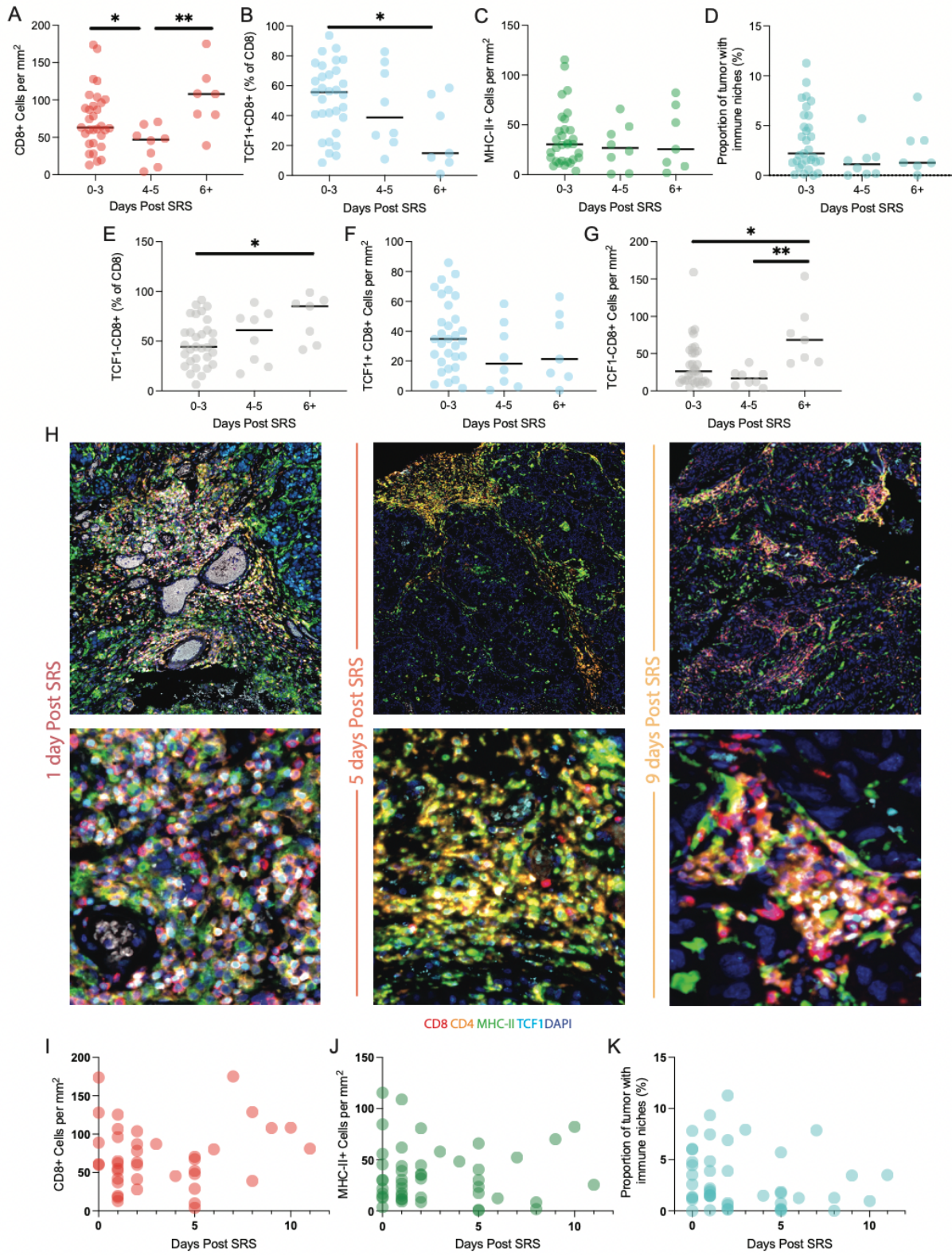


**Figure 3.11: The effect of timing between exposure to radiation therapy and surgical**

**resection on the immune response in brain metastases.** (A) Abundance of CD8<sup>+</sup> cells present in irradiated brain metastasis samples at 0-3, 4-5, or 6+ days following stereotactic radiosurgery (SRS), as measured by CD8<sup>+</sup> cells per mm<sup>2</sup>. \*p=0.0352, \*\*p=0.0039. (B) Proportion of CD8 T cells that are TCF1<sup>+</sup> present in irradiated brain metastasis samples at 0-3, 4-5, or 6+ days following stereotactic radiosurgery (SRS), as measured by percentage of CD8<sup>+</sup> cells that are TCF1<sup>+</sup>. \*p=0.0150. (C) Abundance of MHC-II<sup>+</sup> cells present in irradiated brain metastasis samples at 0-3, 4-5, or 6+ days following stereotactic radiosurgery (SRS), as measured by MHC-II<sup>+</sup> cells per mm<sup>2</sup>. (D) Proportion of tumor tissue occupied by immune niches in irradiated brain metastasis samples at 0-3, 4-5, or 6+ days following stereotactic radiosurgery (SRS). (E) Proportion of CD8 T cells that are TCF1<sup>-</sup> present in irradiated brain metastasis samples at 0-3, 4-5, or 6+ days following stereotactic radiosurgery (SRS), as measured by percentage of CD8<sup>+</sup> cells that are TCF1<sup>-</sup>. \*p=0.0150. (F) Abundance of TCF1<sup>+</sup> CD8<sup>+</sup> cells present in irradiated brain metastasis samples at 0-3, 4-5, or 6+ days following stereotactic radiosurgery (SRS), as measured by TCF1<sup>+</sup> CD8<sup>+</sup> cells per mm<sup>2</sup>. (G) Abundance of TCF1<sup>-</sup> CD8<sup>+</sup> cells present in irradiated brain metastasis samples at 0-3, 4-5, or 6+ days following stereotactic radiosurgery (SRS), as measured by TCF1<sup>-</sup> CD8<sup>+</sup> cells per mm<sup>2</sup>. \*p=0.0111, \*\*p=0.0027. (H) Immunofluorescence staining of irradiated brain metastasis samples from 1 day post SRS, 5 days post SRS, and 9 days post SRS, revealing the presence of aggregated immune infiltrates, or immune niches, at each time point. Top row shows larger areas of tissue, while the bottom row shows zoomed insets from the same region of tissue. Stains shown include CD8, CD4, MHC-II, TCF1, and DAPI. (I) The number of days between SRS and surgical resection plotted with abundance of CD8<sup>+</sup> cells present (as measured by CD8<sup>+</sup> cells per mm<sup>2</sup>) in irradiated brain metastasis samples in corresponding patients. (J) The number of days between SRS and surgical resection plotted with abundance of MHC-II<sup>+</sup> cells

present (as measured by MHC-II<sup>+</sup> cells per mm<sup>2</sup>) in irradiated brain metastasis samples in corresponding patients. (K) The number of days between SRS and surgical resection plotted with the proportion of tumor tissue occupied by immune niches in irradiated brain metastasis samples in corresponding patients.

presence was unchanged (Figure 3.10 C), suggesting that among the T cell populations present in the tumor, the TCF1<sup>+</sup> stem-like compartment may be less affected by radiation. Importantly, we also found that the proportion of the tumor tissue occupied by immune niches is maintained despite exposure to radiation (Figure 3.10 D), further positioning this immune niche and its contained elements as a more radioresistant component of tumor microenvironment.

We were next interested in whether the timing of radiation therapy would have an impact on the effect of this exposure on tumor immune infiltration and organization. Samples were broken into three groups: patients with 0-3 days, 4-5 days, or 6 or more days between radiation therapy and surgery (Figure 3.11 H). Interestingly the largest attenuation in the CD8 T cell response is seen in patients undergoing surgery at 4-5 days after radiation therapy, whereas this attenuation seems to recover by 6 or more days (Figure 3.11 A, I). Similarly, we see that the TCF1<sup>+</sup> cells make up the largest proportion of the T cell response in patients whose surgery most closely follows radiation therapy (Figure 3.11 B, F), whereas the overall T cell response is recovering and reducing this proportion by day 6 or more (Figure 3.11 E, G). Importantly, the presence of MHC-II<sup>+</sup> antigen presenting cells (Figure 3.11 C, J), and most especially, the proportion of tumor issue occupied by immune niches (Figure 3.11 D, K), is unchanged across the time points, again highlighting the relative radioresistance of this organizational phenomenon in tumor tissue.

### **3.4 Discussion.**

As the field of cancer immunology continues to burgeon, it is critically important to understand what mechanisms of the anti-tumor immune response are translatable across tumor types and what features may be more tumor or tissue type specific. Accordingly, after our studies in renal cell

carcinoma established the central role of TCF1<sup>+</sup> stem-like CD8 T cells, which reside in dense antigen presenting intratumoral immune niches, in sustaining the anti-tumor T cell response<sup>43</sup>, we next sought to determine whether this biology was also present in additional tumor types. In particular, we were also interested in probing for the presence of this biology in diverse tumor types, including those generally considered to be “immunologically cold” (e.g. prostate cancer) and those present in tissues generally considered to be “immunologically privileged” (e.g. brain metastases), with the reasoning that if this biology persists in these “difficult” cases, it may further cement its role as a cornerstone of the mechanisms of the anti-tumor immune response.

We began by examining prostate cancers and selected for a subset of highly immunogenic prostate cancer cases (i.e., those with most significant lymphocyte infiltration) in order to best examine the hallmarks of a significant and productive immune response in the setting of this tumor type. In these immunogenic cases, we were able to identify the presence of TCF1<sup>+</sup> stem-like CD8 T cells in the tumor tissue (Figure 3.1 A), and as in renal cell carcinoma, these stem-like CD8 T cells were found to reside in areas of high MHC-II<sup>+</sup> cellularity—that is, in dense, antigen-presenting immune niches (Figure 3.1 B). Interestingly, we did not find a difference in the abundance of these niches in pathologist-selected immunogenic prostate cancer cases and in MSI-High cases (Figure 3.1 C), suggesting that this organization of the intratumoral immune response may be a feature across tumors, regardless of the inciting stimulus for their immunogenicity. Accordingly, this could suggest that this biology may hold tremendous potential for therapeutic exploration.

We next turned to interrogating the landscape of the tumor immune microenvironment in brain metastases. By employing, customizing, and optimizing our highly quantitative

immunofluorescence imaging pipeline (Figure 3.2), we were able to demonstrate the presence of TCF1<sup>+</sup> stem-like CD8 T cells in these brain metastases samples, and we showed that these cells are present regardless of whether the tissue had been previously irradiated or not (Figure 3.3 A-C). These methods also allowed us to appreciate the presence of MHC-II<sup>+</sup> antigen presenting cells in tumor tissue (Figure 3.3 B, C), as well as correlate the size of the stem-like cell population with the magnitude of the overall CD8 T cell response, whereby the T cell response is proportional to the stem-like cell response, regardless of radiation exposure (Figure 3.3 D-F). Additionally, we further established the presence of these important TCF1<sup>+</sup> stem-like CD8 T cells the brain metastases by identifying and phenotyping the cells by flow cytometry (Figure 3.4), which again revealed the presence of these cells in both irradiated and unirradiated samples (Figure 3.5, Figure 3.6).

Further analysis established that these TCF1<sup>+</sup> stem-like CD8 T cells preferentially reside in areas of high MHC-II<sup>+</sup> cellular density (Figure 3.7 A, B) and are on average reside in closer proximity to their nearest antigen presenting cell neighbor than do their TCF1<sup>-</sup> counterparts (Figure 3.7 C). This, similar to what we observed in renal cell carcinoma and immunogenic prostate cancer, suggests that these TCF1<sup>+</sup> stem-like cells prefer to reside in dense, antigen-presenting immune niches in tumors, creating a functional immune outpost in the tumor that supports an ongoing, productive anti-tumor immune response (Figure 3.7 D), which when lost, corresponds to a parallel loss in the overall tumor immune response (Figure 3.8, Figure 3.9 A-C). Importantly, this functional biology is also clinically relevant, not just only in renal cell carcinoma as previously reported, but also in brain metastases, where the abundance of stem-like CD8 T cells or the proportion of tumor tissue occupied by immune niches is associated with improved local control

of brain metastases (Figure 3.9 D, E).

Interestingly, we found that the stem-like cells and these intratumoral immune niches represent a particularly radioresistant feature of the tumor immune microenvironment, whereas exposure to radiation therapy was noted to result in an attenuation of the overall CD8 T cell response, with the most pronounced effect in the TCF1- compartment (Figure 3.10). When investigating the effect of timing of radiation therapy on the anti-tumor immune response, while those tumors resected most closely following radiation had the most pronounced attenuation in the T cell response, the proportion of immune niches present in the tumor tissue was unchanged with respect to radiation exposure (Figure 3.11). These findings further position these immune niches (and the stem-like T cells therein) as an importantly radioresistant faction of the anti-tumor immune response. This may be a critical realization for layering multiple modalities of therapy, as this data reveals that it may be possible to take advantage of the immunostimulatory nature of radiation therapy, without decimating the immune cells already present and functioning in the tumor tissue. Especially as a sustained, strong intratumoral T cell response has been associated with both improved clinical outcomes and improved responses to immunotherapy, such as checkpoint blockade<sup>39-42</sup>, the realization that these all-important TCF1+ stem-like CD8 T cells and their immune niche homes can persist and thrive through radiation therapy may hold great potential for the strategic combination of multiple immune-stimulating treatment modalities, such as sequential administration of radiation therapy and immune checkpoint blockade.

In conclusion, the work discussed herein reveals the presence of TCF1+ stem-like CD8 T cells in diverse tumor types, including immunogenic prostate cancers and brain metastases of several

different cancer types. Importantly, in each of these settings, as we also reported in renal cell carcinoma<sup>43</sup>, these stem-like cells reside in dense, antigen presenting immune niches in tumor tissue, which serve as homes and reservoirs for those stem-like cells to both self-renew as well as differentiate into more terminally differentiated cells and mediate the tumor killing compartment of the anti-tumor T cell response. Thus, while there are numerous ways that the immunogenicity in a tumor can be established<sup>103</sup>, it seems that this level of organization—the intratumoral immune niche—is a central hallmark of immunologically active tumors and of a productive immune response, and if the mechanisms of this organization can be uncovered and therapeutically reproduced, we may unlock the ability to reliably convert an immunogenic stimulus to a sustained, productive anti-tumor immune response. Consequently, these findings not only reveal that this described immunobiology is translatable across tumor types, but also provide critical insight into avenues of further investigation that could lead to novel therapeutic strategies and into opportunities for intelligent design of combination therapeutic strategies, such as sequential radiation therapy and immune checkpoint blockade.

### **3.5 Materials & Methods.**

#### *Immunogenic Prostate Studies*

Tissue selection: In accordance with the U.S. Common Rule and after Institutional Review Board (IRB) approval, RP tissue (or biopsy cores alone in three cases) was collected retrospectively between 2007 and 2019 at Beth Israel Deaconess Medical Center (BIDMC, Boston, MA) and deidentified in accordance with BIDMC IRB protocol #2010-P-000254. Given previous findings of enriched PD-L1 expression and TILs among high-grade cases, we examined 115 total cases that

were GG 4–5 (50 cases), or had other National Comprehensive Cancer Network (NCCN) high-risk features (extracapsular extension or serum PSA >20 ng/dL; 54 cases). We identified 29 total cases (25% of screened cases) with tumor PD-L1 expression  $\geq 5\%$  by IHC; we included an additional three RP cases and three cases with only core biopsies available, all PD-L1–negative but with high TILs [ $\geq 20$  lymphocytes per high-power field (hpf)], forming a cohort of 35 total cases (30% of screened cases). These cases comprised the “immunogenic” cohort. Additional MSI-H cases were analyzed with multiplex panel described below.

IHC: Prostate tissue was fixed in formalin, processed, and embedded in paraffin using standard methods. For each case, the tissue block with the largest dimensions of the dominant tumor plus two or three additional blocks were selected for PD-L1 and CD3 IHC. Additional details are presented in online Supplementary Methods.

Immunogenicity criteria: Immunogenicity was defined as PD-L1 moderate to strong membranous staining in  $\geq 5\%$  of tumor cells; cytoplasmic staining was not considered. High density of TILs, defined as  $\geq 20$  lymphocytes per hpf either present within the tumor cell nests or glands or immediately adjacent to tumor cells (i.e., distance between the lymphocyte and its nearest tumor cell being less than the diameter of an average tumor cell), was used to include six PD-L1–negative cases. All immunostains were evaluated by an experienced pathologist (H. Ye) and a trained MD investigator (C. Calagua).

Multiplex IF analysis: The multiplex IF panel consisted of a previously described panel of antibodies to CD8, PD-1, TCF1, and MHC II, and DAPI counterstaining<sup>43</sup> (Table 3.1).

*Brain Metastases Studies*

Patients: Records of patients treated at two institutions (Emory University and the Levine Cancer Institute) between 2007-2016 were evaluated and reviewed. Data were de-identified according to the Health Insurance Portability and Accountability Act, and all investigation was performed in accordance with the relevant guidelines and regulations. Informed consent was obtained for tissue sample banking; informed consent for this study was waived by the Institutional Review Board that approved the study protocol.

FFPE Samples: Formalin fixed paraffin embedded tissue samples from these patients were stained and analyzed. Unirradiated samples were obtained from the Emory Brain Tumor Bank, and irradiated samples were acquired from the Levine Cancer Institute.

Histology Sample preparation: Sections were deparaffinized in successive incubations with xylene and decreasing concentrations (100, 95, 75, 50, 0%) of ethanol. Antigen retrieval was achieved using Abcam 100x TrisEDTA Antigen Retrieval Buffer (pH = 9) heated under high pressure. Sections were then washed in PBS + 0.1% Tween20 before antibody staining.

Immunofluorescence antibody staining was done using two different techniques: (1) Sections were blocked for 30 min with 10% goat serum in 1x PBS + 0.1% Tween20. Sections were then stained with appropriate primary and secondary antibodies. Primary antibodies were used at a concentration of 1:100 (MHC-II) or 1:150 (CD8, TCF1) and incubated for 1 h at room temperature. Secondary antibodies were used at a concentration of 1:250 (A488, A568) or 1:500 (A647) and

incubated for 30 min at room temperature. Detailed information about antibodies used is listed in Table 3.2. Sections were counterstained with DAPI according to manufacturer instructions (Thermo-Fisher). (2) Using the Opal 7-color IHC kit (Akoya Biosciences) endogenous peroxidase activity was quenched by microwave treatment of the slides with AR buffer. Non-specific binding was blocked with blocking/Ab diluent. After incubation with the primary antibody, the slides were incubated with HRP Ms+Rb secondary antibody and then incubated in the appropriate opal fluorophore for 10 minutes, until staining developed. The slides were finally counterstained with DAPI.

Image capture and analysis: The selected fluorophore panel (1) allowed for simultaneous visualization of three targets and a nuclear stain (DAPI) using a Zeiss Z.1 Slide Scanner equipped with a Colibri 7 Flexible Light Source. Zeiss ZenBlue software was used for post-acquisition image processing. Slides stained with the Opal IHC Kit (2) were scanned using a Perkin Elmer Vectra Polaris. For brightfield imaging, slides were scanned using a Hamamatsu's Nanozoomer slide scanner. Images were analysed using CellProfiler and custom R and python scripts, as previously described<sup>43</sup>. Statistical analysis was carried out using GraphPad Prism 9. Mann-Whitney tests were used to compare unpaired, non-parametrically distributed samples. Simple linear regression was used to evaluate for correlations between variables.

Fresh human sample collection, processing and flow staining: brain metastasis samples were collected after patients underwent craniotomy and surgical resection. Samples were collected direction after resection into Phosphate Buffered Saline. They samples were then processed by getting cut into small pieces, digested with a MACS enzyme cocktail, and then homogenized using

a MACS Dissociator. Digested tumor was washed then through a 70um filter to get a single cell suspension. Samples were then frozen in freezing media (FBS + 10% DMSO) at -80C.

Single cell suspensions from processed human tumor samples were stained with antibodies from Table 3.3. Live/dead staining was done using fixable near-IR or aqua dead cell staining kit (Invitrogen). Cells were permed using the FOXP3 Fixation/Permeabilization kit (eBioscience) for 45 minutes with fixation/permeabilization buffer at 4C and stained with intracellular antibodies in permeabilization buffer for 30mins at 4C. Samples were acquired on a BD Symphony cytometer and analyzed using Flowjo (v10).

### **3.6 Acknowledgements**

#### *Immunogenic Prostate Studies*

The authors gratefully acknowledge the patients and the families of patients who contributed to this study. We wish to acknowledge Ying Huang, PhD and the Molecular Pathology Core Lab at Dana-Farber Cancer Institute for providing multiplex IF on unselected prostatectomy samples, Yue Sun, MD at Beth Israel Deaconess Medical Center for pathology support, and Kai Wucherpfennig, MD, PhD at Dana-Farber Cancer Institute for scientific advice and review of data. Portions of this work utilized the computational resources of the NIH HPC Biowulf cluster. This work was supported by the Intramural Research Program of the NIH, NCI (to A.G. Sowalsky); a PCF Challenge Award 18CHAL09 (to S.P. Balk, D.J. Einstein, H. Ye); NCI grants 1-F30-CA-243250 (to C.S. Jansen), P50 CA090381 (to S.P. Balk), and Developmental Research Project P20 CA233255 (to S.P. Balk and D.J. Einstein); and Department of Defense Awards W81XWH-17-1-0350 (to D.J. Einstein) and W81XWH-16-1-0431 (to A.G. Sowalsky and S.P. Balk).

*Brain Metastases Studies*

C.S.J is supported by a National Cancer Institute grant (1-F30-CA-243250). Z.B. is supported by a National Cancer Institute grant (1-K12-CA-237806-01).

**3.7 Tables****Table 3.1 Immunofluorescence Antibodies**

<b>Target</b>	<b>Antibody Type</b>	<b>Clone</b>	<b>Concentration</b>	<b>Secondary</b>	<b>Concentration</b>
MHC-II (HLA-DR, DP, DQ)	Mouse IgG2a	Tu39	1:100	Goat anti-mouse IgG2a A488	1:250
TCF1	Rabbit	C63D9	1:150	Goat anti-rabbit A568	1:250
CD8	Mouse IgG1	C8/144B	1:150	Goat anti-mouse IgG1 A647	1:250

**Table 3.2 Immunofluorescence Antibodies**

Target	Antibody Type	Clone	Concentration	Secondary
MHC-II (HLA-DR, DP, DQ)	Mouse IgG2a	Tu39	1:100 or 1:50	Goat anti-mouse IgG2a A488 or Opal520
TCF1	Rabbit	C63D9	1:150 or 1:100	Goat anti-rabbit A568 or Opal620
CD8	Mouse IgG1	C8/144B	1:150 or 1:500	Goat anti-mouse IgG1 A647 or Opal570
PD1	Mouse IgG2	EH33	1:50	Opal480

**Table 3.3 Flow Cytometry Antibodies**

Antibody	Fluorochrome	Catalog number	Clone
CD4	BUV496	BD 750980	OKT4
CD8	BUV661	BD 750699	RPA-T8
PD-1	BUV737	BD 612791	EH12.1
CD39	BV421	328214	A1
CD45RA	BV510	304142	HI100
CD3	PerCP-Cy5.5	300430	UCHT1
Tim3	PE	R&D FAB2365P	344823
CD28	BUV395	BD 740308	CD28.2
CD127	PE-Cy7	Biologend 351320	A019D5
CCR7	BV785	Biologend 353230	G043H7
HLA-DR	BV605	Biologend 307640	L243
GranzymeB	A700	BD 560213	GB11
TCF-1	AF488	Cell signaling 6444S	C63D9
Ki67	BV711	Biologend 350516	Ki67
CD69	BV650	Biologend 310934	FN50
FOXP3	PE-Dazzle 594	Biologend 320126	206D
TOX	eFluor 660	Invitrogen 50-6502-82	TXR10

## **Chapter 4: Clinical outcomes following immunotherapy in renal cell carcinoma patients is associated with a pre-existing immune response in tumor tissue**

### **4.1. Introduction**

Renal cell carcinoma has long been noted as an immunogenic tumor, and historically, immunotherapy treatment regimens available to these patients included high dose IL2, which provides objective responses in nearly 20% of patients, but at the cost of substantial toxicity<sup>104, 105</sup>. More recently, immune checkpoint blockade, such as anti-PD1 and anti-PDL1 based therapies, have become common choices for treatment of patients with advanced clear cell renal cell carcinoma, with recent clinical trials leading to FDA approval and breakthrough therapy designations for use of combination tyrosine kinase inhibitor + checkpoint blockade as frontline therapeutic options<sup>106-112</sup>. In addition, the use of checkpoint blockade for resectable renal cell carcinomas at a high risk of recurrence was recently approved in the adjuvant setting, and similar investigations in the neoadjuvant setting are ongoing<sup>113</sup>.

Despite these recent successes and promising pending investigations, the use of immune checkpoint blockade is accompanied by significant risk of on-target off-tumor (immune-mediated) adverse events, and many patients may fail to respond to these therapies, despite their promising successes for other patients. Interestingly, while some biomarkers of response to immunotherapy have been identified in other tumor types and have enabled enhanced patient selection, such as PD-L1 expression, tumor mutation burden, or MSI status, these strategies have not enriched for responders in renal cell carcinoma<sup>56, 57</sup>. Accordingly, enhanced understanding of the mechanisms of the response to immunotherapy in renal cell carcinoma is desperately needed, and biomarkers

of the effective response to checkpoint blockade are vital to improving patient selection and improving treatment options for patients with high risk or advanced renal cell carcinoma.

More than a decade of use of immune checkpoint blockade in human patients has resulted in a great deal of discovery of various features of immune response that may correlate with therapeutic outcomes, and more specifically, it has been reported that several features of CD8 T cells can predict how patients respond to therapy. For example, increased expression of Ki67 in CD8 T cells in the peripheral blood is associated with improved clinical responses in melanoma and lung cancer<sup>114-122</sup>, Other recent reports investigating the TCR repertoire of CD8 T cells in the blood have suggested that the entrance of new TCR clonotypes in the blood following immunotherapy may be associated with improved survival in several tumor types<sup>123-125</sup>. Taken together, these studies reveal that dynamic immune changes seem to suggest that these proliferating CD8 T cells, which are associated with improved clinical outcomes, may be newly activated or recently re-activated clones that were previously dormant<sup>126</sup>.

In addition to rapid and dynamic changes in the CD8 T cell response in the peripheral blood, studies have associated CD8 T cell infiltration in tumor tissues with improved patient survival and response to immune checkpoint blockade<sup>27, 31, 37, 39, 52, 53</sup>. For example, initial work to this effect was shown in melanoma, where it was reported that patients with higher CD8 T cell infiltration into tumor tissue at the time of therapy were more likely to glean clinical benefit from therapy, and analogous findings have subsequently been reported in additional tumor types<sup>37, 39, 44, 45, 52, 127</sup>.

Furthermore, recent studies have identified that there is a subset of CD8 T cells in the tumor that

are central to the mechanism behind clinical efficacy of immune checkpoint blockade. This subset of T cells, stem-like CD8 T cells, is characterized by expression of the transcription factor TCF1+, which we have reported to be critical for maintaining the anti-tumor T cell response in treatment naïve renal cell carcinoma<sup>43</sup> and others have correlated with response to checkpoint blockade in melanoma<sup>44-48</sup>. Together, this illustrates that there is a common thread across tumor types that underlies the disparities of the response to immune checkpoint blockade. Some patients generate a strong T cell response that opposes tumor growth and progression, either endogenously or following immune checkpoint blockade, but others fail to do so, and the maintenance of TCF1+ stem-like CD8 T cells in tumor tissue seems to be one factor in delineating which patients can mount significant anti-tumor T cell responses and which responses may fail<sup>43</sup>. Accordingly, we sought to study the response to immune checkpoint blockade in renal cell carcinoma patients, and more specifically, how the pre-existing intratumoral T cell response supports the later response to immune checkpoint blockade.

## **4.2 Results.**

*TCF1+ stem-like CD8 T cells are identified in archived tumor samples by both immunofluorescence and flow cytometry in RCC patients receiving immunotherapy*

Having identified that TCF1+ stem-like CD8 T cells in renal tumors support a strong CD8 T cell response, which predicts improved patient survival, and having identified that the presence of these stem-like cells in intratumoral immune niches in not only renal tumors, but also prostate tumors and brain metastases, we then wondered if the presence and organization of these stem-like cells

in tumor tissue would affect the clinical response to immune checkpoint blockade.

In a cohort of patients with renal cell carcinoma who went on to receive immune checkpoint blockade following disease progression, we identified archival samples (FFPE blocks and/or fresh frozen tumor tissue) from the patient's resected primary tumor specimen (FFPE cohort: Table 1, fresh frozen cohort: Table 2). As shown in the schematic in figure 4.1 A, these patients underwent partial or radical nephrectomy prior to receiving any systemic therapy. These patients were then monitored for disease recurrence or progression, and then when clinically indicated, received immune checkpoint blockade. Importantly, in these treatment-naïve patients, the latency between surgical resection and initiation of immune checkpoint blockade may constitute months, or in some cases, even years.

In these patient cohorts, we set out to confirm the presence and organization of TCF1+ stem-like CD8 T cells in immune niches in tumor tissue, in both fresh frozen and FFPE tumor samples acquired from surgical resection, as we had previously described in renal cell carcinoma<sup>43</sup>. In Figure 4.1 B, we show how these stem-like CD8 T cells in the tumor are identified by flow cytometry in fresh frozen tumor samples. In Figure 4.2 C-D, we show how phenotypic highlights of these stem-like CD8 T cells, where similar to as previously shown<sup>43</sup>, where stem-like cells have high costimulatory molecule expression, while more terminally differentiated cells have higher checkpoint molecule expression.

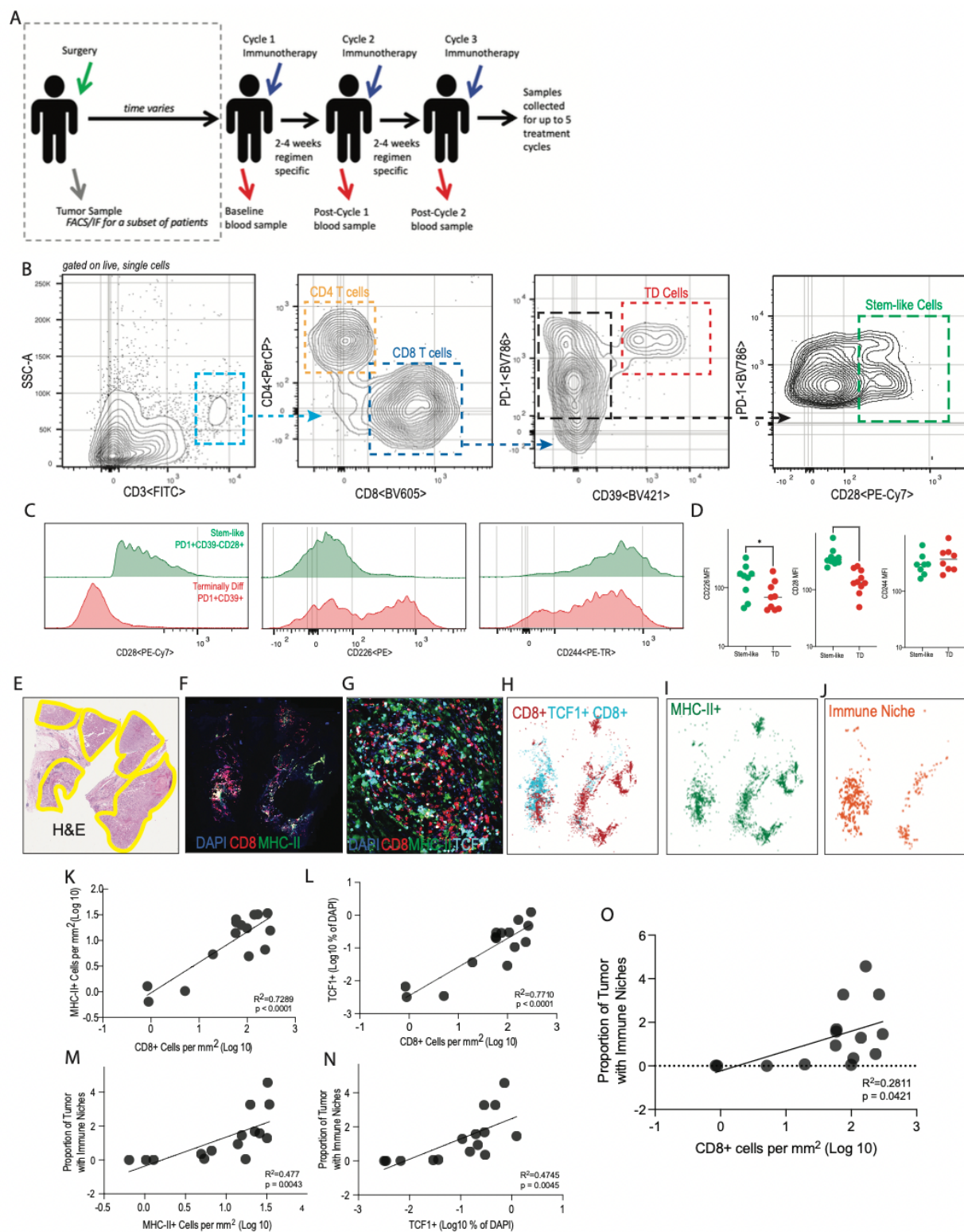


**Figure 4.1: Identification of TCF1+ stem-like CD8 T cells in renal cell carcinoma tumors by**

**flow cytometry and quantitative immunofluorescence imaging.** (A) Study design follows renal cell carcinoma patients throughout disease course, from surgical resection through the reception of immune checkpoint blockade. Tumor samples (FFPE & fresh frozen tissue) were used, and blood was collected at baseline and at each treatment interval. (B) Flow cytometry gating strategy for identifying stem-like CD8 T cells and terminally differentiated CD8 T cells in renal cell carcinoma samples. (C) Flow cytometry-based measurement (mean fluorescence intensity) of selected phenotypic markers on stem-like CD8 T cells (green) and terminally differentiated CD8 T cells (red). (D) Summary data for markers show in C. (E) Renal cell carcinoma sample stained with hematoxylin & eosin and brightfield scanned. Area of tumor tissue outlined in yellow. (F) Renal cell carcinoma sample immunofluorescence stained for CD8, MHC-II, and counter stained with DAPI and fluorescence-scanned. (G) Zoomed inset of whole slide scan of a renal cell carcinoma sample immunofluorescence shown in F, stained for MHC-II, TCF1, and CD8 and counterstained with DAPI. (H-J) A set of three immunomaps, with (H) the x,y location of CD8 T cells shown in red, with the location of TCF1+ CD8 T cells overlaid in cyan, (I) the x,y location of MHC-II+ cells in green, and (J) the local cellular neighborhoods (approximately  $10,000\mu\text{m}^2$ ) occupied by immune niches (orange), which are defined by areas where both TCF1+ CD8 T cells and MHC-II+ cells associate. (K) Correlation between MHC-II+ cell and CD8+ cell infiltration, as measured per  $\text{mm}^2$  ( $R^2=0.7289$ ,  $p<0.0001$ ). (L) Correlation between CD8+ cell infiltration, as measured per  $\text{mm}^2$ , and the proportion of TCF1+ cells (as a percentage of all DAPI+ cells,  $R^2=0.7710$ ,  $p<0.0001$ ). (M) Correlation of the proportion of the tumor occupied by immune niches with the MHC-II+ cell infiltration (as measured per  $\text{mm}^2$ :  $R^2=0.477$ ,  $p=0.0043$ ). (N) Correlation of the proportion of the tumor occupied by immune niches with specifically TCF1+ CD8+ cell infiltration (as measured a percentage of DAPI+ cells:  $R^2=0.4745$ ,  $p=0.0045$ ). (O) Correlation of

the proportion of the tumor occupied by immune niches with the CD8<sup>+</sup> cell infiltration (as measured per mm<sup>2</sup>:  $R^2=0.2811$ ,  $p=0.0421$ ).

We were also able to identify these TCF1<sup>+</sup> stem-like CD8 T cells in intratumoral immune niches by multiplex, quantitative immunofluorescence imaging analysis (similar to as described in Chapters 2 & 3). Adjacent whole slide scans show (Figure 4.1 E) an H&E stain and (Figure 4.2 F) an immunofluorescence stain of a renal cell carcinoma tumor sample, with a zoomed immunofluorescence inset showing the presence of TCF1<sup>+</sup> stem-like CD8 T cells in close association with MHC-II<sup>+</sup> antigen presenting cells (Figure 4.1 G). Using our quantitative imaging analysis methods, we also define the precise locations of all CD8<sup>+</sup> cells in the tumor issue, as well as specify the location of each TCF1<sup>+</sup> stem-like CD8 T cell in the tumor (Figure 4.1 H) and the location of all infiltrating MHC-II<sup>+</sup> antigen presenting cells in the tumor (Figure 4.1 I). Importantly, we can also use this analysis to define which areas contain intratumoral immune niches—that is, local cellular neighborhoods where both TCF1<sup>+</sup> stem-like CD8 T cells and MHC-II<sup>+</sup> antigen presenting cells reside (Figure 4.1 J).

Importantly, as we have shown previously in renal cell carcinoma, immunogenic prostate cancer, and brain metastases, we show that the T cell infiltration into these renal tumors parallels the antigen presenting cell infiltration (Figure 4.1 K), and that this T cell infiltration is supported by a parallel presence of specifically TCF1<sup>+</sup> stem-like CD8 T cells (Figure 4.1 L). We also show that the antigen presenting cell density and the abundance of tumor infiltrating TCF1<sup>+</sup> stem-like cells correlates with proportion of the tumor tissue occupied by immune niche neighborhoods (Figure 4.1 M, N). Most critically, those tumors with the highest proportion of immune niches are also those with the strongest CD8 T cell response (Figure 4.1 O), recapitulating, as we have shown before, that these niches are a vital ingredient in maintaining and sustaining a productive anti-tumor T cell response.

*Pre-existing anti-tumor immunity is an important predictor of later immunologic and clinical response to checkpoint blockade*

We next investigated whether the presence of these stem-like T cells and these immune niches might correlate with clinical outcomes after reception of immune checkpoint blockade. In Figure 4.2, we compare two patients with contrasting outcomes – one patient who responded well, having a complete response with no evidence of active disease (Figure 4.2 A), and one patient who progressed quickly despite immune checkpoint blockade administration (Figure 4.2 B). In the responding patient, quantitative analysis of whole slide immunofluorescence imaging reveals many areas of CD8<sup>+</sup> T cell, and specifically TCF1<sup>+</sup> CD8<sup>+</sup> T cell, infiltration (red, blue, respectively), many areas of MHC-II<sup>+</sup> cell infiltration (green), and importantly, many areas of immune niches (orange), where both TCF1<sup>+</sup> CD8<sup>+</sup> cells and MHC-II<sup>+</sup> cells colocalize (Figure 4.2 A). On the other hand, in the patient with progressive disease, the tumor tissue lacks this same level of immune cellularity, with very few areas of infiltrating CD8<sup>+</sup> T cells, very few areas of infiltrating MHC-II<sup>+</sup> cells, and critically, a near to total absence of areas of immune niches (Figure 4.2 B).

Interestingly, this pattern of infiltration parallels what we observe by flow cytometry in these two patients, both in the surgically resected tumor tissue, as well as in the peripheral blood following reception of immunotherapy. In the responding patient, there a strong T cell response in the resected tumor tissue, whereas in the progressing patient, there is a near total absence of CD8 T cell infiltration (Figure 4.2 C). Similarly, there is a significant burst in activated CD8 T cells (as identified by HLA-DR and CD38 co-expression) in the peripheral blood following administration

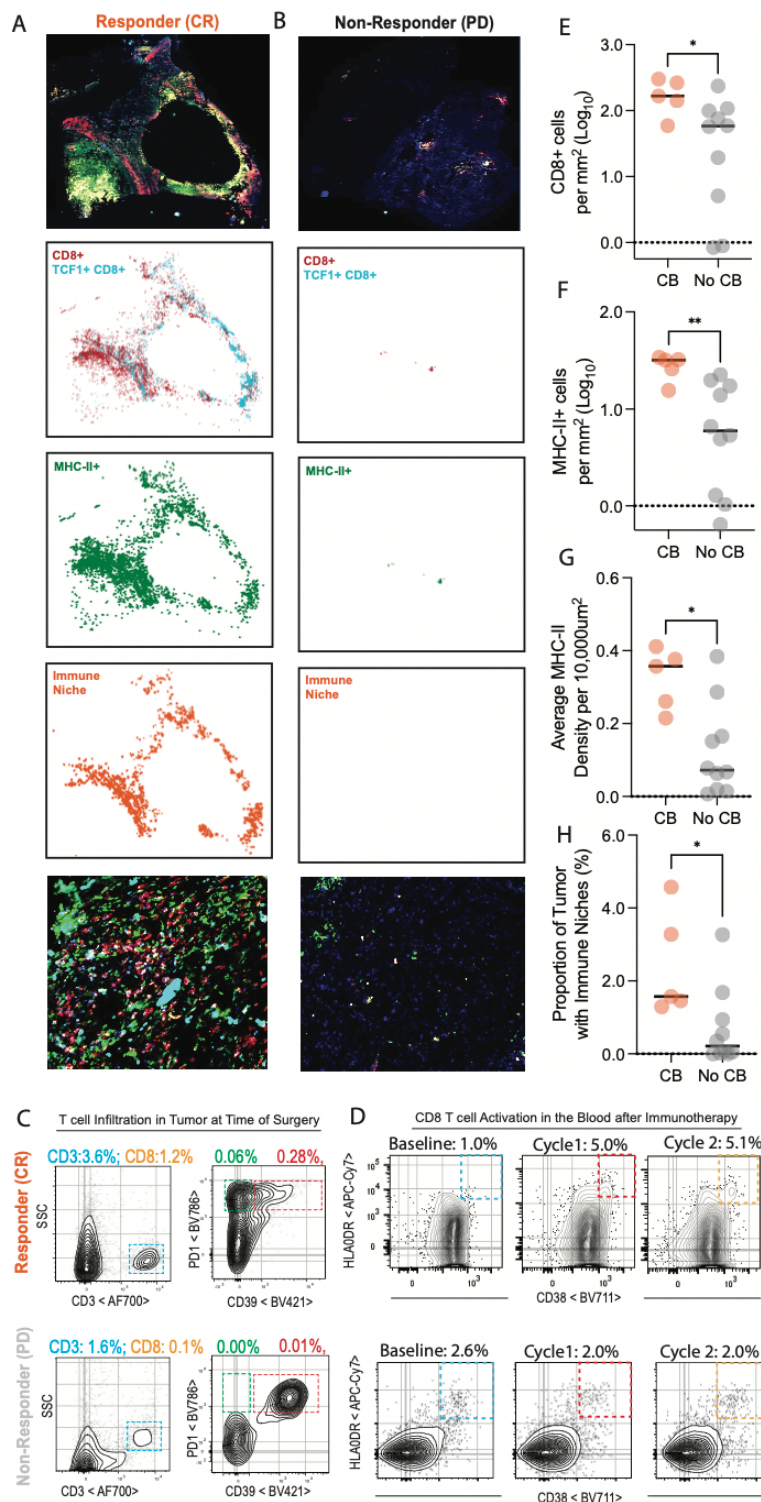


**Figure 4.2: Presence TCF1+ stem-like CD8 T cells in intratumoral immune niches is associated with clinical benefit following immune checkpoint blockade. (A-B) Comparison of a responding patient (A) and non-responding patient (B). From top to bottom, tumor sample**

immunofluorescence stained for CD8 (red), MHC-II (green), TCF1 (cyan) and counterstained with DAPI (blue) and fluorescence slide-scanned. A set of three immunomaps, with (1) the x,y location of CD8 T cells shown in red, with the location of TCF1+ CD8 T cells overlaid in cyan, (2) the x,y location of MHC-II+ cells in green, and (3) the local cellular neighborhoods (approximately  $10,000\mu\text{m}^2$ ) occupied by immune niches (orange), which are defined by areas where both TCF1+ CD8 T cells and MHC-II+ cells associate. At bottom, zoomed insets of whole slide scans, stained for MHC-II (green), TCF1 (cyan), and CD8 (red), and counterstained with DAPI (blue). (C) Flow cytometry showing comparative T cell infiltration, including stem-like CD8 T cells (green) and terminally differentiated T cells (red) in a responding patient (top) and a non-responding patient (bottom). (D) Flow cytometry highlighting the activated CD8 T cell population in the peripheral blood at baseline, after cycle 1, and after cycle 2 of immune checkpoint blockade in a responding patient (top) and a non-responding patient (bottom). (E) Patients with clinical benefit (CB) have more CD8+ cells per  $\text{mm}^2$  than patients without clinical benefit (no CB), ( $p=0.0280$ ). (F) Patients with clinical benefit (CB) have more MHC-II+ cells per  $\text{mm}^2$  than patients without clinical benefit (no CB), ( $p=0.0047$ ). (G) Patients with clinical benefit (CB) have higher average MHC-II+ cellular density per  $10,000\mu\text{m}^2$  than patients without clinical benefit (no CB), ( $p=0.0193$ ). (H) Patients with clinical benefit (CB) have a higher proportion of tumor tissue occupied by immune niches than patients without clinical benefit (no CB), ( $p=0.0186$ ).

of immune checkpoint blockade, when compared to a baseline, pre-treatment sample, whereas this burst in activated cells is absent in the progressing patient (Figure 4.2 D). Taken together, this suggests that pre-existing features of a strong T cell response in the tumor – the presence of many CD8 T cells, maintained by TCF1<sup>+</sup> stem-like in dense antigen presenting niches – may lead to a strong T cell response following immunotherapy, which corresponds with positive clinical outcomes.

This patterns are validated when investigated across multiple patients, when we compare these metrics at the cohort level, where patients with clinical benefit following reception of immune checkpoint blockade harbor increased CD8 T cell and MHC-II<sup>+</sup> antigen presenting cell infiltration (Figure 4.2 E, F), increased MHC-II<sup>+</sup> antigen presenting cell density (Figure 4.2 G), and importantly (Figure 4.2 H), increased levels of intratumoral immune niches when compared to patients without clinical benefit. This further underscores the importance of the TCF1<sup>+</sup> stem-like CD8 T cell, and its home in an intratumoral immune niche, in sustaining the pre-existing immune response to immune checkpoint blockade, which in turn underlies the clinical response to this therapy and mediates positive patient outcomes.

*Pre-existing anti-tumor T cell response is associated with clinical response to immunotherapy*

Having seen that described the importance of the pre-existing anti-tumor immune response by quantitative immunofluorescence imaging analysis, we sought to investigate this concept in a larger cohort, utilizing flow cytometry on fresh frozen banked tumor samples. Using flow cytometry, we can enumerate tumor infiltrating CD8 T cells, and we show that patients with progressive disease following reception of immunotherapy have lower CD8 T cell abundance than

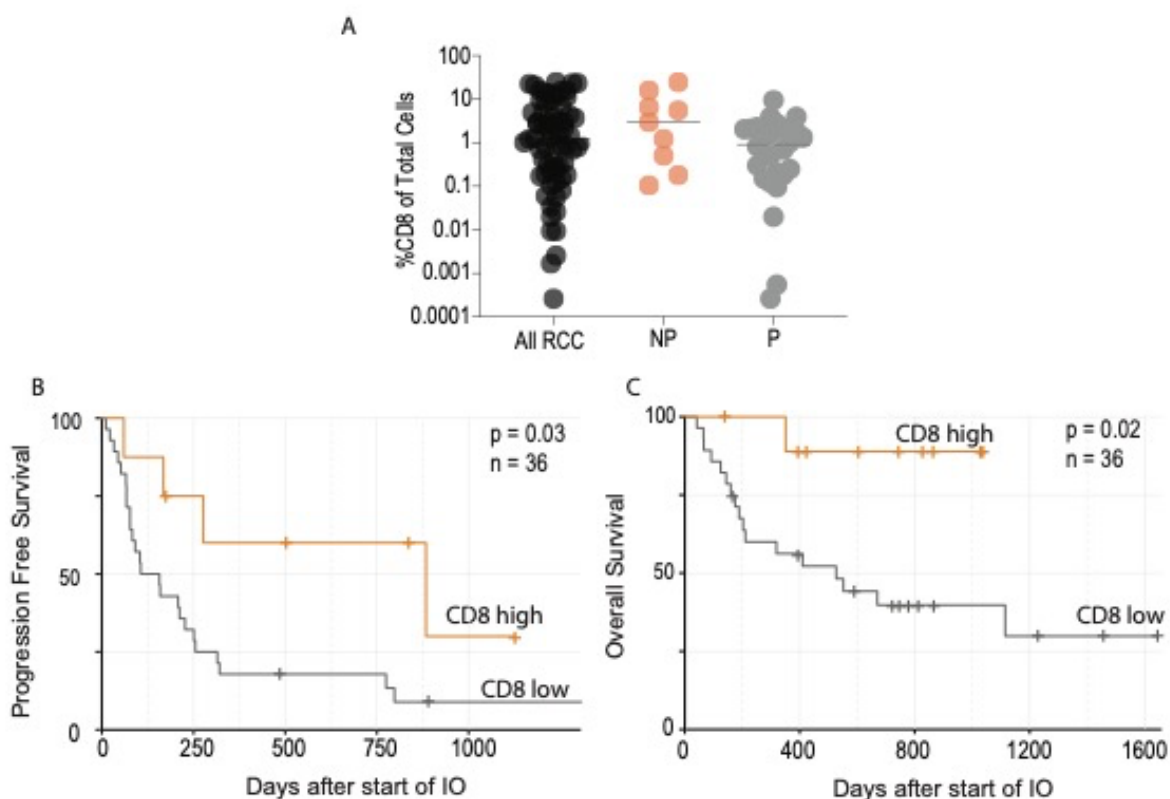


**Figure 4.3 Increased intratumoral infiltration of CD8 T cells is associated with improved progression free and overall survival in renal cell carcinoma patients following immune checkpoint blockade.** (A) Patients with progressive disease have attenuated CD8 T cell infiltration when compared with patients without progressive disease. (B) Patients with higher CD8 T cell infiltration (measured by flow cytometry, as % of total cells) have improved progression free survival as compared to those with lower CD8 T cell infiltration. (C) Patients with higher CD8 T cell infiltration (measured by flow cytometry, as % of total cells) have improved overall survival as compared to those with lower CD8 T cell infiltration.

those patients without progressive disease after immune checkpoint blockade (Figure 4.3 A). Most importantly, patients with increased abundance of CD8 T cells in the tumor tissue at the time of resection—so a stronger pre-existing anti-tumor T cell response—have improved both progression free and overall survival following immune checkpoint blockade (Figure 4.3 B, C). Taken together, this illustrates the crucial role of a pre-existing T cell response, supported by TCF1<sup>+</sup> stem-like CD8 T cells, in the tumor tissue in supporting the later immunologic and clinical response to immunotherapy.

### **4.3 Discussion.**

With our prior work having detailed critical hallmarks of the intratumoral immune response in several tumor types, this study endeavored to examine how these biological mechanisms might be relevant to the immunologic and clinical response to immunotherapy. To do so, we analyzed the both the intratumoral immune response at the time of surgery, as well as the peripheral blood response and clinical response following reception of immune checkpoint blockade (Figure 4.1 A). With this study design, we can use both flow cytometry (Figure 4.1 B-D) and quantitative immunofluorescence imaging (Figure 4.1 E-J) to identify TCF1<sup>+</sup> stem-like CD8 T cells within tumor tissue. With this quantitative imaging analysis, we can characterize these stem-like cells' preferential localization to antigen presenting cell-dense immune niches in the tumor tissue, and demonstrate that the parallel infiltration of MHC-II<sup>+</sup> cells and TCF1<sup>+</sup> stem-like CD8 T cells, and their aggregation into immune niches, supports the maintenance of a strong and productive anti-tumor T cell response (Figure 4.1 H-O).

Importantly, the design of this study allows us track features of a patient's immune response

throughout their entire disease course, beginning at the time of surgery and continuing through the administration of immune checkpoint blockade. Accordingly, it allows us to ask critical questions about whether a patient's intrinsic ability to mount a strong anti-tumor T cell response has bearing on their later propensity to glean clinical benefit from immunotherapy. When we compare patients with disparate clinical outcomes (Figure 4.2 A-D), we can appreciate significant differential between the immune infiltration in a patient with a good clinical outcome (complete response) and one that unfortunately did not (progressive disease). In a patient with clinical benefit (Figure 4.2 A, C-D), we find a strong, intrinsic, intratumoral immune response at the time of surgery, both by flow cytometry and immunofluorescence imaging, that parallels a strong burst of T cell activation in the peripheral blood following immunotherapy. On the contrary, a patient with progressive disease (Figure 4.2 B-D) is found to profoundly lack this same strength of intrinsic immune response, both at in the tumor at the time of surgery and in the peripheral blood following reception of immune checkpoint blockade.

Importantly, these concepts are replicated at the cohort level, where we see that patients experiencing clinical benefit following immune checkpoint blockade are found to have significantly higher levels of immune cell infiltration (specifically, CD8 T cell and MHC-II+ antigen presenting cell, Figure 4.2 E & F), higher levels of MHC-II+ cell density (Figure 4.2 G), and critically, higher proportions of immune niches in the tumor tissue at the time of surgery (Figure 4.2 H), suggesting that a patient's intrinsic ability to mount an anti-tumor immune response may predict their later ability to mount a productive and clinically beneficial response to immunotherapy. Finally, we sought to generalize these findings by measuring simply the CD8 T cell infiltration into tumors at the time of surgery. We find that patients experiencing clinical

benefit have higher CD8 T cell infiltration into their tumors at the time of surgery. Most significantly, we show that stratifying patients into CD8 hi and CD8 low, based on the flow cytometry measurement of the CD8 T cell infiltration into their tumor at the time of surgery, can predict improved both progression free survival and overall survival in renal cell carcinoma patients following administration of immune checkpoint blockade.

In summary, while others have reported an association with tumor infiltrating T cells or with a burst of T cell activation and the response to immunotherapy in isolation and in other tumor types<sup>114, 115, 124, 128</sup>, our studies have drawn a connection between all three of these responses and have specifically shown the importance of these features of the immune response in renal cell carcinoma. Put differently, we show that the intrinsic immunobiology at the time of surgery has an enduring impact on the later immunological and clinical response to immune checkpoint blockade.

Furthermore, we propose that these studies add crucial details to understanding the cellular mechanisms controlling the T cell response to immune checkpoint blockade. The TCF1+ CD8 T cells we describe here and previously are likely those that also proliferate in response to immune checkpoint blockade<sup>46, 67, 68</sup>. When these stem-like cells encounter therapies such as anti-PD1 antibodies, they proliferate, but most importantly give rise to the more terminally differentiated, cytotoxic, effector-like CD8 T cells that are the ones directly responsible for the clearance of tumor cells. Thus, based on these prior studies and the data resultant from our studies, we hypothesize that prior to immunotherapy administration of immunotherapy, there may a pool of tumor specific TCF1+ stem-like CD8 T cells lying dormant that are then unleashed by immune checkpoint

blockade. When re-awakened and unleashed, we propose that these cells, representing a critical biological reservoir, may then proliferate and generate anti-tumor cytotoxic cells. Importantly, it is unclear if these dormant TCF1<sup>+</sup> cells are only present in the tumor, or if the ones unleashed by immune checkpoint blockade to generate a peripheral burst in activated T cells may be preferentially located outside the tumor, such as in draining lymph nodes, and this is a critical question for future study. Based on this hypothesis, we propose that patients with a strong pool of these dormant stem-like CD8 T cells in their tumor and/or lymphatic tissue are those who generate a large burst of newly activated CD8 T cells following immune checkpoint blockade, and that this accounts for ours and others' data showing that measuring T cell infiltration into tumors or T cell activation in the blood is a promising indicator of clinical benefit in patients<sup>27-43</sup>.

In this proposed model, it is also important and interesting to consider what this means for the patients who do not find clinical benefit following immune checkpoint blockade, and several explanations are possible. One possibility is that patients with poor outcomes after immunotherapy lack a strong enough pool of tumor specific TCF1<sup>+</sup> stem-like cells, which results in an insufficiency of the machinery to effectively respond to immune checkpoint blockade. This is supported by our data finding that these patients with poor responses also have diminished presence of both TCF1<sup>+</sup> stem-like cells and their intratumoral immune niche homes. However, another possibility is that in some cases or in some settings, immune checkpoint blockade alone is not a sufficient stimulus to overcome the dormancy of the tumor-specific stem-like T cells. For example, some patients with poor outcomes following immunotherapy may harbor some TCF1<sup>+</sup> stem-like cells, but lack the pre-requisite activating signals (e.g., such as co-stimulatory signals received via CD28 or cognate antigen presenting cells) to incite their differentiation. Further study

should specifically aim to identify which of these scenarios, or what combination of these scenarios, is cause for a lack of clinical and immunological response to immune checkpoint blockade, as this investigation will be essential for improving the response rate of immunotherapy.

#### **4.4 Materials & Methods.**

**Sample Collection, Preparation, and Storage:** Patients were consented under the Emory University Urological Satellite Specimen Bank in accordance with the Institutional Review Board (IRB00055316). Patient blood samples were obtained in cell preparation tubes at baseline and study specific timepoints and processed to cryopreserve peripheral blood mononuclear cells (PBMCs) and plasma. To minimize impact on patient schedules, the collection time points were cycle-dependent, coinciding with scheduled phlebotomy for standard laboratory analysis. Patient tumor samples were collected immediately after undergoing partial or radical nephrectomy. Tumor samples for flow cytometric analysis were harvested in Hank's Balanced Salt Solution, cut into small pieces, digested using Liberase enzyme cocktail (Roche), and homogenized using a MACS Dissociator. Single cell suspensions were obtained, RBC ACK lysed, and stored at  $-80^{\circ}\text{C}$  in freezing media for batch analysis. Samples for immunofluorescence analysis were formaldehyde fixed and embedded in paraffin blocks by Emory Pathology. Unstained and haematoxylin/eosin-stained sections of FFPE blocks were obtained from Emory Pathology.

**Assessment of Therapeutic Response:** Clinical benefit (CB) was defined as a best response of complete response (CR), partial response (PR), or stable disease (SD). Objective response to treatment was determined by using Response Evaluation Criteria in Solid Tumor version 1.1

(RECIST 1.1) (cite 38) by a board-certified radiologist. Re-staging radiograph interval varied among patients on standard of care (SOC) and clinical trial treatments, and in the SOC group modalities may have switched between CT and MRI depending on other clinical factors.

**Flow Cytometry & Fluorescence Activated Cell Sorting:** Single cell suspensions from human tumors and human peripheral blood were stained with antibodies listed below. Live/dead discrimination was performed using fixable Aqua or Near-IR Dead Cell Stain Kit (Invitrogen). Samples were acquired with a Becton Dickinson LSRII and analysed using FlowJo software. For intracellular staining, cells were fixed and permeabilized using the FOXP3 Transcription Factor Staining Buffer Set (eBioscience).

**Immunofluorescence:** Sections were deparaffinized in successive incubations with xylene and decreasing concentrations (100, 95, 75, 50, 0%) of EtOH in ddH<sub>2</sub>O. Antigen retrieval utilized Abcam 100x TrisEDTA Antigen Retrieval Buffer (pH = 9) heated under high pressure and washed in PBS + 0.1% Tween20. Sections were blocked for 30 minutes with 10% goat serum in 1x PBS + 0.1% Tween20 before staining with primary and secondary antibodies. Primary antibodies were used at a concentration of 1:100 (MHC-II) or 1:150 (CD8, TCF1) and incubated for 1 hour at room temperature. Secondary antibodies were used at a concentration of 1:250 (A488, A568) or 1:500 (A647) and incubated for 30 minutes at room temperature. Detailed information about antibodies used is listed below. Sections were counterstained with DAPI according to manufacturer instructions (Thermo-Fisher). Immunofluorescence images were collected using a Zeiss Z.1 Slide Scanner equipped with a Colibri 7 Flexible Light Source, and Zeiss ZenBlue software was used for post-acquisition image processing. CellProfiler<sup>129, 130</sup> and custom R and python scripts were

used for image analysis, as previously described<sup>43</sup>, to determine the xy coordinates of cells within tissue slices, measure fluorescence intensity within each cell, calculate cellular density, and create spatial maps of cell locations and features within the tissue.

Patient survival analysis: Survival analysis of patients was performed using the log-rank test from the R package, Survminer.

#### **4.5 Acknowledgements**

We gratefully acknowledge the patients and the families of patients who contributed to this study, and the clinicians who helped facilitate their contributions. We also wish to acknowledge the Emory Flow Cytometry Core, the Emory Integrated Cellular Imaging Core, the Sowalsky lab at the National Cancer Institute, and Emory's Winship Cancer Institute Cancer Tissue and Pathology Core. Additionally, C.S.J is supported by a National Cancer Institute grant (1-F30-CA-243250).

## 4.6 Tables

**Table 1: Immunofluorescence Imaging Cohort Patient Characteristics**

<b>Table 1</b>		<b>N</b>	<b>%</b>
<b>Total</b>		15	100.00
<b>Age at Time of Surgery</b>	Median (Range)	62 (33-75)	
<b>Sex</b>	Male	9	60.00
	Female	6	40.00
<b>Race</b>	Black/African American	2	13.33
	White/Caucasian	13	86.67
<b>Histologic Subtype</b>	Clear Cell RCC	11	73.33
	Other RCC	4	26.67
<b>Treatment</b>	Nivolumab	3	20.00
	Ipilimumab + Nivolumab	9	60.00
	Study Drug + Ipilimumab + Nivolumab	3	20.00
<b>Histologic Subtype</b>	Clear Cell RCC	11	73.33
	Other RCC	3	20.00
<b>Stage at Diagnosis</b>	I	1	6.67
	II	0	0.00
	III	6	40.00
	IV	8	53.33

**Table 2: Flow Cytometry Cohort Patient Characteristics**

<b>Table 2</b>		<b>N</b>	<b>%</b>
<b>Total</b>		<b>36</b>	<b>100.00</b>
<b>Age at Time of Surgery</b>	<b>Median (Range)</b>	<b>63.3 (32.5-76.6)</b>	
<b>Sex</b>	Male	23	63.89
	Female	13	36.11
<b>Race</b>	Black/African American	9	25.00
	White/Caucasian	27	75.00
<b>Histologic Subtype</b>	Clear Cell RCC	27	75.00
	Other RCC	9	25.00
<b>Treatment</b>	Nivolumab	14	38.89
	Ipilimumab + Nivolumab	12	33.33
	Cabozantinib + Nivolumab	6	16.67
	Levatinib + Nivolumab	1	2.78
	Atezolizumab	1	2.78
	Axitinib + Avelumab	1	2.78
	Study Drug + Ipilimumab + Nivolumab	1	2.78
<b>Histologic Subtype</b>	Clear Cell RCC	27	75.00
	Other RCC	9	25.00
<b>Stage at Diagnosis</b>	I	2	5.56
	II	2	5.56
	III	13	36.11
	IV	19	52.78
<b>%CD8 Strata</b>	High	10	27.78
	Low	26	72.22
<b>%CD8</b>	<b>Median (Range)</b>	<b>1.1 (0.0-24.5)</b>	

**Table 3: Flow Cytometry Antibodies**

Target	Clone	Fluorochrome	Source
CD3	UCHT1	FITC	Biolegend
CD4	OKT4	PerCP	Biolegend
CD28	CD28.2	PE/Cy7	eBioscience
CD39	A1	BV421	Biolegend
CD38	HIT2	BV510	Biolegend
CD38	HIT2	BV711	Biolegend
CD8	RPA-T8	BV605	Biolegend
HLA-DR	L243	BV711	Biolegend
HLA-DR	L243	APC/Cy7	Biolegend
PD-1	29F.1A12	BV786	Biolegend
CD45RA	HI100	BV785	Biolegend
CD25	M-A251	APC	Biolegend
CCR7	G043HI	PE-TR	Biolegend
CD19	HIB19	700	Biolegend
CD14	HCD14	700	Biolegend
Tbet	4B10	421	Biolegend
FOXP3	PCH101	PE	Invitrogen
Ki67	B56	APC	BD Biosciences
GZMB	GB11	700	BD Biosciences

**Table 4: Immunofluorescence Antibodies**

Target	Antibody Type	Clone	Concentration	Secondary	Concentration
MHC-II (HLA-DR, DP, DQ)	Mouse IgG2a	Tu39	1:100	Goat anti-mouse IgG2a A488	1:250
TCF1	Rabbit	C63D9	1:150	Goat anti-rabbit A568	1:250
CD8	Mouse IgG1	C8/144B	1:150	Goat anti-mouse IgG1 A647	1:500

## **Chapter 5: Conclusions and Closing Remarks**

### **5.1. Introduction**

Despite many decades of dedicated research and many advances in both diagnostics and therapeutics, the global disease burden of cancer remains a pressing challenge that causes much suffering and death each year<sup>1</sup>. Recent efforts have particularly focused on the importance of the immune system in the setting of cancer, both in harnessing it in therapeutics to fight cancer growth and development and in exploiting its patterns for use as biomarkers<sup>27-43, 131-133</sup>. An ever-increasing arsenal of immunotherapies are being used as frontline therapies in more and more tumor types, with many of these therapies focusing principally on invigorating the anti-tumor T cell response, such as anti-PD1, anti-PDL1, and anti-CTLA4 based immune checkpoint blockade<sup>107-113, 131-135</sup>. Indeed, it is precisely this anti-tumor T cell response that has also been the focus of much study for use as a biomarker for predicting patient outcomes in several tumor types. As such, understanding the biological mechanisms that support, sustain, and shape the anti-tumor T cell response is a critically important and burgeoning field of study. In this work, we examine this response and uncover key ingredients in the recipe for a robust and productive anti-tumor T cell response in several tumor types and in the setting of the response to immunotherapy.

### **5.2 TCF1+ stem-like T cells in human tumors**

High levels of tumor infiltrating lymphocytes have been associated with a survival benefit or a strong response to immunotherapy in several tumor types<sup>27-43, 131-133</sup>, but, unfortunately, some patients and some tumors fail to possess these high levels of T cell infiltration. However, it is not well understood why some patients are able to mount such a response, while others are not.

Accordingly, this presents a fundamental question—why, and how, is it that some patients' tumors have many T cells, while others do not?

In seeking to answer this question, especially having illustrated a dramatic survival advantage for renal cell carcinoma patients with a strong T cell response (Figure 2.1, Figure 2.2), we report the presence of a stem-like CD8 T cell in human tumors. This stem-like cell, not unlike similar cells documented in the setting of chronic viral infection<sup>46, 64, 70</sup>, is characterized by the expression of the transcription factor TCF1 and has significant expression of costimulatory molecules (e.g. CD28) and lower expression of checkpoint and effector molecules. This stem-like cell can both self-renew, maintaining a pool of these less differentiated cells in the tumor, as well as differentiate into more terminally differentiated, effector-like cells, which lack TCF1 expression and have much higher checkpoint and effector molecule (e.g. PD1, CTLA4, granzyme B, perforin) expression (Figure 2.2, Figure 2.4, Figure 2.5 Figure 2.6). As such, somewhat similar to what has been shown in other settings of chronic antigen exposure (Figure 1.1), we report that these stem-like cells constitute an important reservoir for maintaining a steady supply of anti-tumor T cells that can then carry out effector functions to kill cancer cells, mediating enhanced survival for patients.

Importantly, while our efforts to characterize these T cell populations were first concentrated in renal tumors, we have also demonstrated the presence of these TCF1<sup>+</sup> stem-like CD8 T cells in additional tumor types. We have determined that these special cells are present not only in generally immunogenic tumors, like renal cell carcinoma, but also in subsets of tumor types that are thought to be either generally “immunologically cold” or “immunologically privileged” such as prostate cancer and brain metastases, suggesting that this biology is a critical mechanism that

spans the disease of cancer, despite tissue of origin, average immunogenicity, or ease of circulatory access (Chapter 3). For example, while it is true that prostate tumors tend to harbor a paucity of anti-tumor CD8 T cells, a subset of these tumors do happen to host a stronger T cell response, and in this subset of “immunogenic prostate tumors,” we describe, as in renal tumors, the presence of this TCF1<sup>+</sup> stem-like cell that maintains the anti-tumor T cell response (Figure 3.1). Similarly, these cells are also identified in brain metastases of patients with varied cancers of primary tissue origin, such as breast cancer, non-small cell lung cancer, and melanoma (Figure 3.2, Figure 3.3, Figure 3.4, Figure 3.5, Figure 3.6, Figure 3.10). Interestingly, and importantly, we also demonstrate that these stem-like cells are present in both irradiated and unirradiated brain metastases, indicating their ability to persist despite exposure to ionizing radiation, which is a critical discovery, especially for sequencing multiple modalities of therapy, such as radiation therapy and immune checkpoint blockade (Figure 3.3, Figure 3.5, Figure 3.6, Figure 3.10).

Consequently, the work presented here demonstrates the enduring presence of these cells, not only in a diverse array of tumor types, but also in tissue recesses typically considered to be more “immune privileged,” further underscoring their importance as a cornerstone feature of the anti-tumor T cell response. In summary, herein we demonstrate the presence of stem-like cells in several tumor types, finding that this important cell population correlates with the strength of the total T cell response and thus beginning to shed light on potential mechanisms for how some patients are able to host a strong anti-tumor T cell response, while others are not.

### **5.3 Stem-like T cells reside in an intratumoral immune niche**

After establishing the presence of these stem-like CD8 T cells in human tumors and that their

presence correlates with a strong anti-tumor T cell response, the emergent question then becomes—what maintains and differentiates the stem-like cell population in the tumor? To seek to answer this question, we developed and utilized multiplex, quantitative immunofluorescence imaging methods, in order to understand what cell types might associate with or support the presence of these stem-like T cells in the tumor.

Using these quantitative imaging methods (Figure 2.9), we discovered that these stem-like cells preferentially reside in areas of high antigen presenting cell density, whereas the TCF1- terminally differentiated cells are found more dispersed throughout the tumor (Figure 2.8). Importantly, this finding was replicated in immunogenic prostate tumors (Figure 3.1), as well as in brain metastases (Figure 3.7, Figure 3.8), indicating that both the TCF1+ stem-like T cell and its antigen presenting cell-dense home, which we termed an “intratumoral immune niche,” are trans-tumor type features of the anti-tumor immune response. Put simply, we establish that that the presence of an intratumoral immune niche is a significant feature of immunologically active tumors.

Additionally, when we compare patients with differential clinical outcomes in either renal tumors or brain metastases (Figure 3.8, Figure 3.9), we find that the presence of these immune niches are a hallmark of a strong and productive anti-tumor immune response. In patients with stable or improving disease, a strong T cell response is typically supported by the presence of stem-like CD8 T cells residing in a dense, antigen presenting immune niche. On the other hand, patients with progressive or worsening disease often lack this high immune cellularity, and critically lack “immune niche” neighborhoods, or areas where TCF1+ stem-like T cells colocalize with MHC-II+ antigen presenting cells (Figure 2.8, Figure 2.11, Figure 2.12, Figure 2.14, Figure 3.8). Indeed,

we find that patients with higher average antigen presenting cell density or more areas of “immune niches” have significantly improved outcomes when compared to those with lower antigen presenting cell density or less immune niche areas (Figure 2.13, Figure 3.9), suggesting that the presence of these features in the tumor is indicative of a strong and productive anti-tumor cell response. Interestingly, we find that these intratumoral immune niches are a durable feature of the immune response, persisting despite exposure to radiation therapy, even while this exposure can attenuate the infiltration of other immune cells into the tumor tissue (Figure 3.10, Figure 3.11).

As such, it is clear that the presence of these intratumoral immune niches represents a hallmark of a strong anti-tumor T cell response (Figure 5.1). That is, these immune niches—areas of high antigen presenting cell density—serve as homes for the presence of stem-like CD8 T cells in the tumor. When these niches are present, the stem-like CD8 T cells can survive and thrive, receiving the signals necessary to both self-renew, as well as differentiate and produce new terminally differentiated cells, which then carry out target cell killing, mediating the anti-tumor effect of the T cell response. On the other hand, when these immune niches are lost or absent, the stem-like T cell population is also lacking in the tumor. Without these stem-like cells thriving in the tumor, the production of new terminally differentiated cells is abolished, and the anti-tumor T cell response fails. Thus, the presence of these immune niches represents a cornerstone feature of a productive and effective anti-tumor T cell response, and this immune organization is a key ingredient for ensuring a robust response that may then in turn provide differential survival benefit for patients.

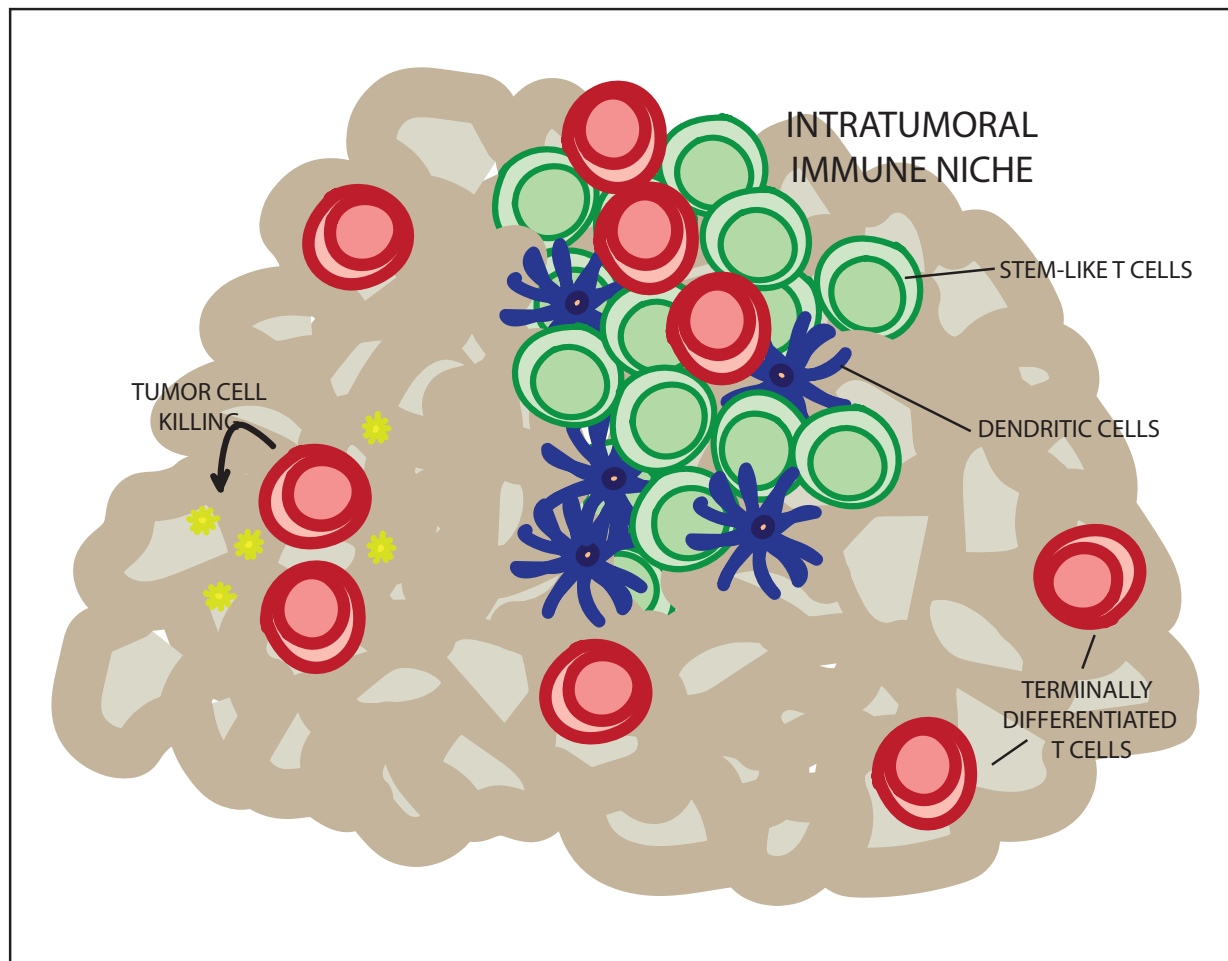


**Figure 5.1: The intratumoral immune niche.** An antigen presenting cell-dense intratumoral immune niches serves as a home for TCF1<sup>+</sup> stem-like CD8 T cells, which both self-renew and give rise to more terminally differentiated CD8 T cells, which can carry out tumor cell killing, arbitrating the anti-tumor effect of the T cell response that provides beneficial outcomes for patients. This immune niche is present in immunologically active tumors and is a ‘hallmark’ of immunogenic cancer, constituting an important mechanistic component of both the endogenous anti-tumor immune response and the response to immunotherapy.

#### **5.4 Immune niches and the response to immunotherapy**

Having found these stem-like T cells in immune niches in tumor tissue to be critical for the maintenance of the intrinsic, endogenous anti-tumor immune response, we also interrogated whether this phenomenon may also have a role in mediating the response to immunotherapy. Interestingly, in renal cell carcinoma patients, we found that patients with a strong endogenous immune response are more likely to derive clinical benefit from immune checkpoint blockade, and we found that this immune response, also previously shown, is supported by a stem-like CD8 T cell that finds its home in intratumoral immune niches (Figure 4.1, Figure 4.2, Figure 4.3).

Importantly, to complete this study, we utilized resected tumor tissue and evaluated the immune cell infiltration and organization therein, and it is important to note that this specimen may be resected months or even years prior to a patient's later reception of immunotherapy (Figure 4.1). This suggests that a patient's intrinsic ability to mount an effective anti-tumor immune response—supported by a stem-like CD8 T cell that resides in dense antigen presenting immune niches in tumor tissue—is vital for determining their later response to immunotherapy (Figure 4.2, Figure 4.3). This is a critical realization, as it may suggest there could be intrinsic factors of a patient's tumor (or a patient's general immune system) that predispose the ability of mount (or not) a productive anti-tumor immune response and thus a clinically beneficial response to immunotherapy. Similarly, this realization could have utility in better stratifying patients for reception or escalation of therapy, where measuring features of a patient's endogenous immune response could indicate whether a patient might be an ideal candidate for immune checkpoint blockade, or whether a patient might be best suited for a different therapeutic modality, given the landscape of their endogenous anti-tumor immune response.

## 5.5 Future studies and concluding remarks

With the field of cancer immunology continuing to boom, the positive effect of a strong anti-tumor T cell response continues to become more and more clear. However, what is less clear is why some patients can mount such a response, while others do not. Accordingly, the work presented herein is of particular importance, as it uncovers pieces of the mechanisms that explain this disparity between patients. Here we establish that the anti-tumor T cell response is maintained by a TCF1+ stem-like CD8 T cell, which both self-renews and differentiates to give rise to more terminally differentiated, effector like cells, and that these stem-like cells are maintained in an antigen presenting cell-dense intratumoral immune niche. We describe the presence of these stem-like cells and immune niches across diverse tumor types, demonstrating the relevance of this model in supporting the T cell response in cancer broadly. In short, we demonstrate that there is an immune niche, containing stem-like T cells and antigen presenting cells, in immunologically active cancers, and that the presence of these niches is a ‘hallmark’ of immunogenic cancers. Further, we demonstrate that these niches support both the immune response that assists improved patient outcomes and the productive response to immune checkpoint blockade.

Accordingly, this work holds great translational potential. For example, the data presented here argues strongly for undertaking rigorous validation study and then for using measures of the anti-tumor T cell response as clinical biomarkers, particularly in renal tumors, as we and others report a strong association between high levels of infiltrating CD8 T cells and improved patient prognoses<sup>27-48</sup>. In renal tumors specifically, the deployment of this biomarker could particularly be of use in at-risk patients, such as those with advanced localized disease (stage III), as a means

to delineate which patients would benefit from immediate therapeutic escalation and which patients are suitable for active surveillance, which is currently a major question in this patient population. Furthermore, given that we also find that the presence of a strong intrinsic anti-tumor T cell response may predict which patients will clinically benefit following immune checkpoint blockade, using measures of the anti-tumor T cell response as clinical biomarkers could also be deployed as a strategy for stratifying which patients should receive immunotherapy and which patients might benefit more from other therapeutic modalities. As only a minority of patients currently respond to immunotherapy<sup>105, 132, 136-139</sup>, using a biomarker in this way might empower for more exact selection of which patients are most appropriate for immunotherapy, especially ongoing study seeks to uncover avenues of increasing the overall response rate to immunotherapy.

An acutely important discovery presented herein is the description of a particular type of peripheral immune organization—the intratumoral immune niche, which maintains and differentiates these stem-like CD8 T cells. While the description of stem-like and terminally differentiated T cells present a functional compartmentalization of the anti-tumor T cell response, the illustration of this type of intratumoral immune organization also presents a kind of physical compartmentalization of the anti-tumor immune response. This work then establishes the appreciation that one way that the immune system efficiently establishes and sustains its activities is through both functional and physical compartmentalization. In that way, not unlike canonical understandings of the immune system's design, where, for example, in the primary and secondary lymphoid tissue “form follows function,” we see that in the anti-tumor T cell response, form and function are inexplicably intertwined. This form of the intratumoral immune niche is necessary for the maintenance of the stem-like T cell population, which sustains the function of the anti-tumor T cell response.

Importantly, several questions remain about the nature of these intratumoral immune niches, and particularly about the mechanisms of their formation and survival in tumor tissue. As these questions continue to take shape, it is useful to start with an understanding of how organization supports immune responses more broadly. The immune system is a highly ordered and organized system, and this organization empowers the carefully orchestrated function of this system.

The organization of the immune system is generally divided between primary, secondary, and tertiary lymphoid tissues. The primary lymphoid organs are those that are responsible for the production of immune cells—the bone marrow and the thymus. The bone marrow is the powerhouse of hematopoiesis, and the thymus plays an indispensable role in T cell differentiation and repertoire selection<sup>140-143</sup>. In both tissues, the organization is carefully orchestrated to empower these functions. For example, with the cortex and the medulla of the thymus harboring specialized stromal and thymic epithelial cells, providing form that supports the immune system functions that occur therein<sup>140</sup>. Similarly, the bone marrow's highly ordered structure also empowers its function, such as through the generation of a carefully designed niche to maintain and protect hematopoietic stem cells, which are critical for continued generation of new blood cells<sup>141-143</sup>.

The organization of the secondary lymphoid tissue—the spleen, the lymph nodes, and Peyer's patches—is also critical to the functionality of the immune system. The structure of this tissue, which harbors both lymphocytes and antigen presenting cells, sets the immune system to be poised for the induction of an effective immune response<sup>144</sup>. These tissues have three primary functions—to attenuate pathogen spread, to facilitate antigen presenting cell contact with rare antigen specific lymphocytes, and to provide a concentration of the factors necessary for the survival and

differentiation of lymphocytes<sup>145-148</sup>. Indeed, the secondary lymphoid organs are specifically designed for efficient adaptation in the face of an infection or otherwise urgent immune response. For example, in an infection, lymph nodes undergo structural remodeling—largely via the plasticity and adaptability of the fibroblastic reticular cells of the lymphoid stroma—to accommodate lymphocyte influx and facilitate antigen presenting cell remodeling<sup>149-153</sup>. In this way, not only does the intrinsic organization of the tissue prepare it for its function, but its form also follows its function in adapting to rapid needs for an immune response.

Broadly, the secondary lymphoid tissue is organized into three main parts—an outer antigen sampling region that is rich in antigen presenting cells, a B cell zone, and a T cell zone<sup>144, 154</sup>. In the antigen sampling region (i.e., subcapsular zone of the lymph node medulla or marginal zone in the spleen) contains aggregates of specialized macrophages and dendritic cells. In the T cell zone (i.e. periarticular lymphatic sheath in the spleen, paracortex in the lymph node, and interfollicular zone in Peyer’s patches), densely packed CD4 and CD8 T cells are found, intermixed with dendritic cells and embedded in sponge-like stroma made of fibroblastic reticular cells<sup>144, 152, 155-160</sup>. These FRCs wrap collagen fibers to form a multidimensional web of conduits, facilitating trafficking throughout the region<sup>144, 160, 161</sup>.

As the outcome of the T cell response to infection relies heavily on a productive encounter between a T cell and its cognate antigen on an antigen presenting cell, it is critical that the microstructure of the lymphoid tissue positions the immune system for success in this interaction. It not only achieves efficient concentration of rare antigen specific T cells, but also distributes antigen to specialized antigen presenting cells<sup>144, 162, 163</sup>. In this way, it is important to appreciate that the

critical players of the lymphoid tissue—the lymphocytes and the antigen presenting cells—cannot act in isolation, but rather only when embedded in this structural context of carefully organized lymphoid tissue. Accordingly, the organization of the tissue—the form—affects the functions carried out therein, and vice versa. The highly orchestrated structure of the tissue sets the stage for the immune cells, but these cells can also adapt this organization to fit their needs over time.

Interestingly, this adaptability and interplay between hematopoietic/immune cells and the structural cells surrounding them is not unique to the primary and secondary lymphoid tissues. In fact, this bidirectional communication and adaptable plasticity is a key feature of empowering immune responses outside the primary and secondary lymphoid tissues as well. For example, highly organized structures that resemble lymphoid tissue have been demonstrated in inflamed, infected, and tumor tissues and are known as tertiary lymphoid structures<sup>87, 164</sup> (Figure 5.2). Importantly, these inducible structures, often termed tertiary lymphoid structures, are not merely a byproduct of significant tissue inflammation, but functionally influence the immune response in these tissues as well. For example, TLS have been shown to improve the clinical course of pulmonary infections but can be pathogenic in the setting of autoimmune diseases, such as Crohn's disease, or in the setting of transplant rejection<sup>165-167</sup>.

Thus, while the precise mechanisms of how these tertiary structures function in the immune response are, as of yet, incompletely appreciated, it is clear that these TLS appear to be at least somewhat functionally and structurally similar to lymph nodes. TLS are defined as aggregations of cells in peripheral tissues comprised of distinct T and B cell compartments, with PNAd<sup>+</sup> high endothelial venules within T cell areas and with follicular dendritic cells, evidence of class

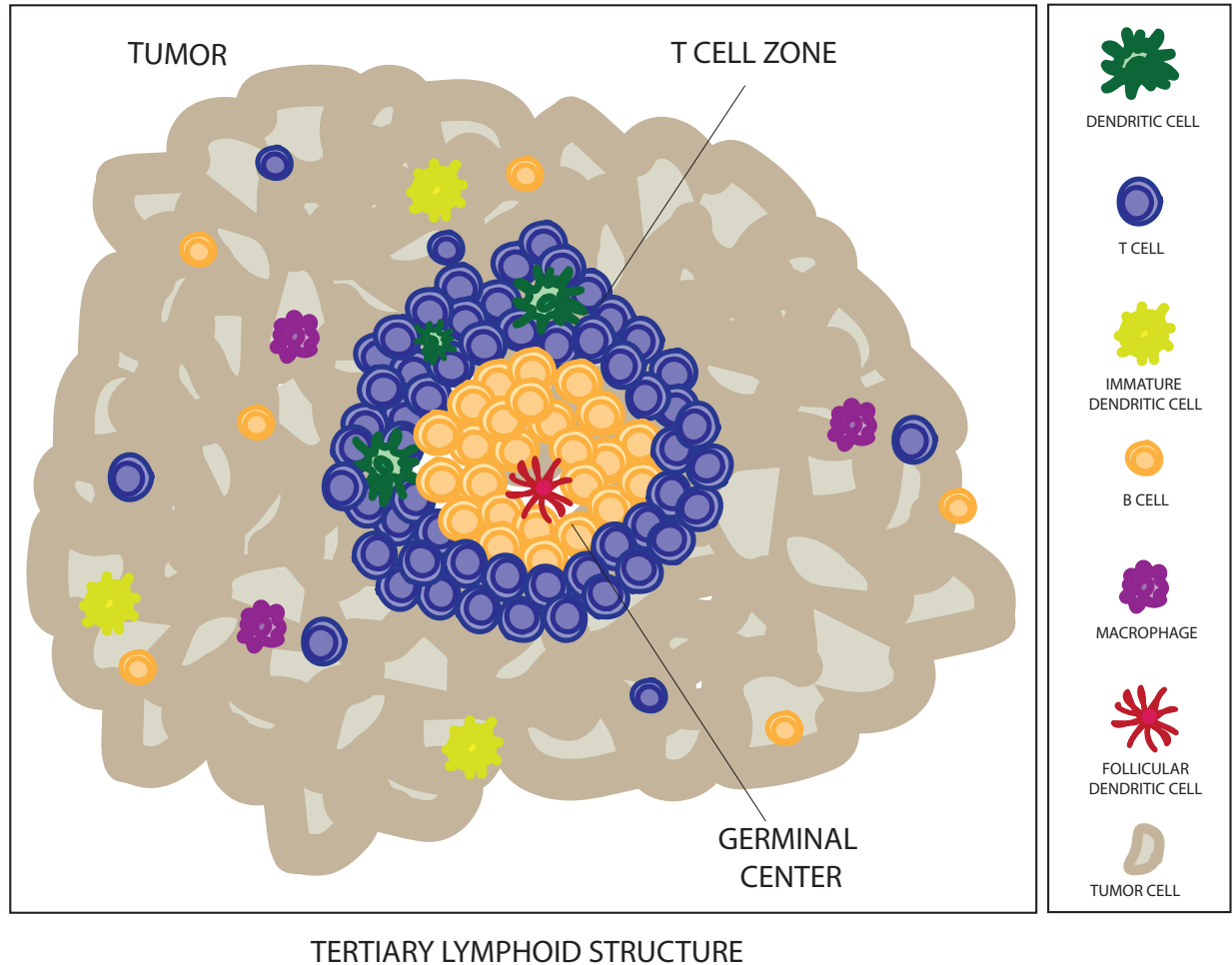


**Figure 5.2 Features of tertiary lymphoid structures.** Tertiary lymphoid structures, as depicted here in tumor tissue, are defined as organizational structures outside the primary and secondary lymphoid tissue that contain distinct T and B cell zones, with follicular dendritic cells and active germinal centers in the B cell zones and mature dendritic cells in the T cell zones.

switching, reactive GCs, and expression of activation induced cytidine deaminase (AID) in B cell areas<sup>87, 168-170</sup>. In essence, these structures mimic the characteristic structures and cell types found in the lymph node and associated with an adaptive immune response—mature DCs situated in a T cell zone, germinal centers with FDCs and B cells, and HEVs. In addition to these structural similarities, TLS and lymph node genesis are suggested to share similar inciting signals—lymphotoxin, TNF $\alpha$ , CCL19/CCL21, CXCL13, and others<sup>87, 171, 172</sup>. For example, ectopic expression of lymphotoxin in mouse models can induce formation of TLS without an offending stimulus (such as infection), and in murine influenza, tertiary lymphoid structures form along the bronchioles, but are erased when lymphotoxin signaling is ablated<sup>166, 170, 172-174</sup>. Importantly, these structures are not unique to lung tissue and have been documented in chronic gastritis, Sjogren's disease, chronic hepatitis C infection, transplant rejection, *heliobacter*-induced hepatitis, and rheumatoid arthritis<sup>167, 175-185</sup>.

Tertiary lymphoid structures have also been described in several tumor types, and in some instances, associated with improved clinical outcomes, such as in non-small cell lung cancer and colorectal cancer<sup>89, 164, 186</sup>. Tertiary lymphoid structures, as in infection and autoimmunity, have been defined as those immune cell aggregations in tumors that harbor T cell zones with mature DCs, germinal centers with follicular dendritic cells and proliferating B cells, and HEVs<sup>87, 164, 168, 169, 187</sup>. Not unlike what has been demonstrated in other settings, the presence of tertiary lymphoid structures in human tumors has been associated with increased chemokine expression (e.g. CCL19/CCL21, CXCL13), adhesion molecules, integrins, and more, and these structures may even contain stromal support networks<sup>164, 188</sup>. Taken together, this suggests that these tumor-related TLS are similar in structure, function, and genesis to those found in autoimmunity and infection,

and that all of these types of TLS share important form and function with secondary lymphoid tissue.

Consequently, several critical questions emerge—what is the role of the TLS in recruiting and maintaining a productive anti-tumor immune response? Are TLS required for a productive anti-tumor immune response? Can tumor-related TLS exist without a productive anti-tumor immune response? What is the prognostic significance of these TLS in various tumor types? And, while many of these questions remain incompletely or entirely unanswered, much has been learned about this biological phenomenon. In some cases (e.g. colorectal cancer, breast cancer, and non-small cell lung cancer, oral squamous cell carcinoma, and others), tumor TLS are associated with high lymphocyte infiltration and with improved clinical outcomes<sup>33, 87, 88, 189-196</sup>. However, other schematics of intratumoral immune organization have been described as well, and it is unclear how these types of organization may differ—in function or in bearing on clinical outcome—from tertiary lymphoid structures. For example, “lymphoid neogenesis” has been reported in lung metastases of melanoma and colorectal cancer patients, and perivascular immune niches have been demonstrated in mouse models of colorectal cancer and melanoma<sup>33, 48, 168, 197</sup>. Indeed, in this work, we report the presence of intratumoral immune niches in renal cell carcinoma<sup>43</sup>, immunogenic prostate cancer<sup>97</sup>, and in brain metastases of varied histologies.

Thus, critical questions about the mechanisms and outcomes of peripheral immune organization remain. For example, it is yet unclear exactly how the immune niches we describe are similar to and different from previously described tertiary lymphoid structures in tumors<sup>33, 87-89, 164, 168-170, 187-196</sup>. While the two organizational types seem to appear to diverge both in organization and in

cellular composition, it is uncertain whether the mechanisms that incite their formation are overlapping or distinct, if one structure's development may precede the other, or whether the structures have differential bearing on the outcome of the anti-tumor T cell response. Accordingly, ongoing study prioritizes these questions, seeking to meticulously compare these two phenomena of peripheral immune cell organization, in hopes of uncovering the mechanisms of how each one forms and the precise direction each provides to the anti-tumor T cell response.

Finally, while the description of this intratumoral immune niche that maintains the anti-tumor T cell response is a significant one, a pressing need then is to understand how these niches form in some patients and perhaps more critically, why these niches fail to form in others. Especially given that patients lacking these immune niches tend to have their disease worsen, it is possible that the failure of these niches' formation is a manifestation of tumor immune escape and that tumors acquire characteristics that inhibit or destroy this foundation for the immune response<sup>198-201</sup>. For example, several genetic mechanisms of immune evasion have been reported—such as loss of MHC<sup>202-204</sup>, acquisition of mutations that provide selective advantages that allow adaptation to avoid immune destruction<sup>205-209</sup>, defects in interferon- $\gamma$  signaling<sup>210-212</sup>, or avoidance of immunogenic cell death<sup>213, 214</sup>. While these studies demonstrate that these mechanisms stymie the anti-tumor immune, it is yet unknown if these mechanisms may impede formation or cause destruction of intratumoral immune niches. Accordingly, a critical future question asks how cancer cell intrinsic biology may affect the formation, or lack thereof, of these immune niches, and how this biology relates to current understandings of immune evasion.

Future study should focus precisely on this question, as continuing to gain understanding of these

niches and how they form will uncover opportunities for therapeutic development. Specifically, as the mechanisms of niche formation are uncovered, this knowledge can be harnessed and exploited to develop therapeutic strategies that seek to incite niche formation or replicate niche function, and thus maintenance of a productive anti-tumor T cell response, in patients whose immune response might otherwise falter. This type of discovery might also hold keys to improving response rates to existing therapies, such as immune checkpoint blockade, which could provide improve and extend quality of life for many patients of varied tumor types. In sum, the work presented herein contributes to a foundational understanding of the mechanisms of the anti-tumor immune response in human cancer and constructs a springboard from which many exciting, high-impact future studies may find footing. As such, it is our single and sincerest goal that this work, and the efforts that follow, may contribute to decreasing the burden of cancer worldwide and to providing hope for patients and their families everywhere.

## Chapter 6: References

1. Siegel RL, Miller KD, Fuchs HE, Jemal A. Cancer statistics, 2022. *CA Cancer J Clin.* 2022;72(1):7-33. Epub 20220112. doi: 10.3322/caac.21708. PubMed PMID: 35020204.
2. Safiri S, Kolahi A-A, Mansournia MA, Almasi-Hashiani A, Ashrafi-Asgarabad A, Sullman MJM, *et al.* The burden of kidney cancer and its attributable risk factors in 195 countries and territories, 1990–2017. *Scientific Reports.* 2020;10(1):13862. doi: 10.1038/s41598-020-70840-2.
3. Dorans KS, Mills KT, Liu Y, He J. Trends in Prevalence and Control of Hypertension According to the 2017 American College of Cardiology/American Heart Association (ACC/AHA) Guideline. *Journal of the American Heart Association.* 2018;7(11):e008888. doi: doi:10.1161/JAHA.118.008888.
4. Mills KT, Stefanescu A, He J. The global epidemiology of hypertension. *Nat Rev Nephrol.* 2020;16(4):223-37. Epub 20200205. doi: 10.1038/s41581-019-0244-2. PubMed PMID: 32024986; PMCID: PMC7998524.
5. Hanahan D, Weinberg RA. The hallmarks of cancer. *Cell.* 2000;100(1):57-70. doi: 10.1016/s0092-8674(00)81683-9. PubMed PMID: 10647931.
6. Hanahan D, Weinberg Robert A. Hallmarks of Cancer: The Next Generation. *Cell.* 2011;144(5):646-74. doi: 10.1016/j.cell.2011.02.013.
7. Hanahan D. Hallmarks of Cancer: New Dimensions. *Cancer discovery.* 2022;12(1):31-46. doi: 10.1158/2159-8290.CD-21-1059.
8. Guo ZS. The 2018 Nobel Prize in medicine goes to cancer immunotherapy (editorial for *BMC cancer*). *BMC cancer.* 2018;18(1):1086-. doi: 10.1186/s12885-018-5020-3. PubMed PMID: 30415640.
9. Custer RP, Bosma GC, Bosma MJ. Severe combined immunodeficiency (SCID) in the

- mouse. Pathology, reconstitution, neoplasms. The American journal of pathology. 1985;120(3):464-77. PubMed PMID: 2412448; PMCID: PMC1887984.
10. Engel AM, Svane IM, Mouritsen S, Rygaard J, Clausen J, Werdelin O. Methylcholanthrene-induced sarcomas in nude mice have short induction times and relatively low levels of surface MHC class I expression. *Apmis*. 1996;104(7-8):629-39.
  11. Shankaran V, Ikeda H, Bruce AT, White JM, Swanson PE, Old LJ, *et al.* IFN $\gamma$  and lymphocytes prevent primary tumour development and shape tumour immunogenicity. *Nature*. 2001;410(6832):1107-11.
  12. Huang P, Westmoreland SV, Jain RK, Fukumura D. Spontaneous nonthymic tumors in SCID mice. *Comp Med*. 2011;61(3):227-34. PubMed PMID: 21819692.
  13. Prochazka M, Gaskins HR, Shultz LD, Leiter EH. The nonobese diabetic scid mouse: model for spontaneous thymomagenesis associated with immunodeficiency. *Proceedings of the National Academy of Sciences of the United States of America*. 1992;89(8):3290-4. doi: 10.1073/pnas.89.8.3290. PubMed PMID: 1373493; PMCID: PMC48852.
  14. Rao S, Gharib K, Han A. Chapter Five - Cancer Immunosurveillance by T Cells. In: Galluzzi L, Rudqvist N-P, editors. *International Review of Cell and Molecular Biology*: Academic Press; 2019. p. 149-73.
  15. Dighe AS, Richards E, Old LJ, Schreiber RD. Enhanced in vivo growth and resistance to rejection of tumor cells expressing dominant negative IFN $\gamma$  receptors. *Immunity*. 1994;1(6):447-56.
  16. Kaplan DH, Shankaran V, Dighe AS, Stockert E, Aguet M, Old LJ, *et al.* Demonstration of an interferon  $\gamma$ -dependent tumor surveillance system in immunocompetent mice. *Proceedings of the national academy of sciences*. 1998;95(13):7556-61.

17. Street SE, Cretney E, Smyth MJ. Perforin and interferon- $\gamma$  activities independently control tumor initiation, growth, and metastasis. *Blood, The Journal of the American Society of Hematology*. 2001;97(1):192-7.
18. van den Broek ME, Kägi D, Ossendorp F, Toes R, Vamvakas S, Lutz WK, *et al*. Decreased tumor surveillance in perforin-deficient mice. *The Journal of experimental medicine*. 1996;184(5):1781-90.
19. Smyth MJ, Thia KY, Street SE, MacGregor D, Godfrey DI, Trapani JA. Perforin-mediated cytotoxicity is critical for surveillance of spontaneous lymphoma. *The Journal of experimental medicine*. 2000;192(5):755-60.
20. Barth RJ, Jr, Mulé JJ, Spiess PJ, Rosenberg SA. Interferon gamma and tumor necrosis factor have a role in tumor regressions mediated by murine CD8<sup>+</sup> tumor-infiltrating lymphocytes. *Journal of Experimental Medicine*. 1991;173(3):647-58. doi: 10.1084/jem.173.3.647.
21. Engels EA, Pfeiffer RM, Fraumeni JF, Kasiske BL, Israni AK, Snyder JJ, *et al*. Spectrum of Cancer Risk Among US Solid Organ Transplant Recipients. *JAMA*. 2011;306(17):1891-901. doi: 10.1001/jama.2011.1592.
22. Penn I. The effect of immunosuppression on pre-existing cancers. *Transplantation*. 1993;55(4):742-7.
23. Birkeland SA, Storm HH, Lamm LU, Barlow L, Blohmé I, Forsberg B, *et al*. Cancer risk after renal transplantation in the Nordic countries, 1964–1986. *International journal of cancer*. 1995;60(2):183-9.
24. Horowitz MM, Gale RP, Sondel PM, Goldman JM, Kersey J, Kolb H-J, *et al*. Graft-versus-leukemia reactions after bone marrow transplantation 1990.
25. Mathé G, Amiel J, Schwarzenberg L, Cattani A, Schneider M, De Vries M, *et al*. Successful

allogenic bone marrow transplantation in man: chimerism, induced specific tolerance and possible anti-leukemic effects. *Blood*. 1965;25(2):179-96.

26. Porter DL, Roth MS, McGarigle C, Ferrara J, Antin JH. Induction of Graft-versus-Host Disease as Immunotherapy for Relapsed Chronic Myeloid Leukemia. *New England Journal of Medicine*. 1994;330(2):100-6. doi: 10.1056/NEJM199401133300204.

27. Galon J, Costes A, Sanchez-Cabo F, Kirilovsky A, Mlecnik B, Lagorce-Pages C, *et al.* Type, density, and location of immune cells within human colorectal tumors predict clinical outcome. *Science*. 2006;313(5795):1960-4. Epub 2006/09/30. doi: 10.1126/science.1129139. PubMed PMID: 17008531.

28. Baier PK, Wimmenauer S, Hirsch T, von Specht BU, von Kleist S, Keller H, *et al.* Analysis of the T cell receptor variability of tumor-infiltrating lymphocytes in colorectal carcinomas. *Tumour Biol*. 1998;19(3):205-12. doi: 10.1159/000030008. PubMed PMID: 9591047.

29. Diederichsen AC, Hjelmberg J, Christensen PB, Zeuthen J, Fenger C. Prognostic value of the CD4+/CD8+ ratio of tumour infiltrating lymphocytes in colorectal cancer and HLA-DR expression on tumour cells. *Cancer Immunol Immunother*. 2003;52(7):423-8. Epub 20030415. doi: 10.1007/s00262-003-0388-5. PubMed PMID: 12695859.

30. Naito Y, Saito K, Shiiba K, Ohuchi A, Saigenji K, Nagura H, *et al.* CD8+ T cells infiltrated within cancer cell nests as a prognostic factor in human colorectal cancer. *Cancer Res*. 1998;58(16):3491-4. PubMed PMID: 9721846.

31. Pages F, Berger A, Camus M, Sanchez-Cabo F, Costes A, Molidor R, *et al.* Effector memory T cells, early metastasis, and survival in colorectal cancer. *N Engl J Med*. 2005;353(25):2654-66. Epub 2005/12/24. doi: 10.1056/NEJMoa051424. PubMed PMID: 16371631.

32. Mlecnik B, Tosolini M, Kirilovsky A, Berger A, Bindea G, Meatchi T, *et al.* Histopathologic-based prognostic factors of colorectal cancers are associated with the state of the local immune reaction. *J Clin Oncol.* 2011;29(6):610-8. Epub 2011/01/20. doi: 10.1200/JCO.2010.30.5425. PubMed PMID: 21245428.
33. Remark R, Alifano M, Cremer I, Lupo A, Dieu-Nosjean MC, Riquet M, *et al.* Characteristics and clinical impacts of the immune environments in colorectal and renal cell carcinoma lung metastases: influence of tumor origin. *Clin Cancer Res.* 2013;19(15):4079-91. Epub 2013/06/21. doi: 10.1158/1078-0432.CCR-12-3847. PubMed PMID: 23785047.
34. Gooden MJ, de Bock GH, Leffers N, Daemen T, Nijman HW. The prognostic influence of tumour-infiltrating lymphocytes in cancer: a systematic review with meta-analysis. *Br J Cancer.* 2011;105(1):93-103. Epub 2011/06/02. doi: 10.1038/bjc.2011.189. PubMed PMID: 21629244; PMCID: PMC3137407.
35. Pagès F, Galon J, Dieu-Nosjean MC, Tartour E, Sautès-Fridman C, Fridman WH. Immune infiltration in human tumors: a prognostic factor that should not be ignored. *Oncogene.* 2009;29:1093. doi: 10.1038/onc.2009.416.
36. Geng Y, Shao Y, He W, Hu W, Xu Y, Chen J, *et al.* Prognostic Role of Tumor-Infiltrating Lymphocytes in Lung Cancer: a Meta-Analysis. *Cellular Physiology and Biochemistry.* 2015;37(4):1560-71.
37. Peranzoni E, Lemoine J, Vimeux L, Feuillet V, Barrin S, Kantari-Mimoun C, *et al.* Macrophages impede CD8 T cells from reaching tumor cells and limit the efficacy of anti-PD-1 treatment. *Proceedings of the National Academy of Sciences of the United States of America.* 2018;115(17):E4041-E50. Epub 2018/04/11. doi: 10.1073/pnas.1720948115. PubMed PMID: 29632196.

38. Sato E, Olson SH, Ahn J, Bundy B, Nishikawa H, Qian F, *et al.* Intraepithelial CD8+ tumor-infiltrating lymphocytes and a high CD8+ / regulatory T cell ratio are associated with favorable prognosis in ovarian cancer. *Proceedings of the National Academy of Sciences of the United States of America.* 2005;102(51):18538-43. doi: 10.1073/pnas.0509182102.
39. Tumeh PC, Harview CL, Yearley JH, Shintaku IP, Taylor EJ, Robert L, *et al.* PD-1 blockade induces responses by inhibiting adaptive immune resistance. *Nature.* 2014;515(7528):568-71. Epub 2014/11/28. doi: 10.1038/nature13954. PubMed PMID: 25428505; PMCID: PMC4246418.
40. Eroglu Z, Zaretsky JM, Hu-Lieskovan S, Kim DW, Algazi A, Johnson DB, *et al.* High response rate to PD-1 blockade in desmoplastic melanomas. *Nature.* 2018;553:347. doi: 10.1038/nature25187  
<https://www.nature.com/articles/nature25187#supplementary-information>.
41. Dhodapkar KM, Gettinger SN, Das R, Zebroski H, Dhodapkar MV. SOX2-specific adaptive immunity and response to immunotherapy in non-small cell lung cancer. *Oncoimmunology.* 2013;2(7):e25205. Epub 2013/09/28. doi: 10.4161/onci.25205. PubMed PMID: 24073380; PMCID: PMC3782159.
42. Daud AI, Loo K, Pauli ML, Sanchez-Rodriguez R, Sandoval PM, Taravati K, *et al.* Tumor immune profiling predicts response to anti-PD-1 therapy in human melanoma. *The Journal of Clinical Investigation.* 2016;126(9):3447-52. doi: 10.1172/JCI87324.
43. Jansen CS, Prokhnjevskaja N, Master VA, Sanda MG, Carlisle JW, Bilen MA, *et al.* An intratumoral niche maintains and differentiates stem-like CD8 T cells. *Nature.* 2019;576(7787):465-70. Epub 20191211. doi: 10.1038/s41586-019-1836-5. PubMed PMID: 31827286; PMCID: PMC7108171.

44. Sade-Feldman M, Yizhak K, Bjorgaard SL, Ray JP, de Boer CG, Jenkins RW, *et al.* Defining T Cell States Associated with Response to Checkpoint Immunotherapy in Melanoma. *Cell*. 2018;175(4):998-1013 e20. doi: 10.1016/j.cell.2018.10.038. PubMed PMID: 30388456.
45. Miller BC, Sen DR, Al Abosy R, Bi K, Virkud YV, LaFleur MW, *et al.* Subsets of exhausted CD8(+) T cells differentially mediate tumor control and respond to checkpoint blockade. *Nat Immunol*. 2019;20(3):326-36. Epub 2019/02/20. doi: 10.1038/s41590-019-0312-6. PubMed PMID: 30778252.
46. Im SJ, Hashimoto M, Gerner MY, Lee J, Kissick HT, Burger MC, *et al.* Defining CD8+ T cells that provide the proliferative burst after PD-1 therapy. *Nature*. 2016;537(7620):417-21. Epub 2016/08/09. doi: 10.1038/nature19330. PubMed PMID: 27501248; PMCID: PMC5297183.
47. Kurtulus S, Madi A, Escobar G, Klapholz M, Nyman J, Christian E, *et al.* Checkpoint Blockade Immunotherapy Induces Dynamic Changes in PD-1(-)CD8(+) Tumor-Infiltrating T Cells. *Immunity*. 2019;50(1):181-94.e6. Epub 2019/01/13. doi: 10.1016/j.immuni.2018.11.014. PubMed PMID: 30635236; PMCID: PMC6336113.
48. Siddiqui I, Schaeuble K, Chennupati V, Fuertes Marraco SA, Calderon-Copete S, Pais Ferreira D, *et al.* Intratumoral Tcf1(+)PD-1(+)CD8(+) T Cells with Stem-like Properties Promote Tumor Control in Response to Vaccination and Checkpoint Blockade Immunotherapy. *Immunity*. 2019;50(1):195-211.e10. Epub 2019/01/13. doi: 10.1016/j.immuni.2018.12.021. PubMed PMID: 30635237.
49. Maleki Vareki S, Garrigós C, Duran I. Biomarkers of response to PD-1/PD-L1 inhibition. *Critical Reviews in Oncology/Hematology*. 2017;116:116-24. doi: <https://doi.org/10.1016/j.critrevonc.2017.06.001>.
50. Patel SP, Kurzrock R. PD-L1 Expression as a Predictive Biomarker in Cancer

Immunotherapy. *Mol Cancer Ther.* 2015;14(4):847-56. Epub 2015/02/20. doi: 10.1158/1535-7163.Mct-14-0983. PubMed PMID: 25695955.

51. Lee J-M, Gulley JL. Checkpoint and PARP inhibitors, for whom and when. *Oncotarget.* 2017;8(56):95036-7. doi: 10.18632/oncotarget.20852. PubMed PMID: PMC5707002.

52. Herbst RS, Soria J-C, Kowanetz M, Fine GD, Hamid O, Gordon MS, *et al.* Predictive correlates of response to the anti-PD-L1 antibody MPDL3280A in cancer patients. *Nature.* 2014;515(7528):563-7. doi: 10.1038/nature14011. PubMed PMID: 25428504.

53. Azimi F, Scolyer RA, Rumcheva P, Moncrieff M, Murali R, McCarthy SW, *et al.* Tumor-infiltrating lymphocyte grade is an independent predictor of sentinel lymph node status and survival in patients with cutaneous melanoma. *J Clin Oncol.* 2012;30(21):2678-83. Epub 2012/06/20. doi: 10.1200/jco.2011.37.8539. PubMed PMID: 22711850.

54. Chen DS, Mellman I. Elements of cancer immunity and the cancer-immune set point. *Nature.* 2017;541(7637):321-30. Epub 2017/01/20. doi: 10.1038/nature21349. PubMed PMID: 28102259.

55. Haffner MC, Guner G, Taheri D, Netto GJ, Palsgrove DN, Zheng Q, *et al.* Comprehensive Evaluation of Programmed Death-Ligand 1 Expression in Primary and Metastatic Prostate Cancer. *The American journal of pathology.* 2018;188(6):1478-85. Epub 2018/03/27. doi: 10.1016/j.ajpath.2018.02.014. PubMed PMID: 29577933; PMCID: PMC5971230.

56. Xu W, Atkins MB, McDermott DF. Checkpoint inhibitor immunotherapy in kidney cancer. *Nat Rev Urol.* 2020;17(3):137-50. Epub 20200204. doi: 10.1038/s41585-020-0282-3. PubMed PMID: 32020040.

57. Davis AA, Patel VG. The role of PD-L1 expression as a predictive biomarker: an analysis of all US Food and Drug Administration (FDA) approvals of immune checkpoint inhibitors. *J*

Immunother Cancer. 2019;7(1):278. Epub 20191026. doi: 10.1186/s40425-019-0768-9. PubMed PMID: 31655605; PMCID: PMC6815032.

58. Topham DJ, Doherty PC. Longitudinal Analysis of the Acute Sendai Virus-Specific CD4<sup>+</sup> T Cell Response and Memory. *The Journal of Immunology*. 1998;161(9):4530.

59. Murali-Krishna K, Altman JD, Suresh M, Sourdive DJ, Zajac AJ, Miller JD, *et al*. Counting antigen-specific CD8 T cells: a reevaluation of bystander activation during viral infection. *Immunity*. 1998;8(2):177-87. doi: 10.1016/s1074-7613(00)80470-7. PubMed PMID: 9491999.

60. Butz EA, Bevan MJ. Massive expansion of antigen-specific CD8<sup>+</sup> T cells during an acute virus infection. *Immunity*. 1998;8(2):167-75. doi: 10.1016/s1074-7613(00)80469-0. PubMed PMID: 9491998; PMCID: PMC2776648.

61. Kalia V, Sarkar S, Gourley TS, Rouse BT, Ahmed R. Differentiation of memory B and T cells. *Current opinion in immunology*. 2006;18(3):255-64.

62. Kaech SM, Hemby S, Kersh E, Ahmed R. Molecular and functional profiling of memory CD8 T cell differentiation. *Cell*. 2002;111(6):837-51.

63. Wherry EJ. T cell exhaustion. *Nature immunology*. 2011;12(6):492-9.

64. Hashimoto M, Kamphorst AO, Im SJ, Kissick HT, Pillai RN, Ramalingam SS, *et al*. CD8 T cell exhaustion in chronic infection and cancer: opportunities for interventions. *Annual review of medicine*. 2018;69:301-18.

65. Zajac AJ, Blattman JN, Murali-Krishna K, Sourdive DJ, Suresh M, Altman JD, *et al*. Viral immune evasion due to persistence of activated T cells without effector function. *J Exp Med*. 1998;188(12):2205-13. Epub 1998/12/22. PubMed PMID: 9858507; PMCID: PMC2212420.

66. Cardenas MA, Prokhnevskaya N, Kissick HT. Organized immune cell interactions within

tumors sustain a productive T-cell response. *International immunology*. 2021;33(1):27-37. doi: 10.1093/intimm/dxaa057. PubMed PMID: 32827212.

67. He R, Hou S, Liu C, Zhang A, Bai Q, Han M, *et al*. Follicular CXCR5- expressing CD8(+) T cells curtail chronic viral infection. *Nature*. 2016;537(7620):412-28. doi: 10.1038/nature19317. PubMed PMID: 27501245.

68. Utzschneider DT, Charmoy M, Chennupati V, Pousse L, Ferreira DP, Calderon-Copete S, *et al*. T Cell Factor 1-Expressing Memory-like CD8(+) T Cells Sustain the Immune Response to Chronic Viral Infections. *Immunity*. 2016;45(2):415-27. doi: 10.1016/j.immuni.2016.07.021. PubMed PMID: 27533016.

69. Leong YA, Chen Y, Ong HS, Wu D, Man K, Deleage C, *et al*. CXCR5(+) follicular cytotoxic T cells control viral infection in B cell follicles. *Nat Immunol*. 2016;17(10):1187-96. Epub 20160803. doi: 10.1038/ni.3543. PubMed PMID: 27487330.

70. Hudson WH, Gensheimer J, Hashimoto M, Wieland A, Valanparambil RM, Li P, *et al*. Proliferating Transitory T Cells with an Effector-like Transcriptional Signature Emerge from PD-1(+) Stem-like CD8(+) T Cells during Chronic Infection. *Immunity*. 2019;51(6):1043-58.e4. Epub 20191203. doi: 10.1016/j.immuni.2019.11.002. PubMed PMID: 31810882; PMCID: PMC6920571.

71. Wu T, Ji Y, Moseman EA, Xu HC, Manghani M, Kirby M, *et al*. The TCF1-Bcl6 axis counteracts type I interferon to repress exhaustion and maintain T cell stemness. *Sci Immunol*. 2016;1(6). Epub 20161209. doi: 10.1126/sciimmunol.aai8593. PubMed PMID: 28018990; PMCID: PMC5179228.

72. Savas P, Virassamy B, Ye C, Salim A, Mintoff CP, Caramia F, *et al*. Single-cell profiling of breast cancer T cells reveals a tissue-resident memory subset associated with improved

prognosis. *Nat Med*. 2018;24(7):986-93. Epub 2018/06/27. doi: 10.1038/s41591-018-0078-7. PubMed PMID: 29942092.

73. Herbst RS, Soria JC, Kowanetz M, Fine GD, Hamid O, Gordon MS, *et al*. Predictive correlates of response to the anti-PD-L1 antibody MPDL3280A in cancer patients. *Nature*. 2014;515(7528):563-7. Epub 2014/11/28. doi: 10.1038/nature14011. PubMed PMID: 25428504; PMCID: PMC4836193.

74. Gallimore A, Dumrese T, Hengartner H, Zinkernagel RM, Rammensee H-G. Protective Immunity Does Not Correlate with the Hierarchy of Virus-specific Cytotoxic T Cell Responses to Naturally Processed Peptides. *The Journal of Experimental Medicine*. 1998;187(10):1647-b. doi: 10.1084/jem.187.10.1647-b.

75. Wherry EJ, Ha S-J, Kaech SM, Haining WN, Sarkar S, Kalia V, *et al*. Molecular Signature of CD8<sup>+</sup> T Cell Exhaustion during Chronic Viral Infection. *Immunity*. 2007;27(4):670-84. doi: 10.1016/j.immuni.2007.09.006.

76. Barber DL, Wherry EJ, Masopust D, Zhu B, Allison JP, Sharpe AH, *et al*. Restoring function in exhausted CD8 T cells during chronic viral infection. *Nature*. 2006;439(7077):682-7. Epub 2005/12/31. doi: 10.1038/nature04444. PubMed PMID: 16382236.

77. Gros A, Robbins PF, Yao X, Li YF, Turcotte S, Tran E, *et al*. PD-1 identifies the patient-specific CD8<sup>+</sup> tumor-reactive repertoire infiltrating human tumors. *The Journal of Clinical Investigation*. 2014;124(5):2246-59. doi: 10.1172/JCI73639.

78. Topalian SL, Hodi FS, Brahmer JR, Gettinger SN, Smith DC, McDermott DF, *et al*. Safety, Activity, and Immune Correlates of Anti-PD-1 Antibody in Cancer. *New England Journal of Medicine*. 2012;366(26):2443-54. doi: 10.1056/NEJMoa1200690.

79. Brahmer JR, Tykodi SS, Chow LQM, Hwu W-J, Topalian SL, Hwu P, *et al*. Safety and

Activity of Anti-PD-L1 Antibody in Patients with Advanced Cancer. *New England Journal of Medicine*. 2012;366(26):2455-65. doi: 10.1056/NEJMoa1200694.

80. Hodi FS, O'Day SJ, McDermott DF, Weber RW, Sosman JA, Haanen JB, *et al*. Improved Survival with Ipilimumab in Patients with Metastatic Melanoma. *New England Journal of Medicine*. 2010;363(8):711-23. doi: 10.1056/NEJMoa1003466.

81. Ahmadzadeh M, Johnson LA, Heemskerk B, Wunderlich JR, Dudley ME, White DE, *et al*. Tumor antigen-specific CD8 T cells infiltrating the tumor express high levels of PD-1 and are functionally impaired. *Blood*. 2009;114(8):1537-44. Epub 2009/05/09. doi: 10.1182/blood-2008-12-195792. PubMed PMID: 19423728; PMCID: PMC2927090.

82. Mlecnik B, Bindea G, Angell HK, Maby P, Angelova M, Tougeron D, *et al*. Integrative Analyses of Colorectal Cancer Show Immunoscore Is a Stronger Predictor of Patient Survival Than Microsatellite Instability. *Immunity*. 2016;44(3):698-711. Epub 2016/03/18. doi: 10.1016/j.immuni.2016.02.025. PubMed PMID: 26982367.

83. Tosolini M, Kirilovsky A, Mlecnik B, Fredriksen T, Mauger S, Bindea G, *et al*. Clinical impact of different classes of infiltrating T cytotoxic and helper cells (Th1, th2, treg, th17) in patients with colorectal cancer. *Cancer Res*. 2011;71(4):1263-71. Epub 2011/02/10. doi: 10.1158/0008-5472.Can-10-2907. PubMed PMID: 21303976.

84. Brummelman J, Mazza EMC, Alvisi G, Colombo FS, Grilli A, Mikulak J, *et al*. High-dimensional single cell analysis identifies stem-like cytotoxic CD8(+) T cells infiltrating human tumors. *J Exp Med*. 2018;215(10):2520-35. doi: 10.1084/jem.20180684. PubMed PMID: 30154266; PMCID: 6170179.

85. Simoni Y, Becht E, Fehlings M, Loh CY, Koo SL, Teng KWW, *et al*. Bystander CD8(+) T cells are abundant and phenotypically distinct in human tumour infiltrates. *Nature*.

2018;557(7706):575-9. Epub 2018/05/18. doi: 10.1038/s41586-018-0130-2. PubMed PMID: 29769722.

86. Akondy RS, Fitch M, Edupuganti S, Yang S, Kissick HT, Li KW, *et al.* Origin and differentiation of human memory CD8 T cells after vaccination. *Nature*. 2017;552(7685):362-7. Epub 2017/12/14. doi: 10.1038/nature24633. PubMed PMID: 29236685.

87. Dieu-Nosjean MC, Goc J, Giraldo NA, Sautes-Fridman C, Fridman WH. Tertiary lymphoid structures in cancer and beyond. *Trends Immunol*. 2014;35(11):571-80. Epub 2014/12/03. doi: 10.1016/j.it.2014.09.006. PubMed PMID: 25443495.

88. Sautes-Fridman C, Petitprez F, Calderaro J, Fridman WH. Tertiary lymphoid structures in the era of cancer immunotherapy. *Nature reviews Cancer*. 2019;19(6):307-25. Epub 2019/05/17. doi: 10.1038/s41568-019-0144-6. PubMed PMID: 31092904.

89. Silina K, Soltermann A, Movahedian Attar F, Casanova R, Uckeley ZM, Thut H, *et al.* Germinal centers determine the prognostic relevance of tertiary lymphoid structures and are impaired by corticosteroids in lung squamous cell carcinoma. *Cancer Res*. 2017. Epub 2017/12/28. doi: 10.1158/0008-5472.CAN-17-1987. PubMed PMID: 29279354.

90. Miron M, Kumar BV, Meng W, Granot T, Carpenter DJ, Senda T, *et al.* Human Lymph Nodes Maintain TCF-1 Memory T Cells with High Functional Potential and Clonal Diversity throughout Life. *The Journal of Immunology*. 2018;ji1800716. doi: 10.4049/jimmunol.1800716.

91. Mandrekar J, J Mandrekar S, Cha S. Cutpoint Determination Methods in Survival Analysis using SAS2003.

92. Contal C, O'Quigley J. An application of changepoint methods in studying the effect of age on survival in breast cancer. *Computational Statistics & Data Analysis*. 1999;30(3):253-70. doi: [https://doi.org/10.1016/S0167-9473\(98\)00096-6](https://doi.org/10.1016/S0167-9473(98)00096-6).

93. Scrucca L, Fop M, Murphy TB, Raftery AE. mclust 5: Clustering, Classification and Density Estimation Using Gaussian Finite Mixture Models. *The R journal*. 2016;8(1):289-317. Epub 2016/11/08. PubMed PMID: 27818791; PMCID: PMC5096736.
94. Love MI, Huber W, Anders S. Moderated estimation of fold change and dispersion for RNA-seq data with DESeq2. *Genome biology*. 2014;15(12):550. doi: 10.1186/s13059-014-0550-8. PubMed PMID: 25516281; PMCID: 4302049.
95. Krueger F, Andrews SR. Bismark: a flexible aligner and methylation caller for Bisulfite-Seq applications. *Bioinformatics* (Oxford, England). 2011;27(11):1571-2. doi: 10.1093/bioinformatics/btr167. PubMed PMID: 21493656; PMCID: 3102221.
96. Gerner MY, Kastenmuller W, Ifrim I, Kabat J, Germain RN. Histo-cytometry: a method for highly multiplex quantitative tissue imaging analysis applied to dendritic cell subset microanatomy in lymph nodes. *Immunity*. 2012;37(2):364-76. Epub 2012/08/07. doi: 10.1016/j.immuni.2012.07.011. PubMed PMID: 22863836; PMCID: PMC3514885.
97. Calagua C, Ficial M, Jansen CS, Hirz T, del Balzo L, Wilkinson S, *et al*. A Subset of Localized Prostate Cancer Displays an Immunogenic Phenotype Associated with Losses of Key Tumor Suppressor Genes. *Clinical Cancer Research*. 2021;27(17):4836-47. doi: 10.1158/1078-0432.CCR-21-0121.
98. Jansen CS, Prokhnevskaya N, Kissick HT. The requirement for immune infiltration and organization in the tumor microenvironment for successful immunotherapy in prostate cancer. *Urol Oncol*. 2019;37(8):543-55. Epub 2018/11/13. doi: 10.1016/j.urolonc.2018.10.011. PubMed PMID: 30446449.
99. Berghoff AS, Fuchs E, Ricken G, Mlecnik B, Bindea G, Spanberger T, *et al*. Density of tumor-infiltrating lymphocytes correlates with extent of brain edema and overall survival time in

patients with brain metastases. *Oncoimmunology*. 2016;5(1):e1057388. Epub 20150609. doi: 10.1080/2162402x.2015.1057388. PubMed PMID: 26942067; PMCID: PMC4760339.

100. Berghoff AS, Kiesel B, Widhalm G, Rajky O, Ricken G, Wöhrer A, *et al*. Programmed death ligand 1 expression and tumor-infiltrating lymphocytes in glioblastoma. *Neuro Oncol*. 2015;17(8):1064-75. Epub 20141029. doi: 10.1093/neuonc/nou307. PubMed PMID: 25355681; PMCID: PMC4490866.

101. Medawar PB. Immunity to homologous grafted skin; the fate of skin homografts transplanted to the brain, to subcutaneous tissue, and to the anterior chamber of the eye. *Br J Exp Pathol*. 1948;29(1):58-69. PubMed PMID: 18865105; PMCID: PMC2073079.

102. Louveau A, Smirnov I, Keyes TJ, Eccles JD, Rouhani SJ, Peske JD, *et al*. Structural and functional features of central nervous system lymphatic vessels. *Nature*. 2015;523(7560):337-41. doi: 10.1038/nature14432.

103. Blankenstein T, Coulie PG, Gilboa E, Jaffee EM. The determinants of tumour immunogenicity. *Nature reviews Cancer*. 2012;12(4):307-13. doi: 10.1038/nrc3246. PubMed PMID: 22378190.

104. Klapper JA, Downey SG, Smith FO, Yang JC, Hughes MS, Kammula US, *et al*. High-dose interleukin-2 for the treatment of metastatic renal cell carcinoma : a retrospective analysis of response and survival in patients treated in the surgery branch at the National Cancer Institute between 1986 and 2006. *Cancer*. 2008;113(2):293-301. doi: 10.1002/cncr.23552. PubMed PMID: 18457330; PMCID: PMC3486432.

105. Yang JC, Sherry RM, Steinberg SM, Topalian SL, Schwartzentruber DJ, Hwu P, *et al*. Randomized Study of High-Dose and Low-Dose Interleukin-2 in Patients With Metastatic Renal Cancer. *Journal of Clinical Oncology*. 2003;21(16):3127-32. doi: 10.1200/JCO.2003.02.122.

106. Motzer RJ, Jonasch E, Boyle S, Carlo MI, Manley B, Agarwal N, *et al.* NCCN Guidelines Insights: Kidney Cancer, Version 1.2021. *J Natl Compr Canc Netw.* 2020;18(9):1160-70. doi: 10.6004/jnccn.2020.0043. PubMed PMID: 32886895.
107. Motzer RJ, Tannir NM, McDermott DF, Frontera OA, Melichar B, Choueiri TK, *et al.* Nivolumab plus Ipilimumab versus Sunitinib in Advanced Renal-Cell Carcinoma. *New England Journal of Medicine.* 2018;378(14):1277-90. doi: 10.1056/NEJMoa1712126. PubMed PMID: 29562145.
108. Motzer RJ, Escudier B, McDermott DF, George S, Hammers HJ, Srinivas S, *et al.* Nivolumab versus Everolimus in Advanced Renal-Cell Carcinoma. *New England Journal of Medicine.* 2015;373(19):1803-13. doi: 10.1056/NEJMoa1510665.
109. Rini BI, Plimack ER, Stus V, Gafanov R, Hawkins R, Nosov D, *et al.* Pembrolizumab plus Axitinib versus Sunitinib for Advanced Renal-Cell Carcinoma. *N Engl J Med.* 2019;380(12):1116-27. Epub 2019/02/20. doi: 10.1056/NEJMoa1816714. PubMed PMID: 30779529.
110. Motzer RJ, Penkov K, Haanen J, Rini B, Albiges L, Campbell MT, *et al.* Avelumab plus Axitinib versus Sunitinib for Advanced Renal-Cell Carcinoma. *N Engl J Med.* 2019;380(12):1103-15. Epub 2019/02/20. doi: 10.1056/NEJMoa1816047. PubMed PMID: 30779531.
111. Motzer R, Alekseev B, Rha S-Y, Porta C, Eto M, Powles T, *et al.* Lenvatinib plus Pembrolizumab or Everolimus for Advanced Renal Cell Carcinoma. *New England Journal of Medicine.* 2021;384(14):1289-300. doi: 10.1056/NEJMoa2035716.
112. Choueiri TK, Powles T, Burotto M, Escudier B, Boursin MT, Zurawski B, *et al.* Nivolumab plus Cabozantinib versus Sunitinib for Advanced Renal-Cell Carcinoma. *New England Journal of Medicine.* 2021;384(9):829-41. doi: 10.1056/NEJMoa2026982.
113. Choueiri TK, Tomczak P, Park SH, Venugopal B, Ferguson T, Chang Y-H, *et al.* Adjuvant

Pembrolizumab after Nephrectomy in Renal-Cell Carcinoma. *New England Journal of Medicine*. 2021;385(8):683-94. doi: 10.1056/NEJMoa2106391.

114. Huang AC, Postow MA, Orlowski RJ, Mick R, Bengsch B, Manne S, *et al*. T-cell invigoration to tumour burden ratio associated with anti-PD-1 response. *Nature*. 2017;545(7652):60-5. Epub 2017/04/12. doi: 10.1038/nature22079. PubMed PMID: 28397821; PMCID: PMC5554367.

115. Huang AC, Orlowski RJ, Xu X, Mick R, George SM, Yan PK, *et al*. A single dose of neoadjuvant PD-1 blockade predicts clinical outcomes in resectable melanoma. *Nature Medicine*. 2019;25(3):454-61. doi: 10.1038/s41591-019-0357-y.

116. Kamphorst AO, Pillai RN, Yang S, Nasti TH, Akondy RS, Wieland A, *et al*. Proliferation of PD-1+ CD8 T cells in peripheral blood after PD-1-targeted therapy in lung cancer patients. *Proceedings of the National Academy of Sciences of the United States of America*. 2017;114(19):4993-8. Epub 2017/04/28. doi: 10.1073/pnas.1705327114. PubMed PMID: 28446615; PMCID: PMC5441721.

117. Dronca RS, Liu X, Harrington SM, Chen L, Cao S, Kottschade LA, *et al*. T cell Bim levels reflect responses to anti-PD-1 cancer therapy. *JCI insight*. 2016;1(6). doi: 10.1172/jci.insight.86014.

118. Fairfax BP, Taylor CA, Watson RA, Nassiri I, Danielli S, Fang H, *et al*. Peripheral CD8(+) T cell characteristics associated with durable responses to immune checkpoint blockade in patients with metastatic melanoma. *Nat Med*. 2020;26(2):193-9. Epub 20200210. doi: 10.1038/s41591-019-0734-6. PubMed PMID: 32042196; PMCID: PMC7611047.

119. Kim KH, Cho J, Ku BM, Koh J, Sun JM, Lee SH, *et al*. The First-week Proliferative Response of Peripheral Blood PD-1(+)CD8(+) T Cells Predicts the Response to Anti-PD-1

Therapy in Solid Tumors. *Clin Cancer Res.* 2019;25(7):2144-54. Epub 20190115. doi: 10.1158/1078-0432.Ccr-18-1449. PubMed PMID: 30647082.

120. Valpione S, Galvani E, Tweedy J, Mundra PA, Banyard A, Middlehurst P, *et al.* Immune awakening revealed by peripheral T cell dynamics after one cycle of immunotherapy. *Nature Cancer.* 2020;1(2):210-21. doi: 10.1038/s43018-019-0022-x.

121. Boland GM, Flaherty KT. Tracking early response to immunotherapy. *Nature Cancer.* 2020;1(2):160-2. doi: 10.1038/s43018-020-0032-8.

122. Ayers M, Lunceford J, Nebozhyn M, Murphy E, Loboda A, Kaufman DR, *et al.* IFN-gamma-related mRNA profile predicts clinical response to PD-1 blockade. *J Clin Invest.* 2017;127(8):2930-40. Epub 2017/06/27. doi: 10.1172/JCI91190. PubMed PMID: 28650338; PMCID: PMC5531419.

123. Wu TD, Madireddi S, de Almeida PE, Banchereau R, Chen Y-JJ, Chitre AS, *et al.* Peripheral T cell expansion predicts tumour infiltration and clinical response. *Nature.* 2020;579(7798):274-8. doi: 10.1038/s41586-020-2056-8.

124. Han J, Duan J, Bai H, Wang Y, Wan R, Wang X, *et al.* TCR Repertoire Diversity of Peripheral PD-1(+)CD8(+) T Cells Predicts Clinical Outcomes after Immunotherapy in Patients with Non-Small Cell Lung Cancer. *Cancer immunology research.* 2020;8(1):146-54. Epub 20191112. doi: 10.1158/2326-6066.Cir-19-0398. PubMed PMID: 31719056.

125. Cha E, Klinger M, Hou Y, Cummings C, Ribas A, Faham M, *et al.* Improved survival with T cell clonotype stability after anti-CTLA-4 treatment in cancer patients. *Sci Transl Med.* 2014;6(238):238ra70. doi: 10.1126/scitranslmed.3008211. PubMed PMID: 24871131; PMCID: PMC4558099.

126. Hui E, Cheung J, Zhu J, Su X, Taylor MJ, Wallweber HA, *et al.* T cell costimulatory

receptor CD28 is a primary target for PD-1-mediated inhibition. *Science*. 2017;355(6332):1428-33. Epub 20170309. doi: 10.1126/science.aaf1292. PubMed PMID: 28280247; PMCID: PMC6286077.

127. Chen PL, Roh W, Reuben A, Cooper ZA, Spencer CN, Prieto PA, *et al*. Analysis of Immune Signatures in Longitudinal Tumor Samples Yields Insight into Biomarkers of Response and Mechanisms of Resistance to Immune Checkpoint Blockade. *Cancer discovery*. 2016;6(8):827-37. Epub 20160614. doi: 10.1158/2159-8290.Cd-15-1545. PubMed PMID: 27301722; PMCID: PMC5082984.

128. Li T, Zhao L, Yang Y, Wang Y, Zhang Y, Guo J, *et al*. T Cells Expanded from PD-1+ Peripheral Blood Lymphocytes Share More Clones with Paired Tumor-Infiltrating Lymphocytes. *Cancer Research*. 2021;81(8):2184-94. doi: 10.1158/0008-5472.CAN-20-2300.

129. Kametsky L, Jones TR, Fraser A, Bray M-A, Logan DJ, Madden KL, *et al*. Improved structure, function and compatibility for CellProfiler: modular high-throughput image analysis software. *Bioinformatics* (Oxford, England). 2011;27(8):1179-80. doi: 10.1093/bioinformatics/btr095.

130. Carpenter AE, Jones TR, Lamprecht MR, Clarke C, Kang IH, Friman O, *et al*. CellProfiler: image analysis software for identifying and quantifying cell phenotypes. *Genome biology*. 2006;7(10):R100. doi: 10.1186/gb-2006-7-10-r100.

131. Pardoll D. Timeline: a decade of advances in immunotherapy. *Nature Medicine*. 2011;17(3):296-. doi: 10.1038/nm0311-296.

132. Huang AC, Zappasodi R. A decade of checkpoint blockade immunotherapy in melanoma: understanding the molecular basis for immune sensitivity and resistance. *Nature Immunology*. 2022. doi: 10.1038/s41590-022-01141-1.

133. Rosenberg SA. Progress in human tumour immunology and immunotherapy. *Nature*. 2001;411(6835):380-4. doi: 10.1038/35077246.
134. Motzer RJ, Powles T, Atkins MB, Escudier B, McDermott DF, Suarez C, *et al*. IMmotion151: A Randomized Phase III Study of Atezolizumab Plus Bevacizumab vs Sunitinib in Untreated Metastatic Renal Cell Carcinoma (mRCC). *Journal of Clinical Oncology*. 2018;36(6\_suppl):578-. doi: 10.1200/JCO.2018.36.6\_suppl.578.
135. Motzer RJ, Rini BI, McDermott DF, Redman BG, Kuzel TM, Harrison MR, *et al*. Nivolumab for Metastatic Renal Cell Carcinoma: Results of a Randomized Phase II Trial. *Journal of Clinical Oncology*. 2015;33(13):1430-7. doi: 10.1200/JCO.2014.59.0703. PubMed PMID: PMC4806782.
136. Darvin P, Toor SM, Sasidharan Nair V, Elkord E. Immune checkpoint inhibitors: recent progress and potential biomarkers. *Experimental & Molecular Medicine*. 2018;50(12):1-11. doi: 10.1038/s12276-018-0191-1.
137. Haslam A, Prasad V. Estimation of the Percentage of US Patients With Cancer Who Are Eligible for and Respond to Checkpoint Inhibitor Immunotherapy Drugs. *JAMA Netw Open*. 2019;2(5):e192535-e. doi: 10.1001/jamanetworkopen.2019.2535. PubMed PMID: 31050774.
138. Webster RM. The immune checkpoint inhibitors: where are we now? *Nature Reviews Drug Discovery*. 2014;13(12):883-4. doi: 10.1038/nrd4476.
139. Sharma P, Hu-Lieskovan S, Wargo JA, Ribas A. Primary, Adaptive, and Acquired Resistance to Cancer Immunotherapy. *Cell*. 2017;168(4):707-23. Epub 2017/02/12. doi: 10.1016/j.cell.2017.01.017. PubMed PMID: 28187290; PMCID: PMC5391692.
140. Blackburn CC, Manley NR. Developing a new paradigm for thymus organogenesis. *Nature Reviews Immunology*. 2004;4(4):278-89. doi: 10.1038/nri1331.

141. Mendelson A, Frenette PS. Hematopoietic stem cell niche maintenance during homeostasis and regeneration. *Nature Medicine*. 2014;20(8):833-46. doi: 10.1038/nm.3647.
142. Zhao E, Xu H, Wang L, Kryczek I, Wu K, Hu Y, *et al*. Bone marrow and the control of immunity. *Cellular & Molecular Immunology*. 2012;9(1):11-9. doi: 10.1038/cmi.2011.47.
143. Tokoyoda K, Hauser AE, Nakayama T, Radbruch A. Organization of immunological memory by bone marrow stroma. *Nature Reviews Immunology*. 2010;10(3):193-200. doi: 10.1038/nri2727.
144. Junt T, Scandella E, Ludewig B. Form follows function: lymphoid tissue microarchitecture in antimicrobial immune defence. *Nature Reviews Immunology*. 2008;8(10):764-75. doi: 10.1038/nri2414.
145. Junt T, Moseman EA, Iannacone M, Massberg S, Lang PA, Boes M, *et al*. Subcapsular sinus macrophages in lymph nodes clear lymph-borne viruses and present them to antiviral B cells. *Nature*. 2007;450(7166):110-4. Epub 20071014. doi: 10.1038/nature06287. PubMed PMID: 17934446.
146. Stoll S, Delon J, Brotz TM, Germain RN. Dynamic imaging of T cell-dendritic cell interactions in lymph nodes. *Science*. 2002;296(5574):1873-6. doi: 10.1126/science.1071065. PubMed PMID: 12052961.
147. Mempel TR, Henrickson SE, Von Andrian UH. T-cell priming by dendritic cells in lymph nodes occurs in three distinct phases. *Nature*. 2004;427(6970):154-9. doi: 10.1038/nature02238. PubMed PMID: 14712275.
148. Schluns KS, Lefrançois L. Cytokine control of memory T-cell development and survival. *Nature Reviews Immunology*. 2003;3(4):269-79.
149. Soderberg KA, Payne GW, Sato A, Medzhitov R, Segal SS, Iwasaki A. Innate control of

adaptive immunity via remodeling of lymph node feed arteriole. *Proceedings of the National Academy of Sciences of the United States of America*. 2005;102(45):16315-20. Epub 20051031. doi: 10.1073/pnas.0506190102. PubMed PMID: 16260739; PMCID: PMC1283434.

150. Angeli V, Ginhoux F, Llodrà J, Quemeneur L, Frenette PS, Skobe M, *et al*. B cell-driven lymphangiogenesis in inflamed lymph nodes enhances dendritic cell mobilization. *Immunity*. 2006;24(2):203-15. doi: 10.1016/j.immuni.2006.01.003. PubMed PMID: 16473832.

151. Schwab SR, Cyster JG. Finding a way out: lymphocyte egress from lymphoid organs. *Nature immunology*. 2007;8(12):1295-301.

152. Bajenoff M, Egen JG, Koo LY, Laugier JP, Brau F, Glaichenhaus N, *et al*. Stromal cell networks regulate lymphocyte entry, migration, and territoriality in lymph nodes. *Immunity*. 2006;25(6):989-1001. Epub 2006/11/23. doi: 10.1016/j.immuni.2006.10.011. PubMed PMID: 17112751; PMCID: PMC2692293.

153. Brown FD, Turley SJ. Fibroblastic Reticular Cells: Organization and Regulation of the T Lymphocyte Life Cycle. *The Journal of Immunology*. 2015;194(4):1389-94. doi: 10.4049/jimmunol.1402520.

154. Fu Y-X, Chaplin DD. Development and maturation of secondary lymphoid tissues. *Annual review of immunology*. 1999;17(1):399-433.

155. Balázs M, Martin F, Zhou T, Kearney J. Blood dendritic cells interact with splenic marginal zone B cells to initiate T-independent immune responses. *Immunity*. 2002;17(3):341-52. doi: 10.1016/s1074-7613(02)00389-8. PubMed PMID: 12354386.

156. Ochsenbein AF, Zinkernagel RM. Natural antibodies and complement link innate and acquired immunity. *Immunol Today*. 2000;21(12):624-30. doi: 10.1016/s0167-5699(00)01754-0. PubMed PMID: 11114423.

157. Phan TG, Grigorova I, Okada T, Cyster JG. Subcapsular encounter and complement-dependent transport of immune complexes by lymph node B cells. *Nature Immunology*. 2007;8(9):992-1000. doi: 10.1038/ni1494.
158. Geijtenbeek TB, Groot PC, Nolte MA, van Vliet SJ, Gangaram-Panday ST, van Duijnhoven GC, *et al*. Marginal zone macrophages express a murine homologue of DC-SIGN that captures blood-borne antigens in vivo. *Blood*. 2002;100(8):2908-16. doi: 10.1182/blood-2002-04-1044. PubMed PMID: 12351402.
159. Farr AG, Berry ML, Kim A, Nelson AJ, Welch MP, Aruffo A. Characterization and cloning of a novel glycoprotein expressed by stromal cells in T-dependent areas of peripheral lymphoid tissues. *J Exp Med*. 1992;176(5):1477-82. doi: 10.1084/jem.176.5.1477. PubMed PMID: 1402691; PMCID: PMC2119410.
160. Katakai T, Hara T, Lee JH, Gonda H, Sugai M, Shimizu A. A novel reticular stromal structure in lymph node cortex: an immuno-platform for interactions among dendritic cells, T cells and B cells. *Int Immunol*. 2004;16(8):1133-42. Epub 20040705. doi: 10.1093/intimm/dxh113. PubMed PMID: 15237106.
161. Gretz JE, Anderson AO, Shaw S. Cords, channels, corridors and conduits: critical architectural elements facilitating cell interactions in the lymph node cortex. *Immunol Rev*. 1997;156:11-24. doi: 10.1111/j.1600-065x.1997.tb00955.x. PubMed PMID: 9176696.
162. von Andrian UH, Mempel TR. Homing and cellular traffic in lymph nodes. *Nature Reviews Immunology*. 2003;3:867. doi: 10.1038/nri1222  
<https://www.nature.com/articles/nri1222#supplementary-information>.
163. Girard J-P, Moussion C, Förster R. HEVs, lymphatics and homeostatic immune cell trafficking in lymph nodes. *Nature Reviews Immunology*. 2012;12:762. doi: 10.1038/nri3298.

164. de Chaisemartin L, Goc J, Damotte D, Validire P, Magdeleinat P, Alifano M, *et al.* Characterization of chemokines and adhesion molecules associated with T cell presence in tertiary lymphoid structures in human lung cancer. *Cancer Res.* 2011;71(20):6391-9. Epub 2011/09/09. doi: 10.1158/0008-5472.CAN-11-0952. PubMed PMID: 21900403.
165. Hwang JY, Randall TD, Silva-Sanchez A. Inducible Bronchus-Associated Lymphoid Tissue: Taming Inflammation in the Lung. *Frontiers in Immunology.* 2016;7:258. doi: 10.3389/fimmu.2016.00258. PubMed PMID: PMC4928648.
166. Randall TD. Chapter 7 - Bronchus-Associated Lymphoid Tissue (BALT): Structure and Function. In: Fagarasan S, Cerutti A, editors. *Advances in Immunology*: Academic Press; 2010. p. 187-241.
167. Sato M, Hirayama S, Matsuda Y, Wagnetz D, Hwang DM, Guan Z, *et al.* Stromal Activation and Formation of Lymphoid-Like Stroma in Chronic Lung Allograft Dysfunction. *Transplantation.* 2011;91(12):1398-405. doi: 10.1097/TP.0b013e31821b2f7a. PubMed PMID: 00007890-201106270-00017.
168. Goc J, Fridman WH, Sautes-Fridman C, Dieu-Nosjean MC. Characteristics of tertiary lymphoid structures in primary cancers. *Oncoimmunology.* 2013;2(12):e26836. Epub 2014/02/06. doi: 10.4161/onci.26836. PubMed PMID: 24498556; PMCID: PMC3912008.
169. Goc J, Germain C, Vo-Bourgais TK, Lupo A, Klein C, Knockaert S, *et al.* Dendritic cells in tumor-associated tertiary lymphoid structures signal a Th1 cytotoxic immune contexture and license the positive prognostic value of infiltrating CD8+ T cells. *Cancer Res.* 2014;74(3):705-15. doi: 10.1158/0008-5472.CAN-13-1342. PubMed PMID: 24366885.
170. Kratz A, Campos-Neto A, Hanson MS, Ruddle NH. Chronic inflammation caused by lymphotoxin is lymphoid neogenesis. *The Journal of Experimental Medicine.* 1996;183(4):1461-

72. doi: 10.1084/jem.183.4.1461.
171. Mebius RE. Organogenesis of lymphoid tissues. *Nat Rev Immunol.* 2003;3(4):292-303. Epub 2003/04/02. doi: 10.1038/nri1054. PubMed PMID: 12669020.
172. Rangel-Moreno J, Moyron-Quiroz JE, Hartson L, Kusser K, Randall TD. Pulmonary expression of CXC chemokine ligand 13, CC chemokine ligand 19, and CC chemokine ligand 21 is essential for local immunity to influenza. *Proceedings of the National Academy of Sciences of the United States of America.* 2007;104(25):10577-82. doi: 10.1073/pnas.0700591104. PubMed PMID: PMC1965555.
173. Moyron-Quiroz JE, Rangel-Moreno J, Kusser K, Hartson L, Sprague F, Goodrich S, *et al.* Role of inducible bronchus associated lymphoid tissue (iBALT) in respiratory immunity. *Nature Medicine.* 2004;10:927. doi: 10.1038/nm1091  
<https://www.nature.com/articles/nm1091#supplementary-information>.
174. GeurtsvanKessel CH, Willart MA, Bergen IM, van Rijt LS, Muskens F, Elewaut D, *et al.* Dendritic cells are crucial for maintenance of tertiary lymphoid structures in the lung of influenza virus-infected mice. *J Exp Med.* 2009;206(11):2339-49. Epub 2009/10/08. doi: 10.1084/jem.20090410. PubMed PMID: 19808255; PMCID: PMC2768850.
175. Nayar S, Campos J, Smith CG, Iannizzotto V, Gardner DH, Mourcin F, *et al.* Immunofibroblasts are pivotal drivers of tertiary lymphoid structure formation and local pathology. *Proceedings of the National Academy of Sciences.* 2019;116(27):13490-7. doi: doi:10.1073/pnas.1905301116.
176. Pitzalis C, Jones GW, Bombardieri M, Jones SA. Ectopic lymphoid-like structures in infection, cancer and autoimmunity. *Nat Rev Immunol.* 2014;14(7):447-62. Epub 20140620. doi: 10.1038/nri3700. PubMed PMID: 24948366.

177. Humby F, Bombardieri M, Manzo A, Kelly S, Blades MC, Kirkham B, *et al.* Ectopic lymphoid structures support ongoing production of class-switched autoantibodies in rheumatoid synovium. *PLoS Med.* 2009;6(1):e1. doi: 10.1371/journal.pmed.0060001. PubMed PMID: 19143467; PMCID: PMC2621263.
178. Timmer TC, Baltus B, Vondenhoff M, Huizinga TW, Tak PP, Verweij CL, *et al.* Inflammation and ectopic lymphoid structures in rheumatoid arthritis synovial tissues dissected by genomics technology: identification of the interleukin-7 signaling pathway in tissues with lymphoid neogenesis. *Arthritis Rheum.* 2007;56(8):2492-502. doi: 10.1002/art.22748. PubMed PMID: 17665400.
179. Sansonno D, De Vita S, Iacobelli AR, Cornacchiulo V, Boiocchi M, Dammacco F. Clonal analysis of intrahepatic B cells from HCV-infected patients with and without mixed cryoglobulinemia. *J Immunol.* 1998;160(7):3594-601. PubMed PMID: 9531323.
180. Sansonno D, Tucci FA, Troiani L, Lauletta G, Montrone M, Conteduca V, *et al.* Increased serum levels of the chemokine CXCL13 and up-regulation of its gene expression are distinctive features of HCV-related cryoglobulinemia and correlate with active cutaneous vasculitis. *Blood.* 2008;112(5):1620-7. Epub 20080612. doi: 10.1182/blood-2008-02-137455. PubMed PMID: 18550853.
181. Winter S, Loddenkemper C, Aebischer A, Räbel K, Hoffmann K, Meyer TF, *et al.* The chemokine receptor CXCR5 is pivotal for ectopic mucosa-associated lymphoid tissue neogenesis in chronic *Helicobacter pylori*-induced inflammation. *Journal of Molecular Medicine (Berlin, Germany).* 2010;88(11):1169-80. doi: 10.1007/s00109-010-0658-6. PubMed PMID: PMC2956061.
182. Lochner M, Ohnmacht C, Presley L, Bruhns P, Si-Tahar M, Sawa S, *et al.* Microbiota-

induced tertiary lymphoid tissues aggravate inflammatory disease in the absence of ROR $\gamma$ t and LTi cells. *The Journal of Experimental Medicine*. 2011;208(1):125-34. doi: 10.1084/jem.20100052.

183. Shomer NH, Fox JG, Juedes AE, Ruddle NH. Helicobacter-induced chronic active lymphoid aggregates have characteristics of tertiary lymphoid tissue. *Infection and immunity*. 2003;71(6):3572-7. Epub 2003/05/23. PubMed PMID: 12761142; PMCID: PMC155770.

184. Thaunat O, Patey N, Caligiuri G, Gautreau C, Mamani-Matsuda M, Mekki Y, *et al*. Chronic Rejection Triggers the Development of an Aggressive Intragraft Immune Response through Recapitulation of Lymphoid Organogenesis. *The Journal of Immunology*. 2010;185(1):717-28. doi: 10.4049/jimmunol.0903589.

185. Baddoura FK, Nasr IW, Wrobel B, Li Q, Ruddle NH, Lakkis FG. Lymphoid neogenesis in murine cardiac allografts undergoing chronic rejection. *Am J Transplant*. 2005;5(3):510-6. doi: 10.1111/j.1600-6143.2004.00714.x. PubMed PMID: 15707405.

186. Dieu-Nosjean MC, Antoine M, Danel C, Heudes D, Wislez M, Poulot V, *et al*. Long-term survival for patients with non-small-cell lung cancer with intratumoral lymphoid structures. *J Clin Oncol*. 2008;26(27):4410-7. Epub 2008/09/20. doi: 10.1200/JCO.2007.15.0284. PubMed PMID: 18802153.

187. Cipponi A, Mercier M, Seremet T, Baurain JF, Theate I, van den Oord J, *et al*. Neogenesis of lymphoid structures and antibody responses occur in human melanoma metastases. *Cancer Res*. 2012;72(16):3997-4007. Epub 2012/08/02. doi: 10.1158/0008-5472.CAN-12-1377. PubMed PMID: 22850419.

188. Shields JD, Kourtis IC, Tomei AA, Roberts JM, Swartz MA. Induction of Lymphoidlike Stroma and Immune Escape by Tumors That Express the Chemokine CCL21. *Science*.

2010;328(5979):749-52. doi: 10.1126/science.1185837.

189. Martinet L, Garrido I, Filleron T, Le Guellec S, Bellard E, Fournie JJ, *et al.* Human solid tumors contain high endothelial venules: association with T- and B-lymphocyte infiltration and favorable prognosis in breast cancer. *Cancer Res.* 2011;71(17):5678-87. Epub 20110816. doi: 10.1158/0008-5472.Can-11-0431. PubMed PMID: 21846823.

190. Solinas C, Garaud S, De Silva P, Boisson A, Van den Eynden G, de Wind A, *et al.* Immune Checkpoint Molecules on Tumor-Infiltrating Lymphocytes and Their Association with Tertiary Lymphoid Structures in Human Breast Cancer. *Front Immunol.* 2017;8:1412. Epub 2017/11/23. doi: 10.3389/fimmu.2017.01412. PubMed PMID: 29163490; PMCID: PMC5670348.

191. Martinet L, Filleron T, Le Guellec S, Rochaix P, Garrido I, Girard J-P. High Endothelial Venule Blood Vessels for Tumor-Infiltrating Lymphocytes Are Associated with Lymphotoxin  $\beta$ -Producing Dendritic Cells in Human Breast Cancer. *The Journal of Immunology.* 2013;191(4):2001-8. doi: 10.4049/jimmunol.1300872.

192. Wirsing AM, Rikardsen OG, Steigen SE, Uhlin-Hansen L, Hadler-Olsen E. Characterisation and prognostic value of tertiary lymphoid structures in oral squamous cell carcinoma. *BMC clinical pathology.* 2014;14:38. Epub 2014/09/02. doi: 10.1186/1472-6890-14-38. PubMed PMID: 25177210; PMCID: PMC4148494.

193. Hiraoka N, Ino Y, Yamazaki-Itoh R, Kanai Y, Kosuge T, Shimada K. Intratumoral tertiary lymphoid organ is a favourable prognosticator in patients with pancreatic cancer. *Br J Cancer.* 2015;112(11):1782-90. Epub 2015/05/06. doi: 10.1038/bjc.2015.145. PubMed PMID: 25942397; PMCID: PMC4647237.

194. Joshi NS, Akama-Garren EH, Lu Y, Lee DY, Chang GP, Li A, *et al.* Regulatory T Cells in Tumor-Associated Tertiary Lymphoid Structures Suppress Anti-tumor T Cell Responses.

Immunity. 2015;43(3):579-90. Epub 2015/09/06. doi: 10.1016/j.immuni.2015.08.006. PubMed PMID: 26341400; PMCID: PMC4826619.

195. Finkin S, Yuan D, Stein I, Taniguchi K, Weber A, Unger K, *et al.* Ectopic lymphoid structures function as microniches for tumor progenitor cells in hepatocellular carcinoma. *Nat Immunol.* 2015;16(12):1235-44. Epub 20151026. doi: 10.1038/ni.3290. PubMed PMID: 26502405; PMCID: PMC4653079.

196. Lee HJ, Park IA, Song IH, Shin SJ, Kim JY, Yu JH, *et al.* Tertiary lymphoid structures: prognostic significance and relationship with tumour-infiltrating lymphocytes in triple-negative breast cancer. *J Clin Pathol.* 2016;69(5):422-30. Epub 20151016. doi: 10.1136/jclinpath-2015-203089. PubMed PMID: 26475777.

197. Stoltzfus CR, Sivakumar R, Kunz L, Olin Pope BE, Menietti E, Speziale D, *et al.* Multi-Parameter Quantitative Imaging of Tumor Microenvironments Reveals Perivascular Immune Niches Associated With Anti-Tumor Immunity. *Frontiers in Immunology.* 2021;12. doi: 10.3389/fimmu.2021.726492.

198. Dunn GP, Old LJ, Schreiber RD. The three Es of cancer immunoediting. *Annu Rev Immunol.* 2004;22:329-60. doi: 10.1146/annurev.immunol.22.012703.104803. PubMed PMID: 15032581.

199. Vinay DS, Ryan EP, Pawelec G, Talib WH, Stagg J, Elkord E, *et al.* Immune evasion in cancer: Mechanistic basis and therapeutic strategies. *Semin Cancer Biol.* 2015;35 Suppl:S185-s98. Epub 20150325. doi: 10.1016/j.semcancer.2015.03.004. PubMed PMID: 25818339.

200. Li J, Byrne KT, Yan F, Yamazoe T, Chen Z, Baslan T, *et al.* Tumor Cell-Intrinsic Factors Underlie Heterogeneity of Immune Cell Infiltration and Response to Immunotherapy. *Immunity.* 2018;49(1):178-93.e7. Epub 20180626. doi: 10.1016/j.immuni.2018.06.006. PubMed PMID:

29958801; PMID: PMC6707727.

201. Li J, Stanger BZ. How Tumor Cell Dedifferentiation Drives Immune Evasion and Resistance to Immunotherapy. *Cancer Res.* 2020;80(19):4037-41. Epub 20200618. doi: 10.1158/0008-5472.Can-20-1420. PubMed PMID: 32554552; PMID: PMC7541560.

202. Burr ML, Sparbier CE, Chan KL, Chan YC, Kersbergen A, Lam EYN, *et al.* An Evolutionarily Conserved Function of Polycomb Silences the MHC Class I Antigen Presentation Pathway and Enables Immune Evasion in Cancer. *Cancer Cell.* 2019;36(4):385-401.e8. Epub 20190926. doi: 10.1016/j.ccell.2019.08.008. PubMed PMID: 31564637; PMID: PMC6876280.

203. Hicklin DJ, Wang Z, Arienti F, Rivoltini L, Parmiani G, Ferrone S. beta2-Microglobulin mutations, HLA class I antigen loss, and tumor progression in melanoma. *The Journal of Clinical Investigation.* 1998;101(12):2720-9. doi: 10.1172/JCI498.

204. Yamamoto K, Venida A, Yano J, Biancur DE, Kakiuchi M, Gupta S, *et al.* Autophagy promotes immune evasion of pancreatic cancer by degrading MHC-I. *Nature.* 2020;581(7806):100-5. Epub 2020/04/22. doi: 10.1038/s41586-020-2229-5. PubMed PMID: 32376951.

205. Collins NB, Al Abosy R, Miller BC, Bi K, Zhao Q, Quigley M, *et al.* PI3K activation allows immune evasion by promoting an inhibitory myeloid tumor microenvironment. *Journal for ImmunoTherapy of Cancer.* 2022;10(3):e003402. doi: 10.1136/jitc-2021-003402.

206. Vidotto T, Melo CM, Castelli E, Koti M, dos Reis RB, Squire JA. Emerging role of PTEN loss in evasion of the immune response to tumours. *British Journal of Cancer.* 2020;122(12):1732-43. doi: 10.1038/s41416-020-0834-6.

207. Thorsson V, Gibbs DL, Brown SD, Wolf D, Bortone DS, Ou Yang T-H, *et al.* The Immune Landscape of Cancer. *Immunity.* 2018;48(4):812-30.e14. doi: 10.1016/j.immuni.2018.03.023.

208. Amankulor NM, Kim Y, Arora S, Kargl J, Szulzewsky F, Hanke M, *et al.* Mutant IDH1 regulates the tumor-associated immune system in gliomas. *Genes Dev.* 2017;31(8):774-86. Epub 20170502. doi: 10.1101/gad.294991.116. PubMed PMID: 28465358; PMCID: PMC5435890.
209. Ruiz de Galarreta M, Bresnahan E, Molina-Sánchez P, Lindblad KE, Maier B, Sia D, *et al.*  $\beta$ -Catenin Activation Promotes Immune Escape and Resistance to Anti-PD-1 Therapy in Hepatocellular Carcinoma. *Cancer discovery.* 2019;9(8):1124-41. Epub 20190611. doi: 10.1158/2159-8290.Cd-19-0074. PubMed PMID: 31186238; PMCID: PMC6677618.
210. Patel SJ, Sanjana NE, Kishton RJ, Eidizadeh A, Vodnala SK, Cam M, *et al.* Identification of essential genes for cancer immunotherapy. *Nature.* 2017;548(7669):537-42. Epub 20170807. doi: 10.1038/nature23477. PubMed PMID: 28783722; PMCID: PMC5870757.
211. Shin DS, Zaretsky JM, Escuin-Ordinas H, Garcia-Diaz A, Hu-Lieskovan S, Kalbasi A, *et al.* Primary Resistance to PD-1 Blockade Mediated by JAK1/2 Mutations. *Cancer discovery.* 2017;7(2):188-201. doi: 10.1158/2159-8290.Cd-16-1223.
212. Gao J, Shi LZ, Zhao H, Chen J, Xiong L, He Q, *et al.* Loss of IFN- $\gamma$  Pathway Genes in Tumor Cells as a Mechanism of Resistance to Anti-CTLA-4 Therapy. *Cell.* 2016;167(2):397-404.e9. Epub 20160922. doi: 10.1016/j.cell.2016.08.069. PubMed PMID: 27667683; PMCID: PMC5088716.
213. Fucikova J, Kepp O, Kasikova L, Petroni G, Yamazaki T, Liu P, *et al.* Detection of immunogenic cell death and its relevance for cancer therapy. *Cell Death & Disease.* 2020;11(11):1013. doi: 10.1038/s41419-020-03221-2.
214. Jin M-Z, Wang X-P. Immunogenic Cell Death-Based Cancer Vaccines. *Frontiers in Immunology.* 2021;12. doi: 10.3389/fimmu.2021.697964.